Large scale behaviour of the freely cooling granular gas

By

Sudhir Narayan Pathak

PHYS10200804005

The Institute of Mathematical Sciences, Chennai

A thesis submitted to the

Board of Studies in Physical Sciences

In partial fulfillment of requirements

For the Degree of

DOCTOR OF PHILOSOPHY

of

HOMI BHABHA NATIONAL INSTITUTE

July, 2014

Homi Bhabha National Institute

Recommendations of the Viva Voce Board

As members of the Viva Voce Board, we certify that we have read the dissertation prepared by Sudhir Narayan Pathak entitled “Large scale behaviour of the freely cooling granular gas" and recommend that it maybe accepted as fulfilling the dissertation requirement for the Degree of Doctor of Philosophy.

_____ Date:

Chair: Purusattam Ray

_____ Date:

Guide/Convener: Rajesh Ravindran

_____ Date:

Member 1: Satyavani Vemparala

_____ Date:

Member 2: Sitabhra Sinha

_____ Date:

External Examiner:

Final approval and acceptance of this dissertation is contingent upon the candidate’s submission of the final copies of the dissertation to HBNI.

I hereby certify that I have read this dissertation prepared under my direction and recommend that it may be accepted as fulfilling the dissertation requirement.

Date:

Place: Guide

STATEMENT BY AUTHOR

This dissertation has been submitted in partial fulfillment of requirements for an advanced degree at Homi Bhabha National Institute (HBNI) and is deposited in the Library to be made available to borrowers under rules of the HBNI.

Brief quotations from this dissertation are allowable without special permission, provided that accurate acknowledgement of source is made. Requests for permission for extended quotation from or reproduction of this manuscript in whole or in part may be granted by the Competent Authority of HBNI when in his or her judgement the proposed use of the material is in the interests of scholarship. In all other instances, however, permission must be obtained from the author.

Sudhir Narayan Pathak

DECLARATION

I, hereby declare that the investigation presented in the thesis has been carried out by me. The work is original and has not been submitted earlier as a whole or in part for a degree / diploma at this or any other Institution / University.

Sudhir Narayan Pathak

DEDICATIONS

To my parents

ACKNOWLEDGEMENTS

It has been a long journey and this thesis has been written with generous help from people around me. It is a great pleasure to thank all those people.

First and foremost, I would like to express my sincere gratitude to my thesis advisor, Prof. Rajesh Ravindran, for his excellent guidance and valuable advice on my thesis work. I wish to thank him for the interesting topics that I learnt and was exposed to in my research. I appreciate his patience and enthusiasm towards developing me as a better researcher.

I am grateful to our collaborators Prof. Dibyendu Das and Prof. Purusattam Ray for insightful discussions and sharing ideas. It was a great oppurtunity to work with Dr. Zahera Jabeen. She has played an important role in the completion of this thesis. I sincerely thank her for the invaluable help in computer programming during the earlier years of PhD.

I am thankful to Prof. Sitabhra Sinha and Prof. Satyavani Vemparala for their encouragement and providing guidance to my thesis work in doctoral committee meetings.

I am also grateful to IMSc administration, librarians and persons in charge of the computing facilities for all their support during my stay at IMSc. They made my stay here as pleasant as possible.

The difficult years of PhD were made easier by friends and I express my thanks to all of them. I had a lot of interesting political/philosophical discussions with Anil, Dhriti, Neeraj, Ramchandra, Sheeraz and Sreejith. Tennis sessions with Abhra, Arghya, Diganta, Joyjit, Gaurav, and Tuhin were the most interesting part of my stay at IMSc. I also thank Anoop, Baskar, Bruno, Chandan, G Arun, Gopal, Joydeep, KK, Ramanathan, Meesum, Raja S, Rajesh, Rohan, Sachin, Soumyajit, Thakur and Yadu for always being a constant

source of joy, laughter and support.

Finally I would like to express my thanks to my sisters Sushma and Sudha, brothers Subodh and Sushil for taking care of the home. Its all because of them that I was able to stay at IMSc for such a long time. No words for my parents as words are not sufficient sometimes.

In case I have missed someone,

Jis jis path pe sneha mila, us us raahi ko dhanyawad

List of Publications arising from the thesis

- **Journal**

  1. **Shock propagation in granular flow subjected to an external impact**

     S. N. Pathak, Z. Jabeen, P. Ray, and R. Rajesh

     Physical Review E **85**, 061301 (2012)

  2. **Shock propagation in a visco-elastic granular gas**

     S. N. Pathak, Z. Jabeen, R. Rajesh, and P. Ray

     AIP Conf. Proc. **1447**, 193 (2012)

  3. **Energy decay in three-dimensional freely cooling granular gas**

     S. N. Pathak, Z. Jabeen, D. Das, and R. Rajesh

     Physical Review Letters **112**, 038001 (2014)

- **Others**

  1. **Inhomogeneous cooling of the rough granular gas in two dimensions**

     S. N. Pathak, D. Das, and R. Rajesh

     arXiv:1407.0855 [cond-mat.soft]; Accepted for publication in Europhysics Letters

Contents

Synopsis

Granular systems are ubiquitous in nature. Examples in day to day life include food grains, coffee beans, powders, steel balls, and sand. At larger length scales, examples include rocks, boulders etc. Planetary rings, intergalactic dust clouds are few examples at the astrophysical scale. The applications of granular physics range from practical use in chemical, pharmaceutical and food industries to clarifying theoretical concepts of non-equilibrium statistical mechanics.

There are two important features associated with granular particles. The first is irrelevance of fluctuations induced by temperature. At room temperature, the energy scale k_BT of temperature is insignificant compared to the typical kinetic and potential energies of a granular particle. Second is the dissipative nature of interaction between particles. Granular particles typically interact only on contact, each collision resulting in a loss of kinetic energy. Due to these features, granular systems often behave differently from the conventional states of matter - solids, liquids and gases - and have tempted people to consider it as an additional state of matter.

A simple model that isolates the effects of inelastic collisions is the granular gas. It is a collection of spheres that move ballistically until they undergo momentum conserving inelastic collisions. If the loss of energy due to collisions is offset by external driving, then the system reaches different types of steady states depending on the details of the problem. A vast amount of literature is devoted to the study of such externally driven granular gases [1, 2, 3]. In the absence of external driving, the system evolves deterministically in time and at long times comes to rest. However, the approach to the steady state can be quite non-trivial. In this thesis, we focus on the large time behaviour of the granular gas in the absence of external driving.

The freely evolving granular gas may be further divided into two sub-classes based on the

initial conditions. In the first, the initial conditions are homogeneous and each particle has an energy drawn from some fixed distribution. We refer to this problem as the freely cooling granular gas (FCGG). In the second, almost all particles are at rest, and a few particles in a localized volume possess non-zero initial kinetic energy. We refer to this problem as the granular explosion problem. We study these two problems using large scale molecular dynamics simulations and scaling analysis. The motivation for studying these problems and the results that we obtain for them are given in detail below.

Freely Cooling Granular Gas (FCGG)

FCGG in three dimensions

FCGG is a well studied model of granular physics. In addition to being a model that isolates the effects of dissipation, it has applications in varied physical phenomena including modelling of granular materials [3], geophysical flows [4], large-scale structure formation in the universe [5] and shock propagation [6, 7]. It is closely connected to the well studied Burgers equation [8], and is an example of ordering system showing nontrivial coarsening behaviour [9].

During the initial stage of evolution of FCGG, the particles remain homogeneously distributed. This homogeneous regime is well understood, based on kinetic theory and numerical simulations [10]. In this homogeneous regime, the kinetic energy $T(t)$ decreases with time t as a power-law $T(t) \sim t^{-2}$ (Haff's law) [11], in all dimensions. At later times, this regime is destabilized by long wavelength fluctuations into an inhomogeneous cooling regime dominated by clustering of particles [12]. In this latter regime, $T(t)$ no longer obeys Haff's law but decreases as a power-law $t^{-\theta_T}$, where $\theta_T \neq 2$ depends only on dimensionality D. Extensive simulations in one [13] and two [14] dimensions show that for large times and for any value of coefficient of normal restitution $r < 1$, FCGG is akin to a sticky gas ($r \to 0$), such that colliding particles stick and form aggregates.

If it is assumed that the aggregates are compact spherical objects, then the sticky limit

corresponds to the well studied ballistic aggregation model (BA). A mean field scaling analysis of BA predicts $\theta_T^{mf} = 2D/(D+2)$ and the presence of a growing length scale $\mathcal{L}_t \sim t^{1/z_{BA}^{mf}}$ with $z_{BA}^{mf} = (D+2)/2$ [15]. The sticky limit is also conjectured to be describable by a Burgers-like equation [13, 14]. This mapping predicts $\theta_T^{BE} = 2/3$ when $D = 1$ and $\theta_T^{BE} = D/2$ when $2 \leq D \leq 4$ [5, 13, 14]. The exponents θ_T^{mf} and θ_T^{BE} coincide with each other in one and two dimensions and also with numerical estimates of θ_T for the FCGG in these dimensions [13, 14]. In three dimensions, they differ with $\theta_T^{mf} = 6/5$ and $\theta_T^{BE} = 3/2$. Thus, it is an open question as to which of the theories, if either, is correct.

To resolve this issue, we study FCGG in three dimensions using large scale event-driven molecular dynamics simulation. There are strong finite size corrections in three dimensions. The energy decay deviates from the power law $t^{-\theta_T}$ in the inhomogeneous regime, for times larger than a crossover time that increases with system size L (L is the linear length of three dimensional simulation volume). We do a finite size scaling,

$$T(t) \simeq L^{-z\theta_T} f\left(\frac{t}{L^z}\right), t, L \to \infty, \tag{1}$$

where z is the dynamical exponent, and the scaling function $f(x) \sim x^{-\theta_T}$ for $x = tL^{-z} \ll 1$. As shown in Fig. 1, the simulation data for different L collapse onto a single curve when $T(t)$ and t are scaled as in Eq. (1) with $\theta_T = \theta_T^{mf} = 6/5$ and $z = z_{BA}^{mf} = 5/2$. The power law $x^{-6/5}$, extending over nearly five decades confirms that the value of decay exponent is $\theta_T = 6/5$, numerically indistinguishable from the mean-field BA. Thus, it conclusively rules out Burgers equation description of FCGG. In Fig. 1, we see that $f(x) \sim x^{-\eta}$ for $x \gg 1$ with $\eta \approx 1.83$, such that at large times $t \gg L^z$, $T(t) \sim L^{1.58} t^{1-.83}$. The decay exponent $\theta_T = 6/5$ is shown to be universal, independent of system parameters.

We also study BA in three dimensions using direct numerical simulation. In these simulations, two colliding particles are replaced with a single spherical particle. The mass, velocity and radius of this new particle is given by mass, linear momentum and volume conservation. We find that θ_T^{BA} (measured in simulations) depends on the density, its value

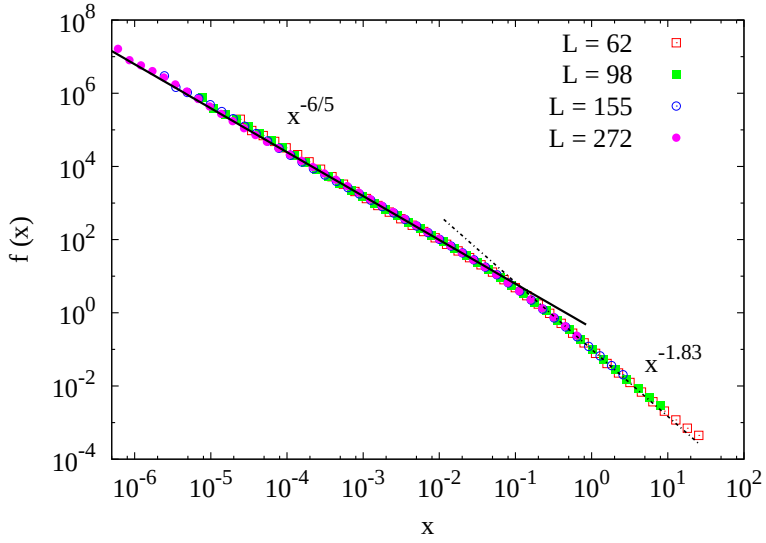

Figure 1: The data for kinetic energy $T(t)$ for different system sizes L collapse onto a single curve when $T(t)$ and t are scaled according to Eq. (1) with $\theta_T = \theta_T^{mf} = 6/5$ and $z = z_{BA}^{mf} = 5/2$. The power law fits are shown by straight lines.

higher than the mean-field value for dilute systems and converging to the mean field prediction of $\theta_T^{mf} = 6/5$ only for high initial density of system.

The energy decay in granular gas and BA at higher densities is similar. To test how far this similarity goes, we compare other statistical properties. First, we compare the cluster size distribution $N(m,t)$, where m is size of a cluster. For the FCGG, $N(m,t)$ consists of two parts: a power law ($\sim m^{-2.7}$) and a peak at large cluster sizes. The power law describes all clusters other than the largest cluster that accounts for the peak. The largest cluster contains a big fraction, nearly $75-80\%$ of the particles. For BA, this distribution is very different, a power law for small cluster sizes ($\sim m^{-0.2}$) and exponential for cluster sizes larger than the mean cluster size. These findings are strikingly different from the predictions for cluster size distribution obtained from the Smoluchowski equation for BA. Second, we compare the velocity distribution $P(v,t)$, where v is any velocity component. $P(v,t)$ has the scaling form $P(v,t) = v_{rms}^{-1}\Phi(v/v_{rms})$, where v_{rms} is the time dependent root mean square velocity. For the FCGG, $\Phi(y)$ is non-Gaussian, and its tail (large y behaviour) is described by $-\ln[\Phi(y)] \sim y^{5/3}$. In sharp contrast to FCGG, for BA, the tail is described by $-\ln[\Phi(y)] \sim y^{0.7}$.

The cluster size and velocity distribution of FCGG and BA are strikingly different from each other, suggesting that the matching of the decay exponent θ_T is a coincidence. Thus, with our simulation of FCGG in three dimensions, we conclude that FCGG fits to neither the ballistic aggregation or a Burgers equation description.

Rough granular gas

Most studies of FCGG consider dissipation only in the normal direction of collision. This is accounted for by the coefficient of normal restitution r. Such particles are called smooth particles and FCGG of such particles is called smooth granular gas (SGG). However, experiments have shown that a correct modelling of collision requires consideration of dissipation in tangential direction of collision, which is done by introducing coefficient of tangential restitution β. Such particles are called rough particles and the corresponding FCGG is called rough granular gas (RGG). Due to change in tangential component of velocities on collision, particles have active rotational degrees of freedom. Kinetic theory studies and numerical simulations of RGG have found that in the homogeneous regime, the translational kinetic energy $T(t)$ and the rotational kinetic energy $K(t)$ both decay as t^{-2}, similar to the Haff's law for SGG [16]. The clustered inhomogeneous regime of the RGG is poorly understood.

Here we study the inhomogeneous regime of RGG in two dimensions using event driven molecular dynamics simulations. We found that in the inhomogeneous regime, $T(t)$ decreases as $T(t) \sim t^{-\theta_T}$, with $\theta_T \approx 1$ independent of r and β. This decay behaviour is similar to SGG in inhomogeneous regime. The rotational energy $K(t)$ decreases with different exponent given by $K(t) \sim t^{-\theta_K}$, with decay exponent $\theta_K \approx 1.6$ again being independent of r and β.

We also study the corresponding ballistic aggregation model. We extend the mean-field scaling analysis of this model to predict $\theta_T^{mf} = \theta_K^{mf} = 1$ in two dimensions. Decay exponents obtained in direct numerical simulation for dense systems are in very good agreement with the scaling analysis predictions. This value of $\theta_K^{mf} = 1$ for ballistic aggregation

is clearly in contradiction with $\theta_K \approx 1.6$ of RGG, concluding that the large time behaviour of RGG is different from ballistic aggregation.

Granular Explosion

FCGG is considered to be one of the simplest model to study granular systems. Even with all its simplicity, its theoretical understanding is challenging. Analytical solution is possible only for a limiting case in one dimension [8]. The experimental study of this system is restricted because of friction and boundary effects. Thus, it is imperative to study simplified versions of FCGG that are tractable analytically and also easier to implement in experiments.

The granular explosion model is analytically more tractable than FCGG [7]. This model is a special case of FCGG, where initially all particles are at rest except few localized ones. The localized energetic particles move and collide with other stationary particles setting them in motion and thus leading to a cascade of collision. It results in the clustering of all moving particles into a spherical-shell, that propagates radially outwards in time, as shown in Fig. 2. The shell formation conserves the radial momentum of the system. Using the radial momentum conservation and simple scaling arguments, it was shown that in D-dimensions radius of disturbance $R(t)$ grows with time t as $R(t) \sim t^{1/(D+1)}$, and the energy of the shell decreases as $E(t) \sim t^{-D/(D+1)}$ [7]. Results from the numerical simulation of hard spheres system were shown to be in very good agreement with these predictions [7].

In simulation of granular explosion model [7], inelasticity of collisions was accounted by simplified model of constant coefficient of restitution r. However, for real systems, r depends strongly on relative velocity v_{rel} of collision. In particular, for realistic visco-elastic model of granular particles, $1 - r \propto v_{rel}^{1/5}$ for $v_{rel} \to 0$ [17]. It is not clear whether the shell structure will form for such realistic velocity dependent r. Thus, we study the granular explosion model with visco-elastic particles using conventional molecular dynamics simulation. We observed that the formation of shell and the scaling results for radius of disturbance and kinetic energy of shell continue to hold for this visco-elastic system. This

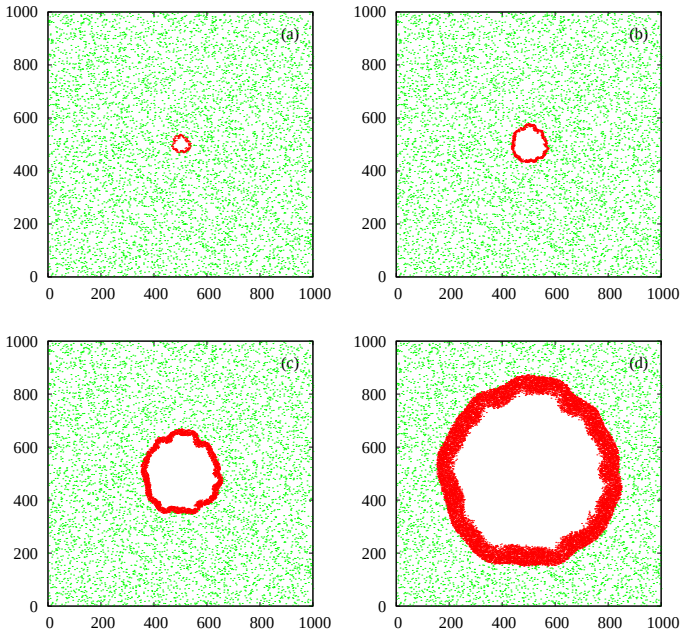

Figure 2: Moving (red) and stationary (green) particles for two dimensional granular explosion following an initial impulse at (500, 500). Panels (a)–(d) correspond to increasing time. The moving particles cluster together to form a shell.

shows that the formation of shell by clustering is independent of details of the dissipation, as long as some dissipation exists.

We apply the above results to a recent experiment on flowing granular material [6]. In this experiment, a dilute monolayer of glass beads flowing down on an inclined plane was perturbed by dropping a steel ball. The impact leads to clustering of particles into a shell, leaving the region inside devoid of glass beads. This shell grows with time and its radius was measured in the experiment using high speed cameras. A theoretical model was proposed and analysed to derive an equation obeyed by the radius. The experimental data was shown to be described very well by the numerical solution of the equation [6].

We note that the granular explosion model discussed above closely resembles the experimental system when one transforms to the center of mass coordinates, and in the limit of large impact energy, when the fluctuations of the particle velocities about the mean flow may be ignored. We show that the earlier theory [6] for the experiment predicts that the radius of disturbance grows logarithmically with time at large times. By a general argu-

ment for hard spheres, we show that the radius can not grow slower than $t^{1/3}$, showing that the theory cannot be right. We then show that the result for radius of disturbance predicted by the radial momentum conservation, $R(t) \sim t^{1/3}$ (in $D = 2$), fits very well to the experimental data except at large times. At long times, the experimental data deviate from the $t^{1/3}$ behaviour, and grows with a different power law $\sim t^{0.18}$. This deviation could be because of two approximations made when equating the granular explosion model with the experiment.

First, we ignored the fluctuations of the velocities of the particles about the mean flow. At earlier times, this approximation is reasonable, as the impact is intense and the typical speeds of displaced particles are much faster than typical velocity fluctuations. However, the fluctuations become relevant at larger times. We modify the granular explosion model to account for these velocity fluctuations. To incorporate these velocity fluctuations, we modify the explosion model by assigning non-zero velocities to the particles that were otherwise at rest in the explosion model. However, the typical velocities of these particles is much smaller than the localised energetic particles. The simulation of this modified model shows that when the velocity of the shell becomes of the order of velocity fluctuations, the sharp shell starts becoming more diffuse and the enclosed empty region disappears. This feature is very similar to as observed in the experiment. With the destabilization of the shell, $R(t)$ deviates from the $t^{1/3}$ power law growth. However, this deviation does not capture the long time behaviour of the radius, $R(t) \sim t^{0.18}$ as observed in the experiment.

Second, we ignored the experimentally observed three dimensional nature of the shell at later times. The shell presumably becomes three dimensional because a fast particle when hemmed in by many surrounding particles may jump out of the plane due to a collision with the floor and friction. This possibility results in radial momentum not being conserved and hence a deviation from $t^{1/3}$ behavior. To incorporate this effect, we modified the granular explosion model in the following way. The two dimensional space

is divided into squares of length equal to the diameter of the particles. Given the grid position of a particle, any particle that is in one of the eight neighbouring squares will be called its neighbour. We remove a particle if it satisfies two criteria, (a) if it has eight or more neighbors, and (b) if its velocity $\vec{v}$ satisfies the hopping criteria $(\vec{v} - \vec{v}_{cm}) \cdot \hat{\vec{v}}_{cm} > \kappa v_{cm}$, where $\vec{v}_{cm}$ is the center of mass velocity of the particle and its neighbours and κ is a constant factor. Our numerical data, obtained from the simulation of this modified model, find that at long times the system crosses over to a different power law growth approximately equal to $t^{0.18}$ provided $\kappa < 0.20$. This is very similar to the growth law seen in the experiment.

List of Figures

List of Tables

Chapter 1

Introduction

In this chapter, we briefly introduce granular systems and in particular freely cooling granular gas, that is the subject matter of this thesis. The organization of the chapters of the thesis is also presented.

1.1 Nonequilibrium Systems

Equilibrium thermodynamics provided much of the conceptual underpinnings for the industrial revolution which had a great impact on the mankind progress during the 19th century. Further conceptual progresses were made with the advent of equilibrium statistical mechanics. However, many systems are inherently not in thermal equilibrium. This class of out-of-equilibrium systems is very large and very diverse, and their study is therefore of great importance. The tools developed to study equilibrium phenomena have been extended to the study of systems that are near to equilibrium.

Natural systems like granular and turbulent flows, living organisms, nanomaterials, and biomolecules are very far from equilibrium. These systems can not be simply studied with our current understanding of equilibrium and near-equilibrium phenomena. Intense

research in past two decades have enabled us with a substantial understanding of far from equilibrium systems. Prototypical models encoding the general features of far from equilibrium have been studied in detail. Examples include active matter, molecular motors and ratchets, turbulence and wave turbulence, random heterogeneous media and granular systems, which is the subject of study of this thesis. Such models have enriched the theoretical understanding of far from equilibrium phenomena with concepts such as fluctuation theorems, non-equilibrium phase transitions, dynamic heterogeneity, fluctuation-induced phenomena, and energy cascades, among others. But, as yet, a comprehensive theory of non-equilibrium statistical mechanics is lacking. This is partly because of sheer diversity of the phenomena involved.

1.2 Granular Systems

Granular systems are omnipresent in nature and are examples of systems far from equilibrium. In our daily lives we come across these systems in the form of food grains, mustard seeds, coffee beans, steel balls, and sand. At larger length scale, we see them in the form of rocks, boulders etc. These systems are present at the astrophysical level with examples such as planetary rings and cosmic dust.

The study of granular physics has practical applications in chemical, pharmaceutical and food industries. These industries deal with transportation and storage of granular materials. There are estimates that we waste 40% of the capacity of our industrial plants because of problems related to transportation of these materials. Improved understanding of granular materials could have significant impact on industry. In addition to practical use, these systems find application in clarifying theoretical concepts of non-equilibrium statistical mechanics.

There are two important aspects that contribute to the unique properties of granular materials. First, granular particles are macroscopic with sizes large enough that Brownian

motion is irrelevant. In other words, fluctuations induced by temperature are irrelevant. At room temperature, the energy scale k_BT of temperature is insignificant compared to the typical kinetic and potential energies of a granular particle. As temperature is irrelevant, system can not explore the whole phase space and exhibits multiple metastable steady states which are far from equilibrium. Each metastable configuration will last indefinitely unless perturbed by external disturbances.

Second is the dissipative nature of interaction between particles. Granular particles typically do not interact through long-range forces, but only when in mechanical contact. Each collision results in a loss of kinetic energy. To explain where the dissipated energy goes, the bulk of particle material is considered as a regular lattice composed of mass points linked by elastic springs. Any collision of a particle leads to deformation of few springs near the surface of particle. These deformed springs takes the dissipated energy and distribute it to all springs. Thus, the energy lost in collision is converted into the internal energy stored in the springs [10]. These aspects make granular systems behave quite differently from conventional solids, liquids and gases [1], and have tempted researchers to consider it as an additional state of matter in it own right.

Traditionally for more than two centuries, scientific studies of granular systems have been the domain of applied engineering research with contributions from notable names such as Coulomb [20], Faraday [21], and Reynolds [22]. For the past two decades, a vast amount of experimental, numerical and theoretical research is devoted within physics to understand the complex static and dynamic behaviour of granular systems [1, 2, 3, 4, 23, 24, 25, 26]. Notable works include, slow relaxation in vibrated sand piles [27, 28, 29, 30], fluid like behaviour similar to those of conventional liquids [31, 32, 33, 34, 35], heterogeneous force chains in granular pile [36, 37, 38], kinetic theory models for granular flows [11, 39, 40, 41], vibration induced convection and heaping [21, 42, 43, 44, 45], vibration induced size separation [46, 47, 48, 49], clustering in granular gases [12, 50, 51, 52].

1.3 Granular Gas

A dilute assembly of granular particles is referred as granular gas. This is a simple model to study the effects of inelastic collisions. In this model, particles move ballistically until they undergo momentum conserving inelastic collisions. Although most of the granular gases in laboratories are man made, there are naturally occurring granular gases such as interstellar dust and planetary rings in outer space.

In the absence of energy input from external sources, these particles dissipate kinetic energy and come to rest. External driving is required to keep the system active. If the loss of energy due to collisions is balanced by external driving, then the system reaches different types of non-equilibrium steady states depending on the details of the problem. A vast amount of research is devoted to the study of such externally driven granular gases [1, 2, 3]. Various driving mechanisms such as gravity [53, 54], vertical [55, 56] and horizontal vibration [57, 58], rotating drums [59, 60], flows of interstitial fluids such as water and air [61, 62], electric and magnetic fields [63, 64] have been implemented [3].

In the absence of external driving, the system evolves deterministically in time, and at large times loses all its energy to come to rest. However, the approach to the steady state can be quite non-trivial. This freely evolving granular gas may be further divided into two sub-classes based on the initial energies of the particles:

- **Freely cooling granular gas (FCGG):** In the first, the particles are homogeneously distributed in space and each particle has an energy drawn from some fixed distribution. We refer to this problem as the freely cooling granular gas (FCGG). FCGG is a well studied model of granular physics. In addition to being a model that isolates the effects of dissipation, it has applications in varied physical phenomena including modelling of dynamics of granular systems [1, 3, 10, 65, 66], geophysical flows [4], large-scale structure formation in the universe [5], and shock propagation [6, 7, 67]. It also belongs to the general class of non-equilibrium systems with limiting cases

being amenable to exact analysis [8, 68], and is an example of an ordering system showing non-trivial coarsening behaviour [9, 69, 70, 71]. The dynamics of this system has close connection with the shock dynamics of the well studied Burgers equation [8, 72, 73, 74, 75].

- **Granular explosion:** In the second, the particles are homogeneously distributed as in FCGG. However, almost all particles are at rest, and a few particles in a localized volume possess non-zero initial kinetic energy. We refer to this model as the granular explosion model. Granular explosion model is a special case of FCGG and its study is motivated from the fact that it has certain advantages over FCGG. The experimental study of FCGG is restricted because of friction and boundary effects. These restrictions can be eliminated in experiments of granular explosion [6]. Also, it is analytically more tractable than FCGG [7].

In this thesis, we study these two problems of freely evolving granular gas using large scale molecular dynamics simulations and scaling analysis. Our particular focus is on the large time behaviour of these systems.

1.4 Organization of the Chapters

The rest of the thesis is organized as follows.

In **Chapter 2**, we review earlier results on FCGG in detail.

In **Chapter 3**, the simulation methods used in this thesis are discussed. We have used two fundamentally different approaches to molecular dynamics simulations. One is conventional force based molecular dynamics for soft-particles, where the Newton's equations of motion for all particles are numerically integrated. In this method, the knowledge of the interaction force is essential. The other is event-driven molecular dynamics for hard-core particles which move freely and interact only on collision. At any stage of evolution, the

next collision occurring in the system is determined, and the position and velocity of two particles involved in the binary collision is updated. This simulation method proceeds through the event of one collision to the next collision, and is much efficient as compared to conventional force based molecular dynamics.

The remaining chapters contain the original work of the thesis.

In **Chapter 4**, we study FCGG in three dimensions. The kinetic energy of FCGG decreases as a power law $t^{-\theta_T}$ at large times t. Two theoretical conjectures exist for the exponent θ_T. One based on mean-field analysis of ballistic aggregation of compact spherical aggregates predicts $\theta_T^{mf} = 2D/(D+2)$ in D dimensions. The other based on Burgers equation describing anisotropic, extended clusters predicts $\theta_T^{BE} = D/2$ when $2 \leq D \leq 4$. We do extensive simulations in three dimensions to find that while θ_T is as predicted by ballistic aggregation, the cluster statistics and velocity distribution differ from it. Thus, the FCGG fits to neither the ballistic aggregation or a Burgers equation description.

In **Chapter 5**, we study large time behaviour of the FCGG of rough particles in two dimensions using large-scale event driven simulations and scaling arguments. During collisions, rough particles dissipate energy in both the normal and tangential directions of collision. At large times, when the system is spatially inhomogeneous, translational kinetic energy and the rotational energy decay with time t as power-laws $t^{-\theta_T}$ and $t^{-\theta_K}$. We numerically determine $\theta_T \approx 1$ and $\theta_K \approx 1.6$, independent of the coefficients of restitution. The inhomogeneous regime of the granular gas has been argued to be describable by the ballistic aggregation model, where particles coalesce on contact. Using scaling arguments, we predict $\theta_T = 1$ and $\theta_K = 1$ for ballistic aggregation. Simulations of ballistic aggregation with rotational degrees of freedom are consistent with these exponents. While θ_T for rough granular gas matches with the corresponding exponent of ballistic aggregation, the exponent θ_K is different. It concludes that the large time behaviour of rough granular gas is different from ballistic aggregation.

In **Chapter 6**, we apply the results of granular explosion to a recent experiment [6] on

flowing granular material. The granular explosion model was studied in [7]. The disturbance created by the initially localized energetic particles leads to formation of spherical-shell of moving particles, whose radius grows with time as $R(t) \sim t^{1/(D+1)}$. In the experiment [6], a dilute monolayer of glass beads flowing down on an inclined plane was perturbed by dropping a steel ball. The impact leads to clustering of particles into a shell, leaving the region inside devoid of glass beads. Noting the resemblance between the experiment and granular explosion, we show that growth of radius predicted in granular explosion $R(t) \sim t^{1/3}$ for $D = 2$ fits very well to the experimental data except at large times. At long times, the experimental data exhibit a crossover to a different power law behaviour, growing as $\sim t^{0.18}$. We attribute this crossover to the problem becoming effectively three dimensional due to accumulation of particles at the shell front. We modify the granular explosion model to incorporate this effect. The simulations of this modified model captures the crossover seen in the experiment.

In **Chapter 7**, we study the granular explosion model with visco-elastic particles using conventional molecular dynamics simulation. In simulations of granular explosion studied in [7], a simplified constant coefficient of restitution r is used to describe collisions. However, for realistic visco-elastic model of granular particles, r is not a constant but depends strongly on relative velocity of collision. We observed that the formation of shell and the scaling result for radius of disturbance continue to hold for the visco-elastic system.

Finally, in **Chapter 8**, we present the principal conclusions that emerge from the work in this thesis, as well as some potential extensions.

Chapter 2

Freely Cooling Granular Gas: A Review

2.1 Introduction

In this chapter we review earlier results for the freely cooling granular gas. In Sec. 2.2, we define the model precisely. During the initial stage of evolution, the system remains homogeneous. This homogeneity allows the development of a Boltzmann type equation for the granular gas, similar to molecular gases. The Boltzmann equation derivation and its solution to obtain the velocity distribution function and dependence of energy on time is reviewed in Sec. 2.3. Due to dissipation, the homogeneous regime is unstable and the system evolves to inhomogeneous regime marked by presence of clusters. This regime is mostly studied in simulations, which we have summarized in Sec. 2.4. In Sec. 2.5, we review a detail study of the homogeneous cooling regime of freely cooling granular gas of rough particles, where dissipation due to frictional interaction is taken into account. The experimental studies of freely cooling granular gas are reviewed in Sec. 2.6. In Sec. 2.7, we review the *ballistic aggregation* model (BA). This model is analytically tractable and is argued to be a description for granular gas in the inhomogeneous regime. The inhomogeneous regime is also argued to be describable by Burgers like equation which we discuss in Sec. 2.8.

2.2 Model

We consider a simple model for a granular particle, a sphere. Consider a collection of N identical particles of mass m and diameter d, distributed homogeneously in D dimensional space with linear length L. The velocities of the particles are initially chosen from a fixed distribution, usually Gaussian or uniform. The system evolves freely, i.e., there is no external driving. The particles move ballistically until they undergo momentum conserving, inelastic collision with other particles. Since collisions are dissipative, the kinetic energy of the system decreases. This freely evolving system is known as the *freely cooling granular gas* (FCGG). In this thesis, we have considered FCGG of three kinds of constituent particles as described below:

2.2.1 Rough Granular Gas (RGG)

The constituents of RGG are particles that dissipate energy in both normal and tangential direction of collision. Consider the collision between two particles i and j. The quantities $\vec{r}_i$, $\vec{v}_i$, $\vec{\omega}_i$ denote the position of the centre, velocity and angular velocity of particle i. The relative velocity of the point of contact, $\vec{g}$ is

$$\vec{g} = (\vec{v}_i - \vec{\omega}_i \times \frac{d}{2}\vec{e}) - (\vec{v}_j + \vec{\omega}_j \times \frac{d}{2}\vec{e}), \tag{2.1}$$

where $\vec{e}$ is unit vector in normal direction of collision, pointing from the centre of particle j to the centre of particle i,

$$\vec{e} = \frac{\vec{r}_i - \vec{r}_j}{|\vec{r}_i - \vec{r}_j|}. \tag{2.2}$$

We denote the normal and tangential components of $\vec{g}$ by $\vec{g}^n$ and $\vec{g}^t$ respectively. The dissipation in normal and tangential directions are quantified by a coefficient of normal restitution r and a coefficient of tangential restitution β, defined through the constitutive

equations [76]:

$$(\vec{g}^{\,n})' = -r\vec{g}^{\,n} \qquad (0 \le r \le 1), \tag{2.3}$$

$$(\vec{g}^{\,t})' = -\beta\vec{g}^{\,t} \qquad (-1 \le \beta \le 1), \tag{2.4}$$

where the primed quantities are the values post-collision. The post-collision velocities may be obtained from linear and angular momentum conservation, combined with the constitutive equations for dissipation, Eqs. (2.3) and (2.4):

$$\begin{aligned}
\vec{v}_i' &= \vec{v}_i - \frac{1+r}{2}\vec{g}^{\,n} - \frac{q(1+\beta)}{2q+2}\vec{g}^{\,t}, \\
\vec{v}_j' &= \vec{v}_j + \frac{1+r}{2}\vec{g}^{\,n} + \frac{q(1+\beta)}{2q+2}\vec{g}^{\,t}, \\
\vec{\omega}_i' &= \vec{\omega}_i + \frac{1+\beta}{d(q+1)}[\vec{e}\times\vec{g}^{\,t}], \\
\vec{\omega}_j' &= \vec{\omega}_j + \frac{1+\beta}{d(q+1)}[\vec{e}\times\vec{g}^{\,t}],
\end{aligned} \tag{2.5}$$

where q is the reduced moment of inertia, $q = I/(md^2/4)$ with I being the moment of inertia. For homogeneous disk $q = 1/2$, and for homogeneous sphere $q = 2/5$. This set of equations [Eq. (2.5)], is commonly known as *collision law*. For simplicity, most of the studies do not consider the velocity dependence of r and β, and treat them as constants.

2.2.2 Smooth Granular Gas (SGG)

The constituents of SGG are particles that dissipate energy only in the normal direction of collision while tangential component of relative velocity remains unchanged. For smooth particles $\beta = -1$, and the above collision law [Eq. (2.5)] reduces to

$$\begin{aligned}
\vec{v}_i' &= \vec{v}_i - \frac{1+r}{2}[(\vec{v}_i - \vec{v}_j)\cdot\vec{e}\,]\,\vec{e}\,, \\
\vec{v}_j' &= \vec{v}_j + \frac{1+r}{2}[(\vec{v}_i - \vec{v}_j)\cdot\vec{e}\,]\,\vec{e}\,.
\end{aligned} \tag{2.6}$$

We have omitted the angular velocity terms as they do not change on collision. This is one of the most widely studied model in the context of freely cooling granular gases.

2.2.3 Visco-Elastic Granular Gas

The interaction between granular particles need not be hard-core (as discussed above) and is more generally modelled by soft-repulsive potential [50, 76]. Here, we discuss *viscoelastic* interaction model [77]. This particular model quite successfully explained the results of an experiment with ice balls [78], which are of importance for the investigation of the dynamics of planetary rings [79].

The interaction force for elastic spheres was derived by Heinrich Hertz [80],

$$F_{\rm el} = \frac{2Y\sqrt{d^{\rm eff}/2}}{3(1-\nu^2)}\xi^{3/2} \equiv \rho\xi^{3/2}, \tag{2.7}$$

where ξ is the compression between colliding spheres. Y and ν are Young modulus and Poisson ratio of the particle material respectively, and ρ is introduced as a short-hand notation for the elastic constant of material. The effective diameter of identical colliding spheres $d^{\rm eff} = d/2$. This interaction law was later extended to the collision of viscoelastic particles [77],

$$F = \rho\xi^{3/2} + \frac{3}{2}A\rho\sqrt{\xi}\dot{\xi}, \tag{2.8}$$

where $\dot{\xi}$ is the compression velocity and the dissipative parameter A is

$$A = \frac{1}{3}\frac{(3\eta_2-\eta_1)^2}{(3\eta_2+2\eta_1)}\frac{(1-\nu^2)(1-2\nu)}{Y\nu^2}. \tag{2.9}$$

The viscous constants η_1, η_2 relate the dissipative stress tensor to the deformation rate tensor. Equation (2.8) is derived with a quasistatic approximation which is valid when the characteristic relative velocity of collision is much less than the speed of sound in the material. This criteria is satisfied for many experimental situations. We mention

that Eq. (2.8) holds if viscoelasticity is the only dissipative process during the particle collision.

The solution of collision process described by

$$\frac{d^2\xi}{dt^2} = \frac{F}{m^{\text{eff}}}, \tag{2.10}$$

where m^{eff} is effective mass and t is time, with initial conditions (assuming that the contact of colliding particles starts at time $t = 0$)

$$\xi(t = 0) = 0 \quad \text{and} \quad \dot{\xi}(t = 0) = g^n, \tag{2.11}$$

gives the coefficient of normal restitution,

$$r = \dot{\xi}(t_{\text{cont}})/\dot{\xi}(0), \tag{2.12}$$

where t_{cont} is the contact duration of colliding particles. These calculations were performed in [81], to obtain r as a series in powers of $(g^n)^{1/5}$,

$$r = 1 - C_1\left(\frac{3}{2}A\right)\left(\frac{\rho}{m^{\text{eff}}}\right)^{2/5}(g^n)^{1/5} + C_2\left(\frac{3}{2}A\right)^2\left(\frac{\rho}{m^{\text{eff}}}\right)^{4/5}(g^n)^{2/5} \pm \ldots, \tag{2.13}$$

where coefficients $C_1 = 1.15344$ and $C_2 = 0.79826$ were obtained analytically and also confirmed by simulations. A general framework has been provided in [81] to evaluate all coefficients of the expansion, but the calculations are quite extensive. A solution similar to Eq. (2.13) has been obtained using dimensional analysis method [17].

System being dissipative, the energy of the system decreases with time. The main quantities of interest are translational kinetic energy $T(t)$ and rotational kinetic energy $K(t)$ defined as

$$T(t) = \frac{2}{D}\left(\frac{1}{N}\sum_{i=1}^{S(t)}\frac{1}{2}m_i\vec{v}_i^{\,2}\right), \tag{2.14}$$

$$K(t) = \frac{2}{2D-3}\left(\frac{1}{N}\sum_{i=1}^{S(t)}\frac{1}{2}I_i\vec{\omega}_i^2\right), \tag{2.15}$$

where m_i and I_i are mass and moment of inertia of particle i. Throughout the thesis, we consider FCGG of identical particles for which $m_i = m$ and $I_i = I$. $S(t)$ is the total number of particles in the system at time t, which for FCGG is $S(t) = N$ at all times. In this thesis, we have also studied ballistic aggregation model (see Sec. 2.7), where particles merge completely on collision to form bigger aggregates. For this system, m_i and I_i are changing with time and total number of particles $S(t)$ decreases with time.

Our discussion of RGG is limited to Sec. 2.5 and Chapter 5. The discussion of visco-elastic granular gas is limited to Chapter 7. Unless otherwise mentioned, everywhere else in the thesis, FCGG refers to hard-sphere SGG with collisions described by constant coefficient of restitution r. For this system, $K(t)$ does not change with time.

2.3 Kinetic Theory

The initial stage of evolution, where the spatial homogeneity of system is preserved is called homogeneous cooling regime (HCR). In this regime, FCGG resembles an ordinary molecular gas of elastic particles, except that $T(t)$ decreases due to inelastic collisions. This regime can be described by Boltzmann equation formalism. The velocity distribution function is given by an expansion around the Maxwell distribution, accounting the deviations from Maxwell distribution by Sonine coefficients.

2.3.1 Haff's Cooling Law

Before we discuss the Boltzmann equation formalism, we show that the temporal decay behaviour of $T(t)$ in HCR can be obtained by simple physical arguments. To this end, we

write a rate equation for $T(t)$ as,

$$\frac{dT}{dt} = \text{collision rate} \times \text{average energy lost in one collision.} \tag{2.16}$$

Now, the typical relative energy lost in one collision is

$$\frac{1}{2}m^{\text{eff}}(v_{12}'^2 - v_{12}^2) = -\frac{1}{2}m^{\text{eff}}v_{12}^2(1-r^2) \propto -(1-r^2)T, \tag{2.17}$$

where v_{12}, v_{12}' are the relative velocity before and after the collision and m^{eff} is the effective mass of colliding particles. In writing Eq. (2.17), we have used the fact that the kinetic energy of relative motion $m^{\text{eff}}v_{12}^2/2$ is on average of the same order as T.

To estimate the average number of collision in unit time, consider a particle moving with average relative velocity v_{12}, while all other particles are fixed scatterers. The volume swept by this particle in unit time $\propto d^{D-1}v_{12}$, giving

$$\text{collision rate} \propto d^{D-1}v_{12}n \propto nd^{D-1}\sqrt{T}, \tag{2.18}$$

where $n = N/L^D$ is the number density. Using Eqs. (2.17) and (2.18), Eq. (2.16) becomes

$$\frac{dT}{dt} \propto -nd^{D-1}(1-r^2)T^{3/2}. \tag{2.19}$$

The solution of Eq. (2.19) for the case r = constant (independent of relative velocity) yields

$$T(t) = \frac{T(0)}{(1+t/t_0)^2} \quad \text{where} \quad t_0^{-1} \propto nd^{D-1}(1-r^2)\sqrt{T(0)}. \tag{2.20}$$

This decay behavior given by Eq. (2.20) is known as Haff's law. For times $t \gg t_0$, $T(t) \sim t^{-2}$. This t^{-2} decay behaviour has been verified in numerical simulations [11, 82] and experiments [83, 84, 85]. We reproduce this decay behaviour with simulations of two dimensional FCGG and is shown in Fig. 2.1.

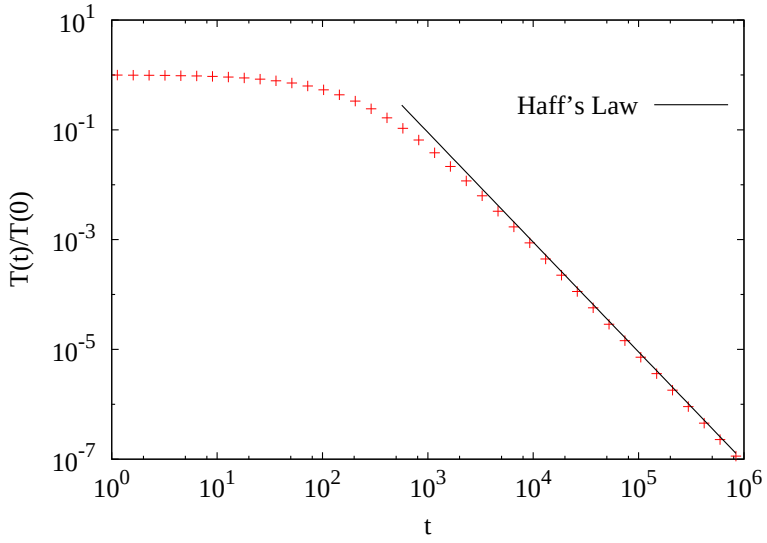

Figure 2.1: The temporal evolution of kinetic energy $T(t)$ for two dimensional freely cooling granular gas. The shown results are with $n = 0.01$ and $r = 0.98$. The solid line is a power law t^{-2}.

2.3.2 Boltzmann Equation

Boltzmann equation is the fundamental theoretical tool of the kinetic theory of gases. This equation governs the time evolution of the velocity distribution function, where it relates the velocity distribution function of the gas particles to the macroscopic properties of particle collisions. The velocity distribution function $f(\vec{r}, \vec{v}, t)$ is defined such that $f(\vec{r}, \vec{v}, t)\, d\vec{r}\, d\vec{v}$ gives the number of particles in the infinitesimal phase-space volume $d\vec{r}\, d\vec{v}$ located at $(\vec{r}, \vec{v})$ at time t. Integrating this function over the full phase-space gives the total number of particles N,

$$\int f(\vec{r}, \vec{v}, t)\, d\vec{r}\, d\vec{v} = N. \tag{2.21}$$

For spatially homogeneous gas the distribution function is independent of $\vec{r}$ and has following properties

$$\int f(\vec{v}, t)\, d\vec{v} = n, \tag{2.22}$$

$$\int \vec{v}\, f(\vec{v}, t)\, d\vec{v} = n \langle \vec{v} \rangle = 0, \tag{2.23}$$

$$\int \frac{1}{2} m v^2 f(\vec{v}, t)\, d\vec{v} = n \left\langle \frac{1}{2} m v^2 \right\rangle = \frac{D}{2} n T(t). \tag{2.24}$$

The above equations relate the moments of f with the macroscopic properties of gas, namely number density n, flow velocity (it is zero as we have assumed isotropic gas with no macroscopic flow) and kinetic energy $T(t)$.

We now outline the derivation of Boltzmann equation for inelastic gases. The number of particles $f(\vec{v}_1, t)\, d\vec{r}_1\, d\vec{v}_1$ in a phase-space volume $d\vec{r}_1\, d\vec{v}_1$ located at $(\vec{r}_1, \vec{v}_1)$ changes over time due to particle collisions. Particles belonging to this velocity interval, after collision will in general move with velocities beyond this interval. Such collisions reduce the number of particles in the considered volume and are called *direct* collisions. On the contrary, *inverse* collisions are collisions in which particles not belonging to this velocity interval (before collision) enter into this interval, increasing the number of particles in the considered phase-space volume.

Consider a direct collision between particles of velocities $\vec{v}_1$ and $\vec{v}_2$. The post-collision velocities are given by

$$\begin{aligned} \vec{v}_1' &= \vec{v}_1 - \frac{1+r}{2}[(\vec{v}_1 - \vec{v}_2)\cdot\vec{e}\,]\,\vec{e}\,, \\ \vec{v}_2' &= \vec{v}_2 + \frac{1+r}{2}[(\vec{v}_1 - \vec{v}_2)\cdot\vec{e}\,]\,\vec{e}\,. \end{aligned} \tag{2.25}$$

To estimate the number of direct collisions ν^- occurring in time Δt, we consider the scattering of particles with velocities $\vec{v}_1$ at particles with velocities $\vec{v}_2$ that yields

$$\nu^-(\vec{v}_1, \vec{v}_2, \vec{e}, \Delta t) = f(\vec{v}_1, t)\, d\vec{v}_1\, d\vec{r}_1 f(\vec{v}_2, t)\, d\vec{v}_2\, d^{D-1}|\vec{v}_{12}\cdot\vec{e}\,|\Delta t\, d\vec{e}. \tag{2.26}$$

Now, we consider an inverse collision between particles of velocities $\vec{v}_1''$ and $\vec{v}_2''$, where the collision leads to post-collision velocities of particles as $\vec{v}_1$ and $\vec{v}_2$,

$$\begin{aligned} \vec{v}_1 &= \vec{v}_1'' - \frac{1+r}{2}[(\vec{v}_1'' - \vec{v}_2'')\cdot\vec{e}\,]\,\vec{e}\,, \\ \vec{v}_2 &= \vec{v}_2'' + \frac{1+r}{2}[(\vec{v}_1'' - \vec{v}_2'')\cdot\vec{e}\,]\,\vec{e}\,. \end{aligned} \tag{2.27}$$

Using $(\vec{v}_1 - \vec{v}_2)\cdot\vec{e} = -r(\vec{v}_1'' - \vec{v}_2'')\cdot\vec{e}$, Eqs. (2.27) can be written as

$$\begin{aligned}\vec{v}_1'' &= \vec{v}_1 - \frac{1+r}{2r}[(\vec{v}_1 - \vec{v}_2)\cdot\vec{e}\,]\,\vec{e}\,,\\ \vec{v}_2'' &= \vec{v}_2 + \frac{1+r}{2r}[(\vec{v}_1 - \vec{v}_2)\cdot\vec{e}\,]\,\vec{e}\,.\end{aligned} \tag{2.28}$$

Considering Eqs. (2.28) as a transformation, $(\vec{v}_1'', \vec{v}_2'') \rightarrow (\vec{v}_1, \vec{v}_2)$, the Jacobian J of the transformation for r = constant, reads $J = 1/r$. Similar to the number of direct collisions, the number of inverse collisions in time Δt is given by

$$\nu^+(\vec{v}_1'', \vec{v}_2'', \vec{e}, \Delta t) = f(\vec{v}_1'', t)\, d\vec{v}_1''\, d\vec{r}_1 f(\vec{v}_2'', t)\, d\vec{v}_2'' d^{D-1}|\vec{v}_{12}'' \cdot \vec{e}\,|\Delta t\, d\vec{e}. \tag{2.29}$$

Using $d\vec{v}_1''\, d\vec{v}_2'' = J d\vec{v}_1 d\vec{v}_2$ in Eq. (2.29) gives

$$\nu^+(\vec{v}_1'', \vec{v}_2'', \vec{e}, \Delta t) = \frac{1}{r^2} f(\vec{v}_1'', t)\, f(\vec{v}_2'', t) d^{D-1}|\vec{v}_{12}\cdot\vec{e}\,|\, d\vec{v}_1\, d\vec{v}_2 d\vec{r}_1 \Delta t\, d\vec{e}. \tag{2.30}$$

With the knowledge of number of direct and inverse collisions for particular values of $\vec{v}_1, \vec{v}_2$ and $\vec{e}$, the total number of collisions which change the number of particles in the considered phase space volume $d\vec{r}_1\, d\vec{v}_1$ can be obtained by integrating over $\vec{v}_2$ and $\vec{e}$. Thus, the increase in the number of particles in the volume $d\vec{r}_1\, d\vec{v}_1$ during the time interval Δt is given by

$$\Delta\,[f(\vec{v}_1, t)]\, d\vec{v}_1 d\vec{r}_1 = \int d\vec{v}_2 d\vec{e}\,\Theta(-\vec{v}_{12}''\cdot\vec{e})\nu^+(\vec{v}_1'', \vec{v}_2'', \vec{e}, \Delta t) - \int d\vec{v}_2 d\vec{e}\,\Theta(-\vec{v}_{12}\cdot\vec{e})\nu^-(\vec{v}_1, \vec{v}_2, \vec{e}, \Delta t), \tag{2.31}$$

where $\Theta(x)$ is the Heaviside step-function

$$\Theta(x) = \begin{cases} 1 & \text{for} \quad x \geq 0, \\ 0 & \text{for} \quad x < 0. \end{cases} \tag{2.32}$$

Only such pairs for which $\vec{v}_{12}\cdot\vec{e} < 0$ for direct collision and $\vec{v}_{12}''\cdot\vec{e} < 0$ for inverse collision lead to an impact. The Θ-function in Eq. (2.31) ensures this condition of col-

lision. To make the two step functions identical, we change the variable $\vec{e} \to -\vec{e}$ in the first integral of Eq. (2.31). This change of variable does not alter the transformation $(\vec{v}_1'', \vec{v}_2'') \to (\vec{v}_1, \vec{v}_2)$, while the Θ-function becomes

$$\Theta(\vec{v}_{12}'' \cdot \vec{e}) = \Theta(-\frac{1}{r}\vec{v}_{12} \cdot \vec{e}) = \Theta(-\vec{v}_{12} \cdot \vec{e}), \tag{2.33}$$

where the property $\Theta(kx) = \Theta(x)$ for any $k > 0$ is used. Now, we divide both sides of Eq. (2.31) by $d\vec{v}_1\, d\vec{r}_1 \Delta t$ and taking the limit $\Delta t \to 0$, we get the Boltzmann equation

$$\frac{\partial}{\partial t} f(\vec{v}_1, t) = d^{D-1} \int d\vec{v}_2 \int d\vec{e}\, \Theta(-\vec{v}_{12}\cdot\vec{e})\, |\vec{v}_{12}\cdot\vec{e}| \left[\frac{1}{r^2} f(\vec{v}_1'', t) f(\vec{v}_2'', t) - f(\vec{v}_1, t) f(\vec{v}_2, t) \right] \equiv I(f, f), \tag{2.34}$$

where $I(f, f)$ is known as collision integral.

In this derivation of Boltzmann equation, we assumed an approximation known as *hypothesis of molecular chaos*. While deriving the rates of direct and inverse collisions, we counted independently the number of scatterers and scattered particles by taking the product of two distributions functions, $f(\vec{v}_1, t)$ and $f(\vec{v}_2, t)$ for direct, and $f(\vec{v}_1'', t)$ and $f(\vec{v}_2'', t)$ for inverse collisions. This holds true only when there are no correlations between particles, otherwise the two-particle distribution function $f_2(\vec{v}_1, \vec{v}_2, \vec{r}_{12}, t)$ for the colliding pairs should be considered. Correlations can be neglected for dilute systems. This approximation of using the product of two one-particle distribution functions is called the *hypothesis of molecular chaos*.

Correlations occur in granular gas because of finite-volume effects, when possible colliders are screened by other particles. To obtain the rates of collisions, the two-particle distribution function $f_2(\vec{v}_1, \vec{v}_2, \vec{r}_{12}, t)$ at the contact distance between the particles $r_{12} = d$ must be known. Enskog suggested an approximation for accounting finite-volume effects:

$$f_2(\vec{v}_1, \vec{v}_2, d, t) \approx g_2(d) f(\vec{v}_1, t) f(\vec{v}_2, t), \tag{2.35}$$

where $g_2(d)$ is the contact value of the equilibrium pair correlation function $g_2(r_{12})$, which is also known as Enskog factor. This function describes the probability that the distance $|\vec{r}_1 - \vec{r}_2|$ between two particles is equal to r_{12}. For a hard-sphere elastic fluid $g_2(d)$ reads [86]

$$g_2(d) = \begin{cases} \frac{1-7\phi/16}{(1-\phi)^2} & \text{for} \quad D = 2, \\ \frac{2-\phi}{2(1-\phi)^3} & \text{for} \quad D = 3, \end{cases} \tag{2.36}$$

where ϕ is the volume fraction. It is shown in simulations that Eq. (2.36) is also very accurate for inelastic hard-spheres [87]. Physically, the factor $g_2(d)$ accounts for the increased collision frequency in dense systems caused by excluded volume effects.

Thus, with this modification [Eq. (2.35)], the Boltzmann equation [Eq. 2.34] becomes Boltzmann-Enskog equation

$$\frac{\partial}{\partial t} f(\vec{v}_1, t) = g_2(d) I(f, f). \tag{2.37}$$

2.3.3 Velocity Distribution and Kinetic Energy

For molecular gases in equilibrium, the velocity distribution is Maxwellian and independent of time t. In granular gases, the energy of the system decreases due to dissipative collisions leading to a time dependent velocity distribution. For near-elastic system ($r \lesssim 1$), the kinetic energy decreases slowly and the system may be considered to be in an equilibrium state at each time instant. With this adiabatic cooling assumption, it has been shown that Eq. (2.37) admits an isotropic scaling solution, where the time dependence of the velocity distribution function is argued to occur through a time dependent average velocity [82, 88],

$$f(\vec{v}, t) = \frac{n}{v_T^D(t)} \tilde{f}\left(\frac{v}{v_T(t)}\right) = \frac{n}{v_T^D(t)} \tilde{f}(c), \tag{2.38}$$

with the scaled velocity $c = v/v_T(t)$. The thermal velocity $v_T(t)$ is defined by

$$T(t) = \frac{1}{2} m v_T^2(t), \tag{2.39}$$

where $T(t)$ is given by second moment of $f(\vec{v}, t)$ as defined in Eq. (2.24).

Substituting the scaled velocity ansatz [Eq. (2.38)] in the Boltzmann-Enskog equation [Eq. (2.37)], and after doing some straightforward algebra [10], one obtains a time-independent equation for the scaled velocity distribution

$$\frac{\mu_2}{D}\left(D + c_1 \frac{\partial}{\partial c_1}\right) \tilde{f}(c_1) = \tilde{I}(\tilde{f}, \tilde{f}), \tag{2.40}$$

and a time-dependent equation for the evolution of kinetic energy

$$\frac{dT}{dt} = -\frac{2\mu_2}{D} \sqrt{\frac{2}{m}} g_2(d) d^{D-1} n T^{3/2}, \tag{2.41}$$

where $\tilde{I}(\tilde{f}, \tilde{f})$ is the dimensionless collision integral,

$$\tilde{I}(\tilde{f}, \tilde{f}) = \int d\vec{c}_2 \int d\vec{e}\, \Theta(-\vec{c}_{12} \cdot \vec{e})\, |\vec{c}_{12} \cdot \vec{e}| \left[\frac{1}{r^2} \tilde{f}(c_1'') \tilde{f}(c_2'') - \tilde{f}(c_1) \tilde{f}(c_2)\right]. \tag{2.42}$$

It is related to $I(f, f)$ as $I(f, f) = n^2 d^{D-1} v_T^{1-D}\, \tilde{I}(\tilde{f}, \tilde{f})$. μ_p is the moment of dimensionless collision integral given by

$$\mu_p \equiv -\int d\vec{c}_1 c_1^p\, \tilde{I}(\tilde{f}, \tilde{f}). \tag{2.43}$$

These moments μ_p do not depend on time as $\tilde{I}(\tilde{f}, \tilde{f})$ is time-independent.

Thus, the Boltzmann equation reduces to a set of two uncoupled equations, one describing the scaled velocity distribution and the other the kinetic energy. The solution of Eq. (2.40) is a complicated mathematical problem and analytical progress can be made only by making approximations. The adiabatic cooling assumption suggests that the velocity distribution is close to Maxwell distribution. Thus, we expand $\tilde{f}(c)$ around the Maxwell dis-

tribution $\phi(c)$ [88, 89], in terms of Sonine polynomials $\{S_p(x)\}$ [see [10] for details about Sonine polynomials],

$$\tilde{f}(c) = \phi(c)\left[1 + \sum_{p=1}^{\infty} a_p S_p(c^2)\right], \tag{2.44}$$

where

$$\phi(c) \equiv \pi^{-D/2} \exp(-c^2). \tag{2.45}$$

The Sonine polynomials expansion is applied to solve the Boltzmann equation [10], i.e., to obtain the Sonine coefficients a_p characterizing the velocity distribution. It can be shown from the definitions of kinetic energy and thermal velocity that the first Sonine coefficient $a_1 = 0$. Neglecting higher Sonine coefficients ($a_p = 0$ for $p > 2$) and characterizing the velocity distribution by the next Sonine coefficient a_2 only, the second coefficient a_2 is obtained to be

$$a_2 = \frac{16\,(1-r)\,(1-2r^2)}{9 + 24D + 8rD - 41r + 30(1-r)\,r^2}. \tag{2.46}$$

This second Sonine coefficient a_2 as a function of r for $D = 2$ and $D = 3$ is plotted in Fig. 2.2. The small value of a_2 has been used to justify the solution of Boltzmann equation by an expansion around the Maxwell distribution. The small value of a_2 also justifies the exclusion of higher Sonine coefficients a_p for $p > 2$. This result for a_2 has been quantitatively confirmed by the Direct Simulation Monte Carlo (DSMC) of the Boltzmann equation [18] as shown in Fig. 2.3 for $D = 3$.

The temporal behaviour of kinetic energy can be easily obtained by integrating Eq. (2.41) yielding

$$T(t) = \frac{T(0)}{(1 + Ct)^2}, \quad \text{with} \quad C = \frac{\mu_2}{D}\sqrt{\frac{2}{m}}\, g_2(d) d^{D-1} n \sqrt{T(0)}. \tag{2.47}$$

This is same as what we obtained using simple physical arguments in Eq. (2.20).

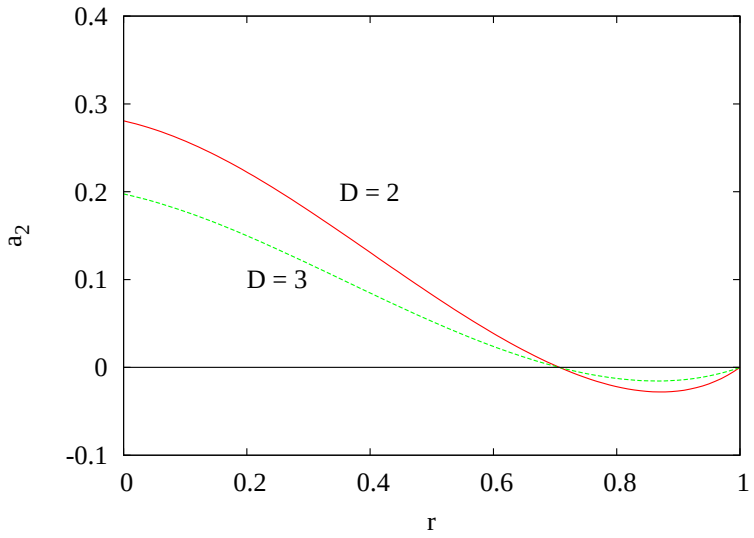

Figure 2.2: Sonine coefficient a_2 vs the coefficient of normal restitution r in two ($D = 2$) and three ($D = 3$) dimensions.

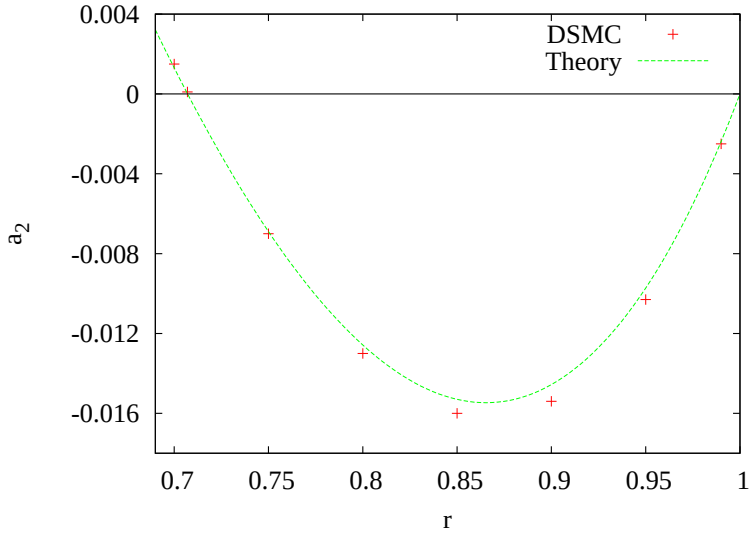

Figure 2.3: Sonine coefficient a_2 vs the coefficient of normal restitution r in $D = 3$. The points show the result of DSMC simulation (data taken from [18])). The line is a plot of theoretical result, Eq. (2.46).

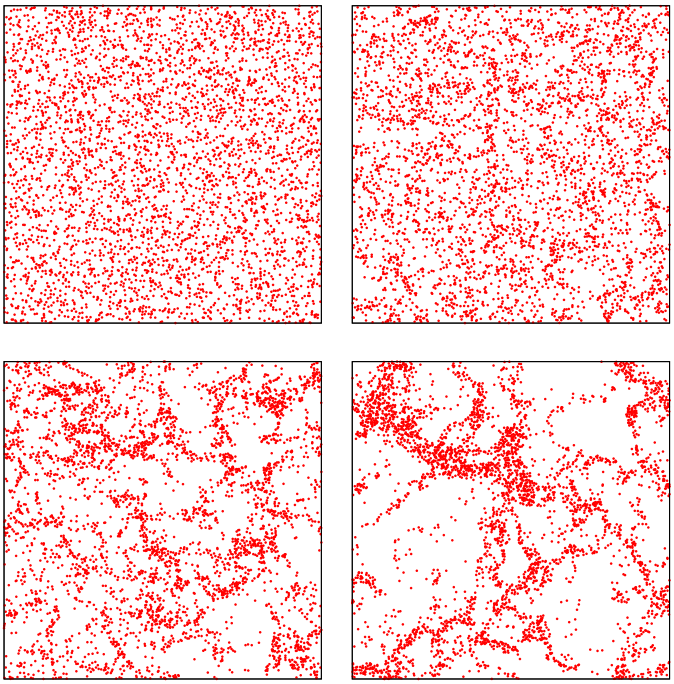

Figure 2.4: Snapshots of freely cooling granular gas in two dimensions, starting from uniform density and evolving to inhomogeneous regime. The coefficient of restitution $r = 0.10$

2.4 Inhomogeneous Cooling Regime

The homogeneous cooling regime is unstable to the formation of high density clusters [12, 90, 91], and the system evolves into inhomogeneous cooling regime where the dynamics of the system is dominated by presence of clusters, as shown in Fig. 2.4 for two dimensional FCGG. These are obtained in numerical simulation of inelastic hard disks. This fact can be understood intuitively. If the density in a region is increased due to fluctuations, the frequency of collision in this region is higher compared to neighboring less dense region. Thus, due to inelastic collisions, the temperature (or kinetic energy) in this dense region decreases resulting in decrease of pressure. The pressure gradient causes movement of particles to the dense region, further increasing the density and decreasing the pressure. Thus, density fluctuations lead to strong clustering in the system. Developing a theory for this regime is a challenging task, thus almost all results in this regime are obtained in simulations.

Brito et al. [92] extended kinetic theory into the inhomogeneous cooling regime using mode coupling methods, and found that in the inhomogeneous regime $T(\tau) \sim \tau^{-D/2}$, where τ is the average number of collisions per particle and not the real time t. The relation between τ and t is unclear [92]. This result agrees with simulations for near-elastic ($r \approx 1$) gases, but fails for large times and strongly inelastic ($r \ll 1$) gases [92].

Ben-Naim et al. [13] studied FCGG in one dimension, where dissipation is modeled by constant coefficient of restitution r. In the inhomogeneous regime, the kinetic energy $T(t)$ decays with time t as a power law $T(t) \sim t^{-\theta_T}$, with $\theta_T = 2/3$. The value of $\theta_T = 2/3$ is universal, independent of dissipation r.

Nie et al. simulated FCGG of hard disks in two dimensions [14]. They found that in the inhomogeneous regime, energy decays as a power-law $T(t) \sim t^{-\theta_T}$ with $\theta_T = 1$. Similar to the one dimensional case, the decay exponent θ_T is independent of r, although its value is different from the one dimensional case.

Chen et al. [93] simulated deformable spheres in two and three dimensions. In two dimensions, θ_T was found to be 1, while for three dimensions it ranges from $\theta_T = 1.35 - 1.6$, depending on the parameters such as the volume fraction and coefficient of restitution. Tube-like clusters were observed in three dimensions [93], which can be compared with the string-like clusters in two dimensions [12]. The three dimensional results were however restricted due to small system sizes and insufficient temporal range.

Miller et al. [94] studied energy decay and clustering in two and three dimensions with hard-sphere gas. The decay exponent θ_T was found to be 1 in two dimensions and $1.1 \pm .1$ in three dimensions. It was found that one large cluster is formed which contains a macroscopic fraction of particles.

Shinde et al. [9, 70, 71] studied FCGG in one dimension where velocity dependent coef-

ficient of restitution is considered. The coefficient of restitution is modeled as

$$r = (1 - r_0) \exp(-|v_{\text{rel}}/\delta|^{\sigma}) + r_0. \tag{2.48}$$

For relative velocity $v_{\text{rel}} \ll \delta$, $r \to 1$, and for $v_{\text{rel}} \gg \delta$, $r \to r_0 < 1$, mimicking the observed behaviour of r in experiments [95, 96, 97]. The parameter σ controls the sharpness of crossover from r_0 to 1 around the crossover scale δ. It was found that the inhomogeneous regime is divided into two regimes by δ, an early regime when $t \ll \delta^{-1}$ and late regime when $t \gg \delta^{-1}$. At early times, the system behaves as a completely inelastic gas conforming to earlier studies [13, 15, 70, 71]. While at late times, the kinetic energy $T(t)$ continues to decay like $t^{-2/3}$ as in early time regime, the spatial structural properties are quite different. In a contrast to the early time regime, the Porod's law for the density and velocity structure function is violated in late time regime [9].

2.5 Homogeneous Cooling of Rough Granular Gas

The rough granular gas (RGG) is defined in Sec. 2.2. The homogeneous cooling regime of RGG has been studied using kinetic theory and numerical simulations in [16], which we briefly summarize in this section. Our summary is restricted to two dimensional RGG, as the results in three dimensions are not qualitatively different from two dimensions [16]. The quantities of interest are the translational energy $T(t)$ and rotational energy $K(t)$ defined in Eqs. (2.14) and (2.15). Assuming that the system is spatially homogeneous, the kinetic theory calculation [16] yields the following coupled differential equations for $T(t)$ and $K(t)$:

$$\frac{dT'}{d\tau} = -AT'^{3/2} + BT'^{1/2}K', \tag{2.49}$$

$$\frac{dK'}{d\tau} = 2BT'^{3/2} - 2CT'^{1/2}K', \tag{2.50}$$

where dimensionless translational kinetic energy $T'(t) = T(t)/T(0)$ and dimensionless rotational kinetic energy $K'(t) = K(t)/T(0)$ is introduced, and time is also scaled as $\tau = G\,T^{1/2}(0)\,t$. $A, B, C,$ and G are constants with their values given by

$$A = \frac{1-r^2}{4} + \frac{\eta}{2}(1-\eta), \tag{2.51}$$

$$B = \frac{\eta^2}{2q}, \tag{2.52}$$

$$C = \frac{\eta}{2q}\left(1 - \frac{\eta}{q}\right), \tag{2.53}$$

$$G = 4d\frac{N}{L^2}\sqrt{\frac{\pi}{m}}g_2(d), \tag{2.54}$$

where $\eta = q(1+\beta)/(2q+2)$, and $g_2(d)$ is the pair correlation function at contact.

To find the asymptotic value of the equipartition ratio $R_{\rm eq} = T'/K'$, we consider the differential equation

$$\frac{dT'}{dK'} = \frac{-AR_{\rm eq} + B}{2BR_{\rm eq} - 2C}. \tag{2.55}$$

The solution of Eq. (2.55) yields

$$R_{\rm eq} = \left(2C - A + \sqrt{(2C-A)^2 + 8B^2}\right)/(4B), \tag{2.56}$$

which is a constant. Thus, after some $\tau > \tau_0$ when $R_{\rm eq}$ has reached the asymptotic constant value as given by Eq. (2.56), both T' and K' have the same decay behaviour. Substituting $K' = T'/R_{\rm eq}$ in Eq. (2.49) gives

$$\frac{dT'}{d\tau} = -FT'^{3/2}, \tag{2.57}$$

where $F = A - B/R_{\rm eq}$. This equation is of the same functional form as for homogeneous cooling of smooth spheres. Its solution is

$$T' = \frac{T'(\tau_0)}{\left[1 + T'(\tau_0)^{1/2}(F/2)(\tau-\tau_0)\right]^2}\,. \tag{2.58}$$

Thus, asymptotically ($\tau \to \infty$) both energies decay as τ^{-2}, which is the Haff's law for

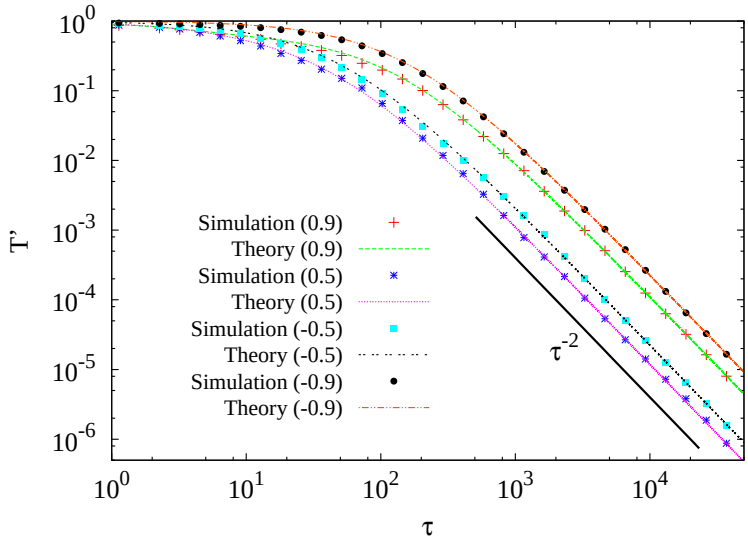

Figure 2.5: Translational kinetic energy T' as a function of scaled time τ for various β (written in brackets).

smooth particles. These analytical results were verified in numerical simulation [16] of hard-core particles using event-driven molecular dynamics simulation. We have reproduced the reported results of Ref. [16] in our simulations. The temporal evolution of T' and K' are shown in Figs. 2.5 and 2.6 respectively, where the simulation result is compared with the theoretical result. The simulation data are for system with $N = 200$, $L = 120$ (volume fraction 0.01) and $r = 0.99$. The value of β is shown in the brackets. Homogeneous discs are considered for which $q = 1/2$. Initially, the normalized energies for the shown data are $T' = 1$ and $K' = 0$. The theoretical results drawn in the figures are obtained by numerical integration of Eqs. (2.49) and (2.50). The match between the theoretical result and simulation data is excellent. At large times, both energies decay like τ^{-2}, as shown by bold line of slope -2. The equipartition ratio $R_{\rm eq}$ is plotted in Fig. 2.7. It saturates to a constant value different from unity, showing that the energy is not equipartitioned between translational and rotational degrees of freedom.

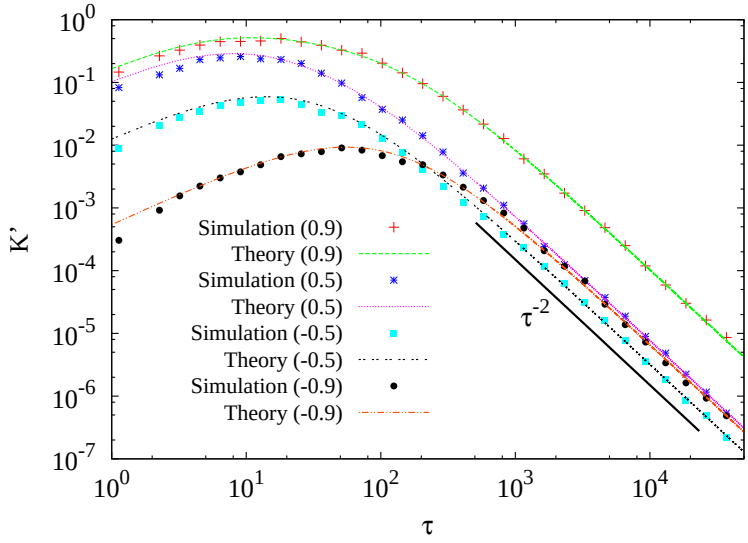

Figure 2.6: Rotational kinetic energy K' as a function of scaled time τ for various β (written in brackets).

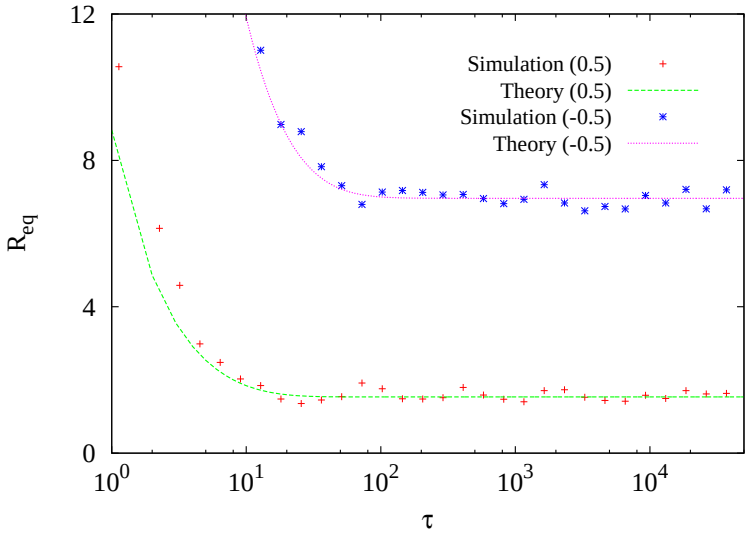

Figure 2.7: Equipartition ratio $R_{\text{eq}} = T'/K'$ as a function of scaled time τ for $\beta = 0.5, -0.5$ (written in brackets).

2.6 Experiments of Freely Cooling Granular Gas

It is extremely hard to probe the dynamical behaviour of FCGG in experiments. In earth-bound experiments, gravity as an external force is always present, due to which the system can not evolve *freely*. Also, the system should be large enough so that the effects of boundary conditions are negligible. Few experiments have overcome these difficulties. We briefly summarize these experiments.

- **Maaß et al. (2008)** [83]: In this experiment, diamagnetic levitation was implemented to compensate gravity. This method is more accessible compared to other methods of compensating gravity such as parabolic flights or satellites. The experimental system was three dimensional. A helium cooled superconducting magnet coil able to generate field strengths upto 20T reduces the gravity to the order of milligravity. The sample consisted of approximately 50-90 round and nearly monodispersed bismuth shots. Bismuth was chosen because of its highly diamagnetic nature. The metallic nature of the sample prevents electrostatic charges, so there is no additional Coulomb interaction. However, bismuth has extremely low coefficient of restitution, nearly 0.33-0.40, which makes the homogeneous cooling regime quite shorter. Magnetic as well as mechanical excitations were used to impart initial energies to the particles. Snapshots of the freely evolving system were recorded at a constant rate of 120 frames per second. The velocity of a particle is then calculated using its position at two consecutive frames. As the cooling process mainly involves the nonclustered particles (in the experiment, it was observed that the velocity of a clustered particle is very low making it determination impossible), the observed quantity in the study was the mean particle speed outside of a possible cluster. Haff's law is seen to describe the experimental data until clustering occurs in the system.

- **Grasselli et al. (2009)** [84]: In this experiment, the freely cooling system consisted

of iron beads enclosed in a two dimensional cell. The wall of the cell was made of glass in order to cancel electrostatic effects and to minimize the friction between the beads and the walls. To remove the effect of gravity, this experiment was performed in zero-gravity situations inside a special equipped airplane undergoing parabolic flights. The temporal evolution of the system was recorded with a high-speed camera at 470 frames per seconds. The coefficient of normal restitution was found to be a constant at large relative velocities, and decreases when the relative velocity decreases. This is in contrast with other experimental findings, where the coefficient of normal restitution increases when the relative velocity decreases. This is because the velocity scale in this experiment is of the order of few centimeters per second, while in previous experiments the typical relative velocity was larger than 1m/s. At such low velocities, adhesive forces are relevant resulting in smaller value of coefficient of normal restitution. The measured kinetic energy decays faster than that predicted by Haff's law with constant coefficient of normal restitution. Better fitting is obtained when rotational degree of freedom is taken into account. A much better fitting is obtained if the Haff's law is modified to take into account the experimentally observed velocity dependent coefficient of restitution.

- **Tatsumi et al. (2009) [85]**: In this experiment, monodispersed zirconium beads were confined in quasi two dimensional cell. The coefficient of restitution of zirconium beads is 0.76 approximately. The experiment was carried out in two types of quasi two dimensional cells: a horizontal cell and a vertical cell. Around 2000 particles for the horizontal cell and 300 particles for the vertical cell were used in experiment. This number is much higher as compared to above discussed Maaß et al. experiment [83]. The cell was kept in vacuum condition to avoid hydrodynamic interaction between particles. The initial velocities of the particles were generated by vibrating the system electromagnetically. Microgravity condition was achieved aboard a parabolic flight of a jet aircraft. Particle motion was captured by a high-speed camera, at a frame rate of 1kHz. As long as clustering is absent in the system,

experimental data fits very well to the Haff's law.

2.7 Ballistic Aggregation

In this section, we discuss the Ballistic Aggregation (BA) model (also called *sticky gas*) [see Ref. [98] for a review]. In the following subsections, we first describe the model in detail, followed by the mean-field scaling analysis of BA, and the simulation results of this model. In the last subsection, we discuss connection between BA and Burgers equation in one dimension.

2.7.1 Model

In the BA model, particles move ballistically and on collision merge to become a new particle, whose shape is assumed to be spherical. To each particle i located at $\vec{r}_i$, we associate a velocity $\vec{v}_i$, a mass m_i and a radius a_i. Consider the collision between particles i and j. The mass m' of the new particle is given by mass conservation

$$m' = m_i + m_j, \tag{2.59}$$

and its velocity $\vec{v'}$ is given by linear momentum conservation

$$m'\vec{v'} = m_i\vec{v}_i + m_j\vec{v}_j. \tag{2.60}$$

The radius a' of the new particle is obtained from volume conservation: $a'^D = a_i^D + a_j^D$. The position $\vec{r'}$ of the new particle is obtained from the conservation of center of mass:

$$m'\vec{r'} = m_i\vec{r}_i + m_j\vec{r}_j. \tag{2.61}$$

We can further consider particles having rotational degree of freedom and associate an angular velocity $\vec{\omega}_i$. The moment of inertia is given by $I_i = qm_i a_i^2$, where q is a number which depends on dimensionality and the distribution of mass inside a particle. Its value is $1/2$ for a homogeneous disk, and $2/5$ for a homogeneous sphere.

The new angular velocity $\vec{\omega'}$ is obtained from conservation of angular momentum. Let $I' = qm'a'^2$ be the moment of inertia of the new particle. Then,

$$I'\vec{\omega'} = I_i\vec{\omega}_i + I_j\vec{\omega}_j + \frac{m_i m_j}{m_i + m_j}(\vec{r}_i - \vec{r}_j) \times (\vec{v}_i - \vec{v}_j). \tag{2.62}$$

Equations (2.59)–(2.62) completely determine the mass, velocity, position and angular velocity of the new particle. We note from Eqs. (2.59) and (2.60) that translational velocities are independent of rotational motion. Except Chapter 5, everywhere else in this thesis, we study BA without considering the rotational degrees of freedom.

2.7.2 Scaling Analysis of Ballistic Aggregation

Carnevale et. al. [15] carried out the mean-field scaling analysis of BA, and we recapitulate the analysis in this subsection. Consider a collection of spheres distributed randomly in a D-dimensional space. Initially at time $t = 0$, the spheres are of average radius a_0, average mass m_0, and with average separation l_0. The velocities have root mean square (rms) value of u_0.

Initially at $t = 0$, the collision time τ_0 is the ratio of the volume per particle to the rate at which a sphere sweeps out the volume,

$$\tau_0 = l_0^D / u_0 a_0^{D-1}, \tag{2.63}$$

this expression being valid only at $t = 0$, when l_0, a_0 and u_0 are the characteristic scales of the system. We define $N(t/\tau_0)$ as the expected number of initial spheres that have

aggregated into a single sphere at t. At $t_1 \equiv s\tau_0$, we have a new initial condition with scales

$$l_1 = N_1^{1/D} l_0, \tag{2.64}$$

$$m_1 = N_1 m_0, \tag{2.65}$$

$$a_1 = N_1^{1/D} a_0, \tag{2.66}$$

$$u_1 = u_0 / N_1^{1/2}, \tag{2.67}$$

$$\tau_1 = N_1^{(D+2)/2D} \tau_0, \tag{2.68}$$

where $N_1 \equiv N(s)$. The scaling for u_1 in Eq. (2.67) is obtained using central limit theorem. The momentum of an aggregate is the sum of N_1 random vectors of typical length $m_0 u_0$, giving the expected size of the resultant random momentum as $N_1^{1/2} m_0 u_0$. Dividing it by m_1 gives Eq. (2.67).

Now, consider $t_2 = s\tau_1 = sN_1^{1/\theta_T^{mf}} \tau_0$, where $\theta_T^{mf} = 2D/(D+2)$. At t_2, the expected size of an aggregate can be calculated using either $t = 0$ or $t = t_1$ as the initial condition. According to the first case, $N(t_2/\tau_0) = N(sN_1^{1/\theta_T^{mf}})$ initial particles have aggregated into a single sphere at t_2. According to the second case, each aggregate at t_2 is composed of $N(t_2/\tau_1) = N_1$ particles from t_1, and each particle at t_1 is composed of N_1 initial particles. Therefore,

$$N(sN(s)^{1/\theta_T^{mf}}) = N(s)^2 \quad \text{or} \quad N(s) \sim s^{\theta_T^{mf}}. \tag{2.69}$$

Thus, the typical mass of an aggregate grows as $M_t \sim t^{\theta_T^{mf}}$. The typical number of aggregates then decreases as $n_t \sim t^{-\theta_T^{mf}}$, since total mass is conserved. With typical velocity $v_t \sim t^{-\theta_T^{mf}/2}$, the kinetic energy of the system is given by

$$T(t) \sim n_t M_t v_t^2 \sim t^{-\theta_T^{mf}} \quad \text{with} \quad \theta_T^{mf} = 2D/(D+2). \tag{2.70}$$

Volume fraction ϕ	Decay exponent θ_T^{BA}
0.0008	1.12
0.0079	1.12
0.0393	1.10
0.3925	1.03
0.6280	1.00

Table 2.1: Table showing the dependence of decay exponent θ_T^{BA} on volume fraction ϕ for two dimensional BA. Data are taken from [19].

2.7.3 Simulation Results for Ballistic Aggregation

Numerical simulations of BA in one dimension [15] with point particles and a variety of initial distribution of positions and velocities find $\theta_T^{BA} = 2/3$ validating the mean-field prediction. Exact solution of BA in one dimension finds $\theta_T^{BA} = 2/3$ matching with the mean-field and simulation result. However, simulations in two dimensions show significant deviations from the mean-field prediction [19, 99]. The BA model in $D \geq 2$ is different from $D = 1$. The size of particles, which can be scaled out in $D = 1$ becomes a relevant variable in $D \geq 2$. In $D = 1$, aggregation is a purely binary process, while in higher dimensions owing to the spatial extension of newly formed aggregate, it may overlap with other particles leading to a chain of multiple aggregation. The possibility of multiparticle aggregation is higher for denser systems, thus making decay exponent θ_T^{BA} density dependent. Table 2.1 shows θ_T^{BA} for varying volume fraction ϕ, for two dimensional BA. For dilute systems, its value is very different from the mean-field value of one. Its value increases with increase in density and saturates at the mean-field value.

The deviation from the mean-field value is because of the incorrect assumption that velocities of original particles contained within an aggregate are uncorrelated [19]. In general, particles moving towards each other are more likely to collide compared to particles that are moving away from each other, breaking the no-correlation assumption. It is shown that mean-field no-correlation assumption is essentially the Maxwell model in context of ballistic processes [19, 100]. The Maxwell model is obtained by replacing the relative velocity in the Boltzmann equation by the root mean square velocity and this approxima-

tion allows for analytical progress of problem. The Maxwell model is an uncontrolled approximation to the Boltzmann equation and the exponents found with this approach are generally erroneous [19].

2.7.4 Burgers Equation and Ballistic Aggregation

In this subsection, we recapitulate the solution of Burgers equation in one dimension [74, 101] and its connection with ballistic aggregation as established in [74].

The one dimensional Burgers equation for the velocity field $u(x,t)$ is

$$\frac{\partial u}{\partial t} + u\frac{\partial u}{\partial x} = \frac{1}{R}\frac{\partial^2 u}{\partial x^2}, \tag{2.71}$$

where x is space coordinate, t is time. $R = u_0 l_0/\nu$ is Reynolds number with the characteristic velocity u_0 and length l_0 of the initial velocity field and ν is kinematic viscosity. We are interested in the solution of Eq. (2.71) in high Reynolds numbers limit $R \gg 1$ and large times $t \gg 1$, under arbitrary continuous initial conditions $u(x,0)$, specified in an infinite domain, $-\infty < x < \infty$. The Hopf–Cole transformation,

$$u = -\frac{2}{wR}\frac{\partial w}{\partial x}, \tag{2.72}$$

transforms nonlinear Eq. (2.71) into a linear diffusion equation for $w(x,t)$,

$$\frac{\partial w}{\partial t} = \frac{1}{R}\frac{\partial^2 w}{\partial x^2}. \tag{2.73}$$

Solving Eq. (2.73) for w and then using Eq. (2.72) gives

$$u(x,t) = \frac{\int_{-\infty}^{\infty} \frac{x-x'}{t} \exp\left[-\frac{R}{2}Z(x,x',t)\right] dx'}{\int_{-\infty}^{\infty} \exp\left[-\frac{R}{2}Z(x,x',t)\right] dx'}, \tag{2.74}$$

where

$$Z(x, x', t) = \frac{(x - x')^2}{2t} + \int_{x_0}^{x'} u(x'', 0)dx'', \tag{2.75}$$

where x_0 is an arbitrary constant. Now, for a fix value of x and $t > 0$, and in the inviscid limit of $R \gg 1$, the most important contribution to the integral will come from the immediate neighborhood of point X, which is given by absolute minimum of $Z(x, x', t)$.

$$X = \min_{x'} Z(x, x', t). \tag{2.76}$$

Thus, Eq. (2.74) reduces to

$$u(x, t) = \frac{x - X}{t}. \tag{2.77}$$

We note that Eq. (2.77) does not generally represent a straight line since X is a function of x and t. Now, to examine the dependence of X on x and t, we consider a geometric interpretation of the minimum condition. As shown in Fig. 2.8, first we construct the curve

$$s(x') = -\int_{x_0}^{x'} u(x'', 0)dx'' + s(x_0), \tag{2.78}$$

which is completely determined by the initial velocity field of the problem. Second, we construct a parabola

$$S(x') = \frac{(x' - x)^2}{2t} + C, \tag{2.79}$$

whose axis is the line $x' = x$, and whose vertex becomes flatter with increasing t. Hence, we have a different parabola for different x and t. We start with a large positive value of constant C, so that the everywhere the S curve is well above the s curve. This is always possible with the assumption that $s(x') < \infty$ for all x'. Now, the minimum condition $dZ/dx' = 0$ gives

$$\frac{dS}{dx'} = \frac{ds}{dx'}. \tag{2.80}$$

In words, when the minimum condition is satisfied, the tangents to both curves, $S(x')$ and $s(x')$ are parallel. The minima value X can thus be obtained by bringing the S curve down

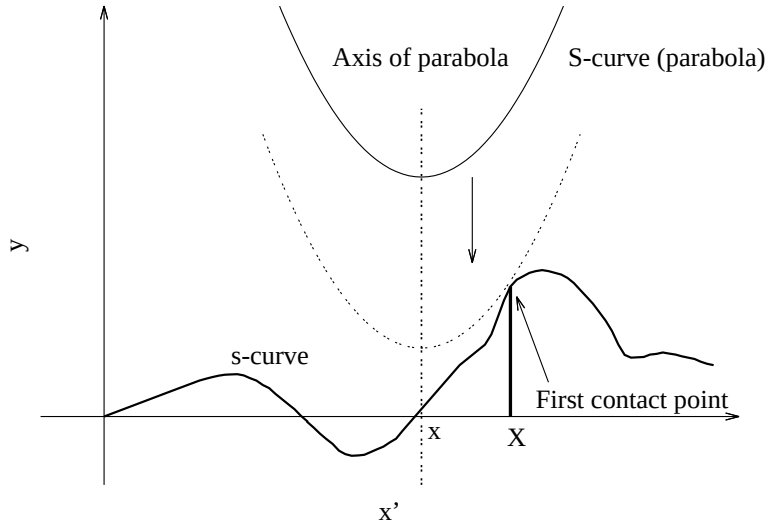

Figure 2.8: Initial data curve (s-curve) and the parabola S.

by decreasing the value of C, until it touches the s curve for the first time (see Fig. 2.8), at which instant both curves have a common tangent at the point of contact. The point X, where the contact occurs for the first time determines the absolute minimum of Z for fixed x and t,

$$Z(x, x', t)|_X = (S(x, x', t) - s(x, x', t) - C)|_X = -C. \tag{2.81}$$

Now, to obtain u as a function of x for a fixed t, we must shift the axis of parabola $S(x')$. The above described method for determining the absolute minimum through first contact point can then be interpreted by requiring that the parabola $S(x')$ shall glide over the s curve without ever cutting it. Thus, each position x of the axis will give the corresponding X and $u(x, t)$ can then be determined using Eq. (2.77).

It is possible that parabola $S(x')$ touches the $s(x')$ curve at two points simultaneously. This possibility is higher for large t, when the parabola is rather flat. In such cases, Eq. (2.76) has a double root. When $t >> 1$, all first contact points are closer to the tops of the s curve, as the parabola is much flatter than the s curve (see Fig. 2.9). We denote the abscissa of the ith top of such kind by η_i, where $i = 0, \pm1, \pm2$,....and η_0 is the top closest to the origin. For the chosen x, the abscissae of the two first contact points are denoted by X_i and X_{i+1}. Since, $X_i \approx \eta_i$ and $X_{i+1} \approx \eta_{i+1}$, the function $s(x')$ can be expanded around η_i and η_{i+1},

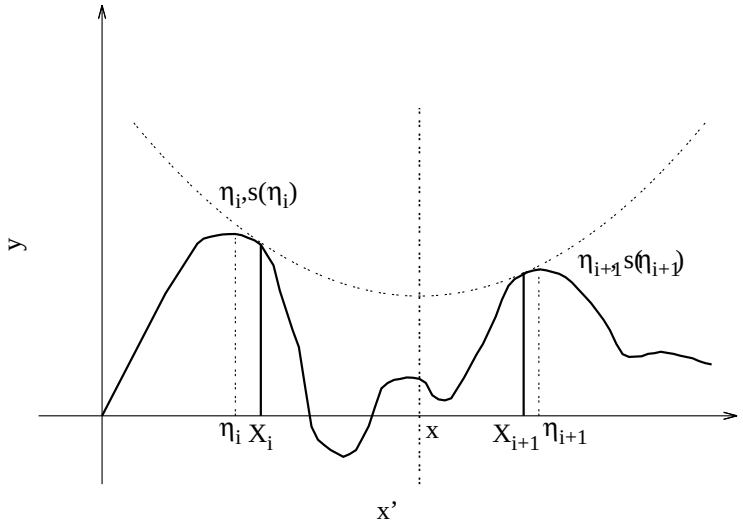

Figure 2.9: A parabola in double contact with the s-curve.

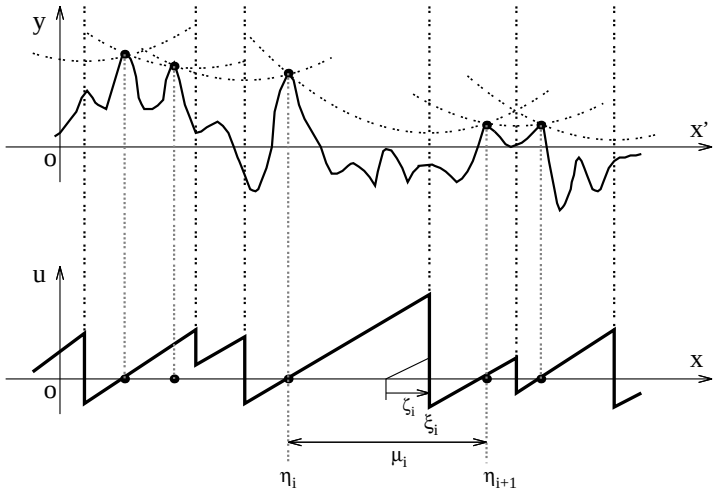

Figure 2.10: A sequence of parabolas in double contact with the s-curve and the corresponding velocity field.

and the integral [Eq. 2.74] is evaluated as the sum of contributions from these two parts yielding,

$$u(x,t) = \frac{1}{t}\left(x - \frac{\eta_i + \eta_{i+1}}{2}\right) - \frac{1}{2t}(\eta_{i+1} - \eta_i)\tanh\left[\frac{R}{4t}(\eta_{i+1} - \eta_i)(x - \xi_i)\right], \tag{2.82}$$

where ξ_i is given by

$$\xi_i = \frac{\eta_i + \eta_{i+1}}{2} - \frac{s(\eta_{i+1}) - s(\eta_i)}{\eta_{i+1} - \eta_i}t + \frac{t}{R(\eta_{i+1} - \eta_i)}\ln\left(\frac{s''(\eta_{i+1})}{s''(\eta_i)}\right). \tag{2.83}$$

This solution is valid in the region $\frac{1}{2}(\xi_{i-1} + \xi_i) < x < \frac{1}{2}(\xi_i + \xi_{i+1})$ and for $R \gg 1$, $t \gg 1$.

For very large R such that $R \gg t \gg 1$, Eqs. (2.82) and (2.83) reduce to

$$u(x,t) = \begin{cases} \frac{x-\eta_i}{t} & \text{for} \quad \frac{\xi_{i-1}+\xi_i}{2} < x < \xi_i, \\ \frac{x-\eta_{i+1}}{t} & \text{for} \quad \xi_i < x < \frac{\xi_i+\xi_{i+1}}{2}, \end{cases} \tag{2.84}$$

and

$$\xi_i = \frac{\eta_{i+1} + \eta_i}{2} - \frac{s(\eta_{i+1}) - s(\eta_i)}{\eta_{i+1} - \eta_i}t. \tag{2.85}$$

Equation (2.84) represents a discontinuity or a shock of strength μ_i/t located at ξ_i, where

$$\mu_i = \eta_{i+1} - \eta_i. \tag{2.86}$$

It is easy to show that the shock moves with the velocity ζ_i/t, where

$$\zeta_i = \xi_i - \frac{\eta_{i+1} + \eta_i}{2}, \tag{2.87}$$

which is equal to the velocity at the centre of the shock. It can be easily seen from Eq. (2.85) that ξ_i coincides with the axis of the parabola passing through the two tops $(\eta_i, s(\eta_i))$ and $(\eta_{i+1}, s(\eta_{i+1}))$ of s curve.

Thus, as shown in Fig. 2.10, the velocity profile is represented by a sequence of vertical

lines (shocks) connected by oblique lines of slope $1/t$. The positions of shocks are given by $\{\xi_i\}$, and $\{\eta_i\}$ gives the positions where the oblique lines intersect $x-$ axis. These shocks move at different speeds determined by Eq. (2.87) and therefore collide with each other from time to time. On collision, the shocks coalesce into one, with the strength of resultant shock given by sum of the strengths of colliding shocks.

We consider the following two observations

1. The advance velocity ζ_i/t and the strength of shocks multiplied by t, μ_i are invariant in time except at the instant of collision.

2. μ_i and $\mu_i\zeta_i/t$ are conserved at each collision. To see this, consider collision between two shocks at ξ_i and ξ_{i+1}. The strength of resultant shock is given by

$$\mu' = \eta_{i+2} - \eta_i = (\eta_{i+2} - \eta_{i+1}) + (\eta_{i+1} - \eta_i) = \mu_i + \mu_{i+1}. \tag{2.88}$$

   It is easy to show that $\mu'\zeta'/t$ given by,

$$\frac{\mu'\zeta'}{t} = \frac{1}{t}(\eta_{i+2} - \eta_i)(\xi' - \frac{\eta_{i+2} + \eta_i}{2}), \tag{2.89}$$

   with

$$\xi' = \frac{\eta_{i+2} + \eta_i}{2} - \frac{s(\eta_{i+2}) - s(\eta_i)}{\eta_{i+2} - \eta_i}t, \tag{2.90}$$

   can be written as

$$\frac{\mu'\zeta'}{t} = \frac{\mu_i\zeta_i}{t} + \frac{\mu_{i+1}\zeta_{i+1}}{t}. \tag{2.91}$$

Thus, there is a one-to-one correspondence between the shock dynamics of Burgers equation and the dynamics of aggregating particles in ballistic aggregation (BA). A shock at ξ_i with strength μ_i and velocity ζ_i/t can be thought of an aggregate in BA with mass μ_i, moving with velocity ζ_i/t. These quantities are invariant in time except at the time of collision. Equations (2.88) and (2.91) establish the mass and momentum conservation respectively.

2.8 Freely Cooling Granular Gas and Burgers Equation

In this section, we discuss in detail two previous works on FCGG [13, 14], which we mentioned very briefly in Sec. 2.4. These works argue for a Burgers equation like description for the large time behaviour of FCGG.

Ben-Naim et al. [13] studied FCGG in one dimension using event driven molecular dynamics simulation. The dissipation is accounted by constant coefficient of restitution r. To circumvent inelastic collapse (whose detailed discussion we defer to Sec. 3.3.6), where infinite collisions occur in finite time imposing practical difficulties in event-driven simulation of the system, a cutoff velocity δ was introduced. Collisions are elastic when relative velocity is lower than δ, otherwise inelastic with constant r. The decay of kinetic energy $T(t)$ with time t is shown in Fig. 2.11. At initial times, the system remains homogeneous and it decays as $T(t) \sim t^{-2}$ (Haff's law). After an r - dependent crossover (the crossover time diverges in the elastic limit $r \to 1$), the system evolves into inhomogeneous regime and it decay behaviour changes to a different power-law, $T(t) \sim t^{-\theta_T}$, with $\theta_T = 2/3$. The value of $\theta_T = 2/3$ is universal, independent of r. The curves for different r are indistinguishable in the inhomogeneous regime, and are also indistinguishable from the ballistic aggregation ($r = 0$) data. It was also noted that with $\delta = 0$, the simulation does not progress. We note that the mean-field scaling analysis [Eq. (2.70)] as well as the exact solution of BA [8] predict the decay exponent to be 2/3 in one dimension.

With these observations, it was proposed that the FCGG is asymptotically in the universality class of a completely inelastic, sticky gas [13]. A simple physical picture was provided to understand this universality. Consider a collision between one moving particle and cluster of N stationary particles in one dimension, where all particles are identical. At any collision particle identities are considered to be exchanged, so that in an elastic collision the particles merely pass through each other, while suffer a small deflection for small inelasticity. The result of a collision between a particle with velocity v and another

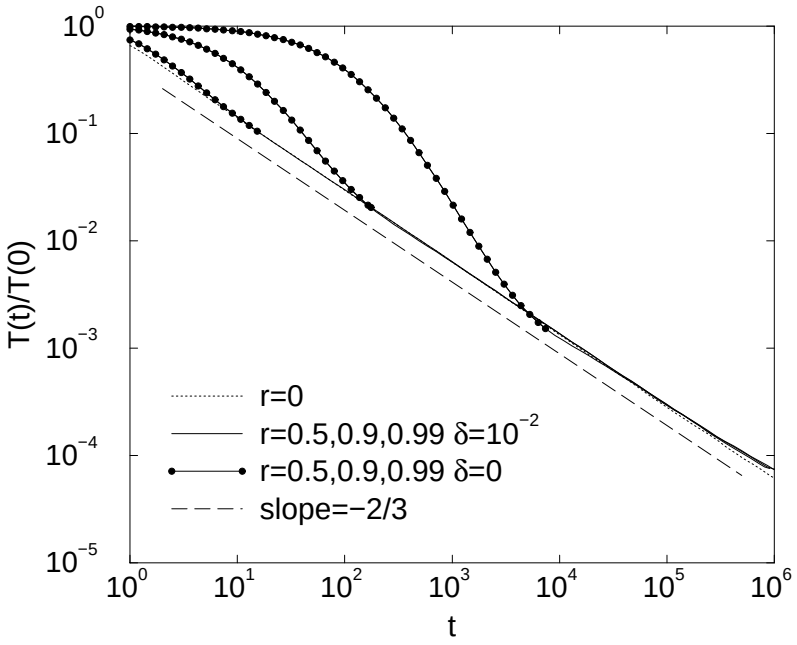

Figure 2.11: The temporal decay of kinetic energy $T(t)$ for one dimensional FCGG, for various r. Data for $r = 0$ (BA) case is also shown. This figure is taken from [13].

particle with velocity u is given by

$$v \to v - \epsilon\,(v - u), \tag{2.92}$$

where $\epsilon = (1 - r)/2$. Thus, each collision between the incident particle and the next stationary particle in the cluster reduces the incident particle velocity by roughly ϵ. The incident velocity after N collisions is $v_N \approx 1 - N\epsilon$. Now, for the particle to pass through the cluster, $N < \epsilon^{-1}$. For this range of cluster sizes, the system remains spatially homogeneous and energy decay follows Haff's law. If the cluster size is bigger than the critical cluster size $N_c(\epsilon) \sim \epsilon^{-1}$, the incident particle is absorbed as if the coefficient of restitution is $r = 0$. As clustering is more prominent in highly inelastic systems, lesser inelastic system remains in homogeneous regime for longer times. Once the system crosses to the inhomogeneous regime, system with any value of $r < 1$ behaves like $r = 0$.

Further confirmation of this universal behaviour is obtained by the measurement of velocity distribution [13]. It was found that in the inhomogeneous regime, the normalized

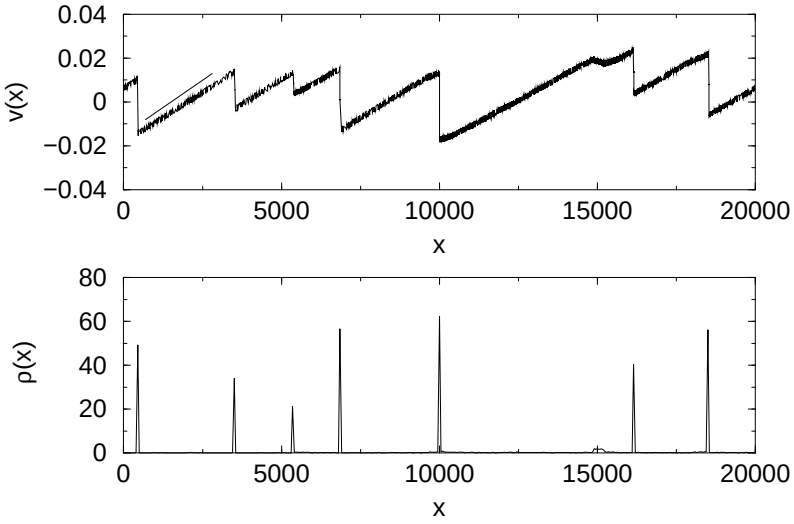

Figure 2.12: Shock profile of one dimensional FCGG. Density and velocity in the inhomogeneous regime are plotted. A line with slope t^{-1} is plotted for reference. This figure is taken from [13].

velocity distribution,

$$P(v,t) \sim t^{1/3}\Phi(vt^{1/3}), \tag{2.93}$$

is described by an identical scaling function $\Phi(z)$ for all values of $r < 1$, including $r = 0$. The scaling function $\Phi(z)$ was found to be Gaussian [13].

This universal behaviour, i.e., the convergence of all $r < 1$ curves to $r = 0$ shows that the inhomogeneous regime of FCGG is described by sticky gas with $r = 0$ being the fixed point. Since sticky gases are described by the inviscid limit of the Burgers equation as discussed in Sec. 2.7.4, it was concluded that this continuum theory also describes the asymptotics of the FCGG in the thermodynamic limit [13]. This conclusion was further supported by comparing the velocity field profile. Shown in Fig. 2.12 is the velocity field of one dimensional FCGG [13], which is similar to the velocity profile of the Burgers equation solution (see Fig. 2.10). The $1/t$ slopes of the linear segments of the profile are consistent with Burgers equation prediction (see Eq. 2.77).

It was speculated that $r = 0$ remains the fixed point even in higher dimensions $D > 1$ as well [13]. It was shown in [5] that in higher dimensions, Burgers equation $\vec{v}_t + \vec{v} \cdot \nabla\vec{v} =$

$\nu\nabla^2\vec{v}$ approximately describes the sticky gas in the inviscid limit $\nu \to 0$. Using this correspondence, it was predicted that kinetic energy decreases as [5, 13].

$$T(t) \sim \begin{cases} t^{-D/2} & \text{for} \quad 2 \le D \le 4, \\ t^{-2} & \text{for} \quad D > 4. \end{cases} \tag{2.94}$$

Nie et al. simulated FCGG of hard disks in two dimensions [14]. They found that in the inhomogeneous regime, energy decays as a power-law $T(t) \sim A(r)t^{-\theta_T}$ with $\theta_T = 1$. Similar to the one dimensional case, the decay exponent θ_T is independent of r, but unlike one dimensional case, $T(t)$ has a dependence on r through the prefactor $A(r)$. It was observed that the dependence of $A(r)$ on r becomes weaker for dilute systems, suggesting completely universal behaviour in the dilute limit. The observed decay exponent $\theta_T = 1$ is predicted by both, the mean-field scaling analysis [Eq. (2.70)] and the correspondence with Burgers equation [Eq. (2.94)]. In the inhomogeneous regime, the velocity distribution function $P(v, t)$ is described by universal scaling function $\Phi(z)$ independent of coefficient of restitution r,

$$P(v, t) \sim \frac{1}{v_{rms}^2}\Phi\left(\frac{v}{v_{rms}}\right). \tag{2.95}$$

In simulations, the scaling function was found to be a Gaussian [14]. Thus $r = 0$ is indeed the fixed point in two dimensions as speculated in [13].

To quantify collective motions and the corresponding velocity fluctuations in the inhomogeneous regime, the local kinetic energy E_k and the local thermal energy E_{th} was also measured in simulations [14]. The local kinetic energy is defined as $E_k = \frac{1}{2}\langle\rho u^2\rangle$ with the density ρ and the velocity $\vec{u} = (u_x, u_y)$ obtained by averaging the corresponding quantities over a small region. The local thermal energy $E_{th} = \frac{1}{2}\langle(v_x - u_x)^2 + (v_y - u_y)^2\rangle$ is obtained by subtracting the average local velocity $\vec{u}$ from the particle velocity $\vec{v}$. The ratio of thermal to kinetic energy is shown in Fig. 2.13. Initially, the thermal energy is large compared to the kinetic energy, indicating that particles move independently and there are no collective

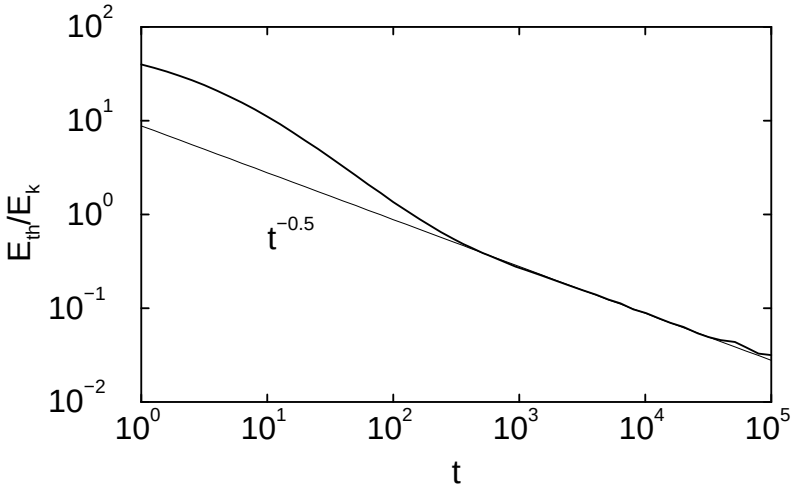

Figure 2.13: The ratio of the thermal energy E_{th} to the kinetic energy E_k as a function of time. A line of slope $-1/2$ is plotted for reference. This figure is taken from [14].

motions in the system. However, at larger times in the inhomogeneous regime, thermal energy becomes much smaller than the kinetic energy, showing the dominance of coherent motion of particles in the system. Collective motion was earlier observed in numerical simulations [12, 87, 90, 93] and as well as suggested by linear stability analysis of the hydrodynamic equations [12, 87]. At long times, the ratio was found to decay with time as $E_{th}/E_k \sim t^{-0.5}$. The thermal energy $E_{th} = \frac{1}{2}\langle(\Delta v)^2\rangle$ quantifies local velocity fluctuations, Δv. As E_k decays as t^{-1}, $\Delta v \sim t^{-3/4}$. The local velocity fluctuations $\Delta v \sim t^{-3/4}$, are small compared to the typical velocity $v \sim t^{-1/2}$, as $\Delta v/v \sim t^{-1/4}$. The relatively small velocity fluctuations imply presence of strong velocity correlations and a well-defined average local velocity. Thus, a hydrodynamic description is plausible for the inhomogeneous regime of FCGG.

Hydrodynamical equations of mass, momentum and energy balance [11, 12], can be used to describe the collective motion of granular flow. As the thermal energy, i.e., the temperature T, is negligible compared with the kinetic energy, the system can be expanded around zero temperature. In particular, the pressure term in the momentum equation can be ignored due to the fact that $p \sim T$, while keeping the viscosity term since $\nu \sim T^{1/2}$.

Therefore, the governing equations are given as,

$$\partial_t \rho + \partial_\alpha(\rho u_\alpha) = 0, \tag{2.96}$$

$$\partial_t(\rho u_\alpha) + \partial_\beta(\rho u_\alpha u_\beta) = \partial_\beta \pi_{\alpha\beta}, \tag{2.97}$$

$$\pi_{\alpha\beta} = \partial_\alpha(\rho \nu u_\beta) + \partial_\beta(\rho \nu u_\alpha) - \partial_\gamma(\rho \nu u_\gamma)\delta_{\alpha\beta}, \tag{2.98}$$

taken in the limit of vanishing viscosity, $\nu \to 0$. α, β, γ refer to spatial coordinates x,y, and repeated indices are summed. The above equations are similar to the two dimensional Burgers equation supplemented by the continuity equation [5, 101]. In two dimensions, the formation of shocks corresponds to dense, thin, stringlike clusters as observed in Ref. [12], where particles move parallel to the cluster orientation.

Chapter 3

Computational Methods

3.1 Introduction

Computer simulations are an important tool for studying granular materials. In the absence of a comprehensive theory of granular matter, computer simulations play an important role in developing phenomenology. Among the simulation methods for granular systems, a widely used method is Molecular Dynamics. In conventional Molecular Dynamics (MD) simulation, Newton's equations of motion of all particles in the system are integrated numerically. This method is used for simulating systems with continuous interaction potential. A major improvement in the conventional MD simulation is possible when the particles in the simulation are considered hard. This efficient method is known as Event Driven Molecular Dynamics (ED). In this chapter we describe these two simulation methods in detail.

3.2 Molecular Dynamics Simulations

Granular systems are a collection of macroscopic particles, interacting only on mechanical contact. Quantum effects being not important, the dynamics of this many-body system is governed by Newton's equation of motion. The motion of a particle i is determined by the total force $\vec{F}_i$ exerted on i by all the other particles j, $j \neq i$, $1 \leq j \leq N$:

$$m\frac{d^2\vec{r}_i}{dt^2} = \vec{F}_i, \quad 1 \leq i \leq N, \tag{3.1}$$

where $\vec{r}_i$ is the position of particle i at time t, and m is the mass of a particle. N is the total number of particles in the system. In general, this system of coupled nonlinear differential equations [Eq. (3.1)] can not be solved analytically. The approximate numerical solution of these equations determines the evolution of the system, and is called Molecular Dynamics (MD). This MD is also known as conventional MD or force-based MD. Since granular particles are rather rigid, their repulsive interaction force grows steeply with the compression once the particles are in contact. This rigid nature demands very small integration time step for the computation of trajectories to obtain stable results. Thus, the MD simulation of granular systems is computationally time consuming.

In this thesis, we have used MD to simulate visco-elastic particles. The interaction force between these particles is discussed in detail in Sec. 2.2.3.

3.2.1 Integration Scheme

Once the interaction force is specified, what remains is to numerically integrate Eq. (3.1). In this thesis, we have used Runge-Kutta scheme for numerical integration. Runge-Kutta is a single-step method in the sense that information at only one previous step is required to compute the solution at its present time. Higher order accuracy is achieved by considering intermediate times. Since a differential equation of order l can be reduced to

a system of l first-order equations, we below present Runge-Kutta scheme for solving a first-order differential equation. Consider a first-order differential equation for y with t as the independent variable:

$$\frac{dy}{dt} = f(t, y), \tag{3.2}$$

where the function $f(t, y)$ is known. In Runge-Kutta method, with the value of function y known at $t = t_n$, $y(t = t_n) \equiv y_n$, its value at next step $t_{n+1} = t_n + h$ is computed using a formula of the form

$$y_{n+1} = y_n + h \sum_{i=1}^{z} w_i k_i, \tag{3.3}$$

where h is the integration time step and w_i's are constants. The k_i's are given by

$$k_i = f(t_n + \alpha_i h, y_n + \sum_{j=1}^{i-1} \beta_{ij} k_j), \tag{3.4}$$

where α_i and β_{ij} are constants with $\alpha_1 = 0$. To obtain all these constants, we expand Eq. (3.3) using Taylor series about (t_n, y_n) and match terms up to the required order in h. We here illustrate the procedure for second-order Runge-Kutta method for which $z = 2$. Rearranging and expanding Eq. (3.3)

$$\begin{aligned} y_{n+1} - y_n &= h[w_1 f(t_n, y_n) + w_2 f(t_n + \alpha_2 h, y_n + \beta_{21} k_1)], \\ h y_n' + \frac{h^2}{2} y_n'' + \ldots &= h[w_1 f(t_n, y_n) + w_2 f(t_n + \alpha_2 h, y_n + \beta_{21} h f)], \\ hf + \frac{1}{2} h^2 (f_t + f f_y) + \ldots &= h(w_1 f + w_2 f) + h^2 w_2 (\alpha_2 f_t + \beta_{21} f f_y) + \ldots, \end{aligned} \tag{3.5}$$

where $f = f(t_n, y_n)$, and f_t, f_y are the partial derivatives computed at the same point. Comparing coefficients upto the second order expansion in h from Eq. (3.5) yields:

$$w_1 + w_2 = 1, \quad w_2 \alpha_2 = \frac{1}{2}, \quad w_2 \beta_{21} = \frac{1}{2}. \tag{3.6}$$

Thus, we have three nonlinear equations in four unknowns, which can be solved for w_1, w_2 and β_{21} in terms of α_2. Three standard choices for α are 1/2, 2/3 and 1, yielding following

formulas:

$$y_{n+1} = y_n + hf\left(t_n + \frac{1}{2}h, y_n + \frac{1}{2}hf_n\right), \tag{3.7}$$

$$y_{n+1} = y_n + \frac{1}{4}h\left[f(t_n, y_n) + 3f\left(t_n + \frac{2}{3}h, y_n + \frac{2}{3}hf_n\right)\right], \tag{3.8}$$

$$y_{n+1} = y_n + \frac{1}{2}h\left[f(t_n, y_n) + f\left(t_n + h, y_n + hf_n\right)\right]. \tag{3.9}$$

These are the three standard second-order Runge-Kutta methods for solving differential equation. However, the classical and the most widely used Runge-Kutta method is of fourth order given by:

$$\begin{aligned} y_{n+1} &= y_n + \frac{h}{6}(k_1 + 2k_2 + 2k_3 + k_4), \\ k_1 &= f(t_n, y_n), \\ k_2 &= f(t_n + \frac{1}{2}h, y_n + \frac{1}{2}k_1), \\ k_3 &= f(t_n + \frac{1}{2}h, y_n + \frac{1}{2}k_2), \\ k_4 &= f(t_n + h_n, y_n + k_3). \end{aligned} \tag{3.10}$$

This formula can be derived by expanding Eq. (3.3) upto fourth order in h. The algebra is however quite cumbersome. This fourth-order Runge-Kutta scheme (RK4) is fairly stable for most of the physical problems. Apart from the above mentioned scheme, there are many other fourth-order Runge-Kutta methods.

3.3 Event Driven Molecular Dynamics Simulations

The conventional MD is widely used for simulating systems where the interaction can be expressed in terms of continuous potentials. In conventional MD, the equations of motion are integrated numerically with a time step that is much smaller than the smallest time scale in the problem. The restriction of small time step renders the simulations time con-

suming. In a system where there are no long-range interactions and particles interact only on collision, a major improvement in the computational efficiency is possible if we take the alternative route of step potentials. If the typical duration of a collision is much shorter than the mean free time between successive collisions, collisions can be considered instantaneous. This idealization of considering the collisions to be instantaneous assumes that the particles are perfectly hard, and is sometimes called hard-sphere approximation. In this hard-spheres system, particles follow linear trajectories until they encounter a collision. Collision being an instantaneous process, all collisions in the system are binary. A collision changes the velocities of the involved particles according to a collision law while velocities of other particles remain unchanged. Thus, we have the information about the position and velocity of every particle at every instant. With this information, the future collision events can be easily calculated. This simulation method which proceeds with the discrete events of collision is called Event Driven Molecular Dynamics (ED). This method relying on the series of events is much more efficient than the conventional MD involving time consuming numerical integrations. This method has found enormous success in the study of granular gases as these systems satisfy very well both criteria required by this method: (a) No long-range interaction, and (b) Granular particles are sufficiently hard for the interactions to be instantaneous.

A sketch of event driven algorithm

1. Initialize the positions $\vec{r}_i$, velocities $\vec{v}_i$ and angular velocities $\vec{\omega}_i$ of all particles $1 \leq i \leq N$, at time $t = 0$.

2. Find the earliest occurring collision in the system. For this we must know the time of occurrence of all possible future collisions.

3. Advance the system to the time of occurrence of this earliest collision.

    - The new positions of all particles can be easily computed as particles are mov-

ing ballistically with their present velocities.

- The velocities of colliding particles can be computed from the collision law which gives the post-collision velocities in terms of pre-collision velocities.
- The velocities of other particles remain unchanged.

4. Repeat step 2 – 3 for the desired number of times.

The details needed to execute these steps are explained in following subsections for a system of identical hard-spheres with mass m and diameter d:

3.3.1 Initialization

The positions $\vec{r}_i$, velocities $\vec{v}_i$ and angular velocities $\vec{\omega}_i$ of all particles are assigned at the start of simulation. Care should be taken that there is no overlap between particles as ED simulation deals with hard-particles.

3.3.2 Predicting Future Collisions

Since the ED simulation progresses with collisions events, we must have the information about the next collision occurring in the system, the colliding partners and the time of collision. Two particles i, j moving with velocities $\vec{v}_i$, $\vec{v}_j$ and at positions $\vec{r}_i$, $\vec{r}_j$ at present time t will collide in future at time t^*_{ij} if

$$|(\vec{r}_i + (t^*_{ij} - t)\vec{v}_i) - (\vec{r}_j + (t^*_{ij} - t)\vec{v}_j)| = d, \tag{3.11}$$

has a solution t^*_{ij} with $t^*_{ij} > t$. Defining $\vec{r}_{ij} = \vec{r}_i - \vec{r}_j$ and $\vec{v}_{ij} = \vec{v}_i - \vec{v}_j$, above equation can be rewritten as

$$(t^*_{ij} - t)^2 + 2(t^*_{ij} - t)\frac{\vec{r}_{ij} \cdot \vec{v}_{ij}}{\vec{v}^2_{ij}} + \frac{\vec{r}^2_{ij} - d^2}{\vec{v}^2_{ij}} = 0. \tag{3.12}$$

For a collision to occur, particles must approach each other, thus

$$\vec{r}_{ij} \cdot \vec{v}_{ij} < 0. \tag{3.13}$$

Equation (3.12) has real solutions if

$$\left[\frac{\vec{r}_{ij} \cdot \vec{v}_{ij}}{\vec{v}_{ij}^2}\right]^2 + \frac{d^2 - \vec{r}_{ij}^2}{\vec{v}_{ij}^2} > 0. \tag{3.14}$$

The particles i, j will collide at t_{ij}^* only when Eqs. (3.13) and (3.14) are satisfied. The time t_{ij}^* is given by the solution of Eq. (3.12) and is

$$t_{ij}^* - t = -\frac{\vec{r}_{ij} \cdot \vec{v}_{ij}}{\vec{v}_{ij}^2} - \sqrt{\left(\frac{\vec{r}_{ij} \cdot \vec{v}_{ij}}{\vec{v}_{ij}^2}\right)^2 + \frac{d^2 - \vec{r}_{ij}^2}{\vec{v}_{ij}^2}}. \tag{3.15}$$

The numerical evaluation of Eq. (3.15) in a computer algorithm is not stable. This is because, for very small distances on the particle surfaces ($d \approx |\vec{r}_{ij}|$), the difference of two almost equally large numbers has to be computed which leads to large numerical errors. A mathematically equivalent expression of Eq. (3.15) which is also numerically stable is:

$$t_{ij}^* - t = \frac{\vec{r}_{ij}^2 - d^2}{-\vec{r}_{ij} \cdot \vec{v}_{ij} + \sqrt{\left(\vec{r}_{ij} \cdot \vec{v}_{ij}\right)^2 + \vec{v}_{ij}^2 (d^2 - \vec{r}_{ij}^2)}}. \tag{3.16}$$

Thus, we determine the future collision time t_{ij}^* of all pairs (i, j). The minimum of these gives the earliest future collision time t^*.

3.3.3 Linear Motion

With the system at its present state at time t and the earliest future collision at time t^*, the position of the particles at time t^* is given by:

$$\vec{r}_i(t^*) = \vec{r}_i(t) + (t^* - t)\vec{v}_i(t), \quad 1 \le i \le N. \tag{3.17}$$

3.3.4 Collision Law

Collision alters the velocities of the involved particles deterministically. The collision law determines the post-collision velocities in terms of their pre-collision velocities and coefficient of restitutions. The collision law for rough and smooth particles is discussed in Sec. 2.2.1 and Sec. 2.2.2 respectively.

3.3.5 Cell Division

In order to determine the earliest occurring collision in the system, we must calculate the collision time for all pairs of particles. There are $N(N-1)/2$ pairs and this makes the algorithm inefficient. The efficiency can be considerably improved by dividing the simulation region into small cells whose edge length exceeds the particle diameter d. Particles are associated to different cells according to there position coordinates. Particles occupying same cell or adjacent cells are called neighbours. With this construction, instead of calculating the collision time of a particle with all other $N-1$ particles, we calculate its collision time with neighbouring particles only. It is quite likely for a particle to collide with particles other than its neighbours. Such collisions are taken into account by introducing an additional event known as *cell-crossing*. Cell-crossing is the event of a particle leaving its present cell and crossing to an adjacent cell. This can be easily computed. A particle can collide with particles other than its neighbours only after cell-crossing. Thus, in the event of cell-crossing of a particle, we calculate the future collision time of this particle with its new neighbors. In this way the algorithm never misses any collision. Incorporating cell-crossing events introduces additional work but overall this algorithm makes the number of collision pairs for a particle local and independent of the system size N, greatly improving the efficiency.

3.3.6 Inelastic Collapse

In this subsection, we discuss *inelastic collapse*, a hindrance for event driven simulation of hard inelastic particles, and the proposed methods to avoid inelastic collapse.

Shida and Kawai [102] considered three inelastically colliding point particles on a line. The coefficient of restitution r is assumed to be a constant. It was found that for certain initial velocities of particles, these three particles undergo infinite collisions in finite time, as shown in below sketch, and form one cluster with all particles having the same position and same velocity. The collapse of three particles requires r to be less than $7-4\sqrt{3}$ [102]. This system was further investigated by McNamara and Young [51], where it was found that when r is greater than $7-4\sqrt{3}$, more than three particles are needed for inelastic collapse to occur. It was shown that for r close to 1, the minimum number of particles needed to trigger inelastic collapse is given by $-\ln(1-r)/(1-r)$ [51].

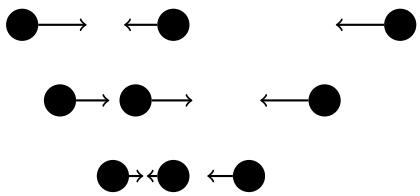

Sketch of an inelastic collapse. For certain initial velocities of particles, the particle in the middle collides alternately with the particle on the left and right leading to vanishing relative velocity and relative position.

Inelastic collapse is not a pathology of one-dimension, as it has been observed in simulation of hard-disks in two-dimensions [90]. It was found that a group of particles align themselves in a straight line and undergo infinite number of collisions in a finite time along that straight line. Inelastic collapse is also observed for particles with rotational degrees of freedom. It was found that the critical value of r for inelastic collapse to occur is larger than for particles without rotational degrees of freedom [103].

Inelastic collapse does not occur for realistic interactions such as viscoelastic interaction.

It is because of dependence of coefficient of restitution on relative velocity of collision. For viscoelastic particles, r is not a constant but increases towards the elastic value of one with decreasing relative velocity. As a result of which, the restriction on r for inelastic collapse to occur is not satisfied for an infinite number of collisions. As soon as the relative velocity is lower than a critical velocity, r becomes higher than the restricted value and eventually the cluster dissolves [104].

Inelastic collapse is a major problem in event driven molecular dynamics simulation of hard core inelastic particles. With a particle undergoing very large number of collisions in a short time, the simulation practically can not proceed beyond that time. Several tricks have been implemented to avoid inelastic collapse. Luding and McNamara introduced the TC model [105], where each collision is assumed to last for a small finite time t_c. If a particle collides again within this time t_c, the second collision is considered as elastic. This model does not satisfy the condition of upper limit on r and interrupts the infinite sequence of collisions. Deltour and Barrat [87] used the idea of rotating the velocities after the collision by a small angle (less than 5°) to avoid inelastic collapse.

A widely used method to circumvent inelastic collapse, suggested in Ref. [51] and first implemented in Ref. [13] is the introduction of a cutoff velocity δ. Collisions are considered inelastic only when the normal relative velocity of collision is greater than this cutoff velocity δ, otherwise elastic. This trick does not obey the restriction on r for the inelastic collapse to occur. It also qualitatively captures the experimentally observed behaviour, where r is seen to be a function of the relative velocity [95, 96]. The value of parameter δ is generally chosen to be sufficiently small compared to the typical relative velocity of collisions in the system. It then affects only those few particles involved in inelastic collapse, and the dynamics of the system is mainly governed by inelastic collisions. We have implemented this particular trick in all of our simulations.

Chapter 4

Energy Decay in Three-Dimensional Freely Cooling Granular Gas

4.1 Introduction

In Chapter 2, we reviewed previous studies on freely cooling granular gas (FCGG) to a good extent. We briefly summarize the important results to make this chapter self-contained. In this chapter, our FCGG consists of hard-core smooth particles. For this system, translational kinetic energy $T(t)$ (defined in Eq. (2.14)) decreases with time t, while rotational energy $K(t)$ (Eq. (2.15)) is conserved. Our primary interest is clustering of particles due to inelastic collisions and the temporal evolution of $T(t)$ at large times t.

At initial times of the evolution of FCGG, particles remain homogeneously distributed and kinetic theory predicts that $T(t)$ decreases as $(1 + t/t_0)^{-2}$ (Haff's law) where the time scale $t_0 \propto (1 - r^2)^{-1}$ for constant coefficient of restitution r [11]. At later times, this regime is destabilized by long wavelength fluctuations into an inhomogeneous cooling regime dominated by clustering of particles [12, 90, 91]. In this latter regime, $T(t)$ no longer obeys Haff's law but decreases as a power law $t^{-\theta_T}$, where θ_T depends only on

dimension D [13, 14]. Direct experiments on inelastic particles under levitation [83] or in microgravity [84, 85] confirm Haff's law. However, being limited by small number of particles and short times, they do not probe the inhomogeneous regime giving no information about θ_T.

Two theoretical conjectures exist for the exponent θ_T. Extensive simulations in one [13] and two [14] dimensions show that for any $r < 1$, the system is akin to a *sticky gas* ($r \to 0$), such that colliding particles stick and form aggregates. If it is assumed that the aggregates are compact spherical objects, then the sticky limit corresponds to the well studied ballistic aggregation model (BA). For BA in the dilute limit and the mean field assumption of uncorrelated aggregate velocities, scaling arguments lead to $\theta_T^{mf} = 2D/(D+2)$ and the presence of a growing length scale $\mathcal{L}_t \sim t^{1/z_{BA}^{mf}}$ with $z_{BA}^{mf} = (D+2)/2$ [15]. In one dimension, BA is exactly solvable and $\theta_T^{BA} = \theta_T^{mf}$ [8, 72]. However, in two dimensions and for dilute systems, it has been shown that θ_T^{mf} is smaller than the numerically obtained θ_T^{BA} by 17% because of strong velocity correlations between colliding aggregates [19, 99].

The sticky limit has also been conjectured [13, 14] to be describable by Burgers-like equation (BE) [101]. This mapping is exact in one dimension [74] and heuristic in two and higher dimensions [14], and leads to $\theta_T^{BE} = 2/3$ in $D = 1$, $\theta_T^{BE} = D/2$ for $2 \le D \le 4$, and $\theta_T^{BE} = 2$ for $D > 4$ [5, 106, 107].

The exponents θ_T^{mf} and θ_T^{BE} coincide with each other in one and two dimensions and also with numerical estimates of θ_T for the FCGG in these dimensions [13, 14]. In three dimensions, they differ with $\theta_T^{mf} = 6/5$ and $\theta_T^{BE} = 3/2$. However, simulations that measure θ_T in three dimensions have been inconclusive, being limited by small system sizes and times, and the measured value of θ_T ranges from $\theta_T = 1.35 - 1.6$ [93] to $\theta_T \sim 1$ [94, 108]. Thus, it remains an open question as to which of the theories, if either, is correct.

To resolve this issue, in this chapter we study the FCGG in three dimensions using event-driven molecular dynamics simulations. We conclude that $\theta_T \approx \theta_T^{mf}$, conclusively ruling out θ_T^{BE} as a possible solution. Comparing with the results of three dimensional BA,

we find that θ_T^{mf} describes the energy decay in BA only when densities are high and multiparticle collisions are dominant. We also find that the cluster size and the velocity distributions of the particles in the FCGG and BA are strikingly different from each other.

The rest of the chapter is organized as follow. In Sec. 4.2, the details of the model and simulation are provided. The simulation results for kinetic energy decay, cluster size distribution and velocity distribution, for FCGG and BA are compared in Sec. 4.3. The chapter is finally concluded in Sec. 4.4.

4.2 Simulation Details

Consider N identical hard-sphere particles distributed uniformly within a periodic three-dimensional box of linear length L and with initial velocities chosen from a normal distribution. The mass and diameter of the particles are set equal to one. All lengths, masses and times are measured in units of particle diameter, particle mass, and initial mean collision time. The system evolves in time without any external input of energy. All particles move ballistically until they undergo momentum conserving, deterministic collisions with other particles. Particles are considered smooth for which the collisions are described by the collision law, Eq. (2.6).

As discussed in Sec. 3.3.6, to avoid inelastic collapse, the coefficient of restitution r is generally chosen to be r_0 (a constant less than unity) for $v_{rel} > \delta$ and 1 (elastic) for $v_{rel} < \delta$, where v_{rel} is the normal component of the relative velocity of the colliding particles and δ is a velocity scale. Thus, only in the limit $\delta \to 0$, all collisions are described by constant coefficient of restitution.

However, the velocity scale δ is relevant experimentally and not just a computational tool. Experimentally, $r(v_{rel})$ approaches 1 when the v_{rel} tends to zero, i.e., $1 - r(v_{rel}) = g(v_{rel}/\delta)$, where $g(x) \sim x^\sigma + O(x^{2\sigma})$, for $x \ll 1$ and $g(x) \sim 1 - r_0$ for $x \to \infty$ [95, 96]. It has also been argued that a constant coefficient of restitution leads to an incomplete description

of granular gas dynamics [9, 70, 71, 81]. Experimentally, the exponent σ takes a variety of values. Within the framework of viscoelastic theory, $\sigma = 1/5$ [10]. A simple model where the above features can be captured is [9]

$$r = (1 - r_0) \exp\left[-\left(\frac{v_{rel}}{\delta}\right)^{\sigma}\right] + r_0. \tag{4.1}$$

For $v_{rel} \ll \delta$, $r \to 1$, and for $v_{rel} \gg \delta$, $r \to r_0 < 1$, capturing the experimentally seen behaviour. The exponent σ characterizes the sharpness of transition from r_0 to 1 around δ. For $\sigma = \infty$, $r = r_0$, for $v_{rel} > \delta$ and 1 otherwise, which is the above described constant coefficient of restitution model.

We simulate both systems, FCGG of hard particles and BA using large scale event-driven molecular dynamics simulations [109, 110] for system sizes up to $N = 8 \times 10^6$. For the hard-core gas, the simulation results are for system with constant coefficient of restitution (independent of v_{rel}), with $\sigma = \infty$ in Eq. (4.1) unless otherwise mentioned.

4.3 Simulation Results

In the following subsections, we first present results for the kinetic energy decay with time for FCGG and BA, followed by the comparison of cluster size and velocity distribution.

4.3.1 Temporal Decay of Kinetic Energy

We first present results for the decrease of kinetic energy with time for the FCGG. As shown in Fig. 4.1, we find that for $r_0 = 0.10$ and volume fraction $\phi = 0.208$, the homogeneous regime is very short-lived and the inhomogeneous regime is reached at early times. However, the energy decay deviates from the universal power law $t^{-\theta_T}$ for times larger than a crossover time that increases with system size L. We assume that $T(t)$ obeys the

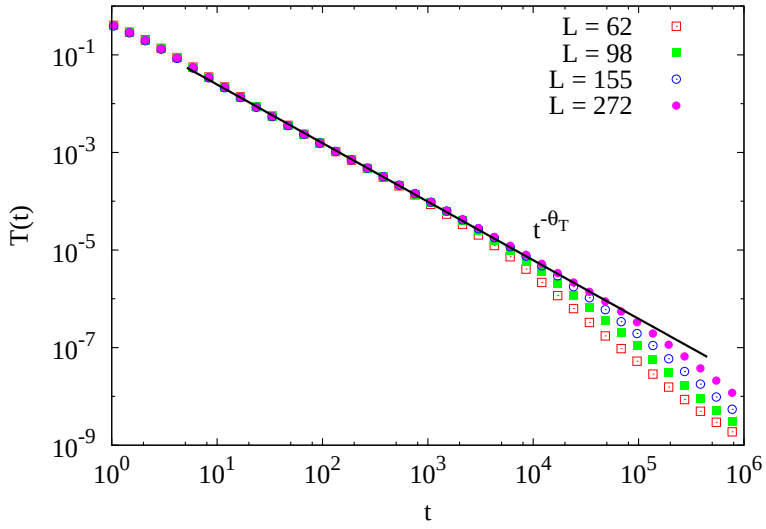

Figure 4.1: The data for kinetic energy $T(t)$ vs time t for different system sizes L. The data are for $\phi = 0.208$, $r_0 = 0.1$, and $\delta = 10^{-4}$.

finite size scaling form

$$T(t) \simeq L^{-z\theta_T} f\left(\frac{t}{L^z}\right), \quad t, L \to \infty, \tag{4.2}$$

where z is the dynamical exponent, and the scaling function $f(x) \sim x^{-\theta_T}$ for $x = tL^{-z} \ll 1$. The simulation data for different L collapse onto a single curve (see Fig. 4.2) when $T(t)$ and t are scaled as in Eq. (4.2) with $\theta_T = \theta_T^{mf} = 6/5$ and $z = z_{BA}^{mf} = 5/2$. The power law $x^{-6/5}$ extends over nearly five decades, confirming that the energy decay in the FCGG in three dimensions has the exponents that are numerically indistinguishable from the mean-field BA. The data conclusively rules out $\theta_T^{BE} = 3/2$ as being the correct exponent. From Fig. 4.2, we see that $f(x) \sim x^{-\eta}$ for $x \gg 1$ with $\eta \approx 1.83$, such that at large times $t \gg L^z$, $T(t) \sim L^{1.58} t^{-1.83}$.

We now show that θ_T measured from the data in Fig. 4.2 is independent of the volume fraction ϕ, coefficient of restitution r_0, and cutoff velocity δ. The systems with varying ϕ are prepared by fixing $L = 272$ and varying N from $2 \times 10^6 (\phi = 0.052)$ to $8 \times 10^6 (\phi = 0.208)$. With increasing ϕ, we find that the crossover from homogeneous ($T(t) \sim t^{-2}$) to inhomogeneous regime ($T(t) \sim t^{-6/5}$) occurs at earlier times [see Fig. 4.3]. In the inhomogeneous regime, the curves are indistinguishable from each other. Thus, we see

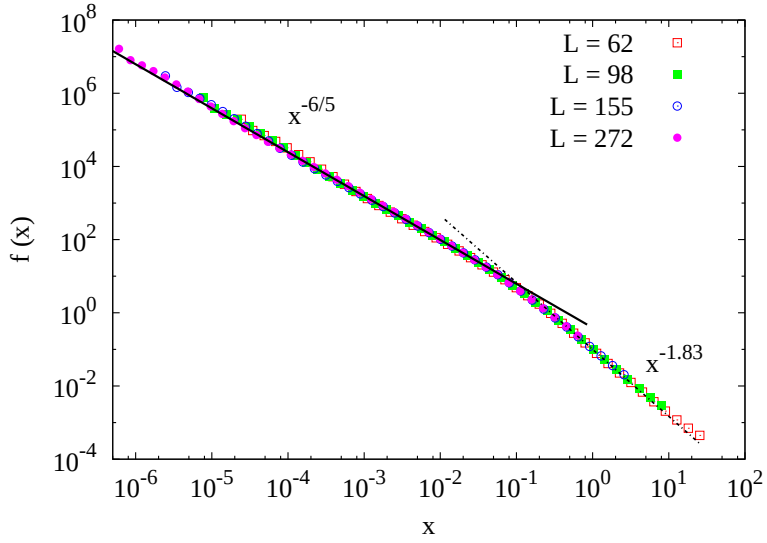

Figure 4.2: The data for kinetic energy $T(t)$ for different system sizes L collapse onto a single curve when t and $T(t)$ are scaled as in Eq. (4.2) with $\theta_T = \theta_T^{mf} = 6/5$ and $z = z_{BA}^{mf} = 5/2$. The power law fits are shown by straight lines. The data are for $\phi = 0.208$, $r_0 = 0.1$, and $\delta = 10^{-4}$.

that the exponent $\theta_T = 6/5$ holds even in the limit $\phi \to 0$. Similarly, with increasing r_0, though the inhomogeneous regime sets in at later times, it nevertheless exists with the same power law $t^{-\theta_T}$ [see Fig. 4.4]. Similar behaviour has been observed in one and two dimensions [13, 14]. We also find no discernible dependence of the data on the parameter δ [see Fig. 4.5]. However, we note that at much larger times ($\sim \delta^{-2/\theta_T}$), collisions become mostly elastic and $T(t)$ stops decreasing with time [13, 111]. A non-zero δ also results in non-trivial coarsening [9].

Finally, we simulate the system using a more realistic velocity dependent coefficient of restitution as in Eq. (4.1) with finite σ. Figure 4.6 shows the decay of $T(t)$ with t for varying σ, where it decays with exponent $\theta_T = 1.2$ independent of σ. Thus, the decay exponent for the velocity dependent coefficient of restitution is indistinguishable from the constant coefficient of restitution value of $\theta_T = 1.2$.

We note that θ_T^{mf} need not be equal to the actual BA exponent θ_T^{BA} [19, 99]. We study this discrepancy in three dimensions by simulating BA directly. Two colliding particles are replaced with a single particle whose volume is the sum of the volumes of the colliding

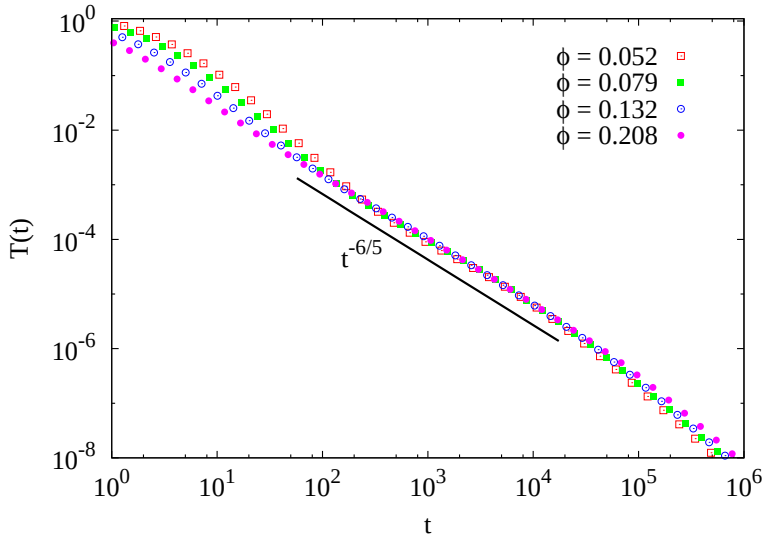

Figure 4.3: The dependence of kinetic energy $T(t)$ on volume fraction ϕ. The solid line is a power law $t^{-6/5}$. The data is for $r_0 = 0.10$, $\delta = 10^{-4}$.

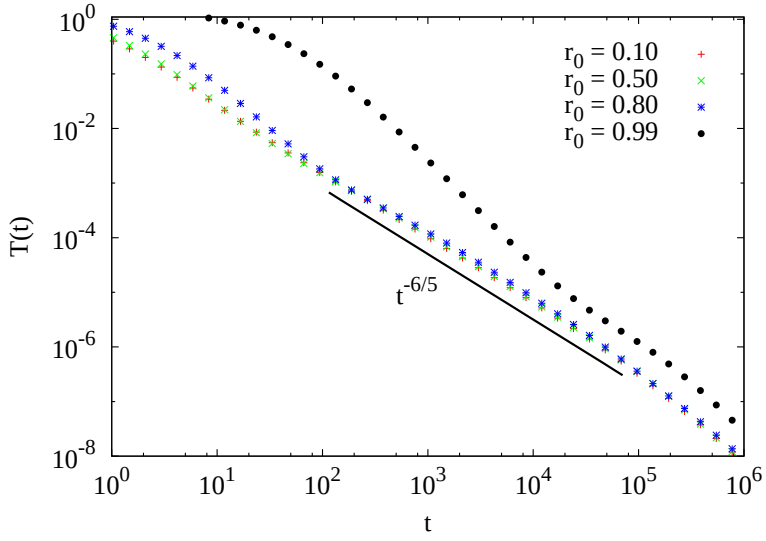

Figure 4.4: The dependence of kinetic energy $T(t)$ on coefficient of restitution r_0. The solid line is a power law $t^{-6/5}$. The data is for $\phi = 0.208$, $\delta = 10^{-4}$.

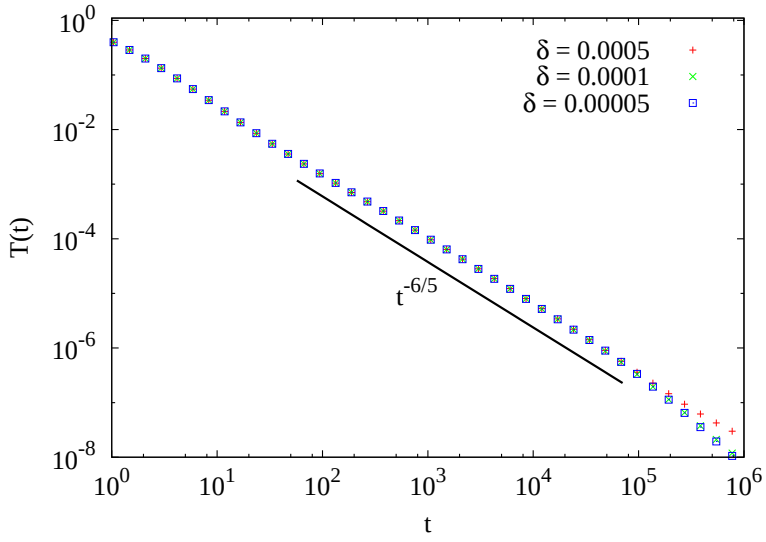

Figure 4.5: The dependence of kinetic energy $T(t)$ on cutoff velocity δ. The solid line is a power law $t^{-6/5}$. The data is for $\phi = 0.208$, $r_0 = 0.10$.

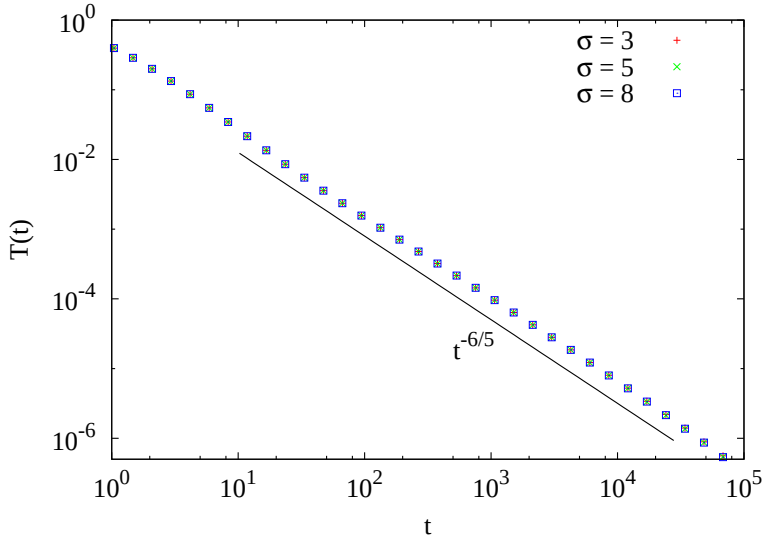

Figure 4.6: The variation of kinetic energy $T(t)$ with time t for a velocity dependent coefficient of restitution [see Eq. (4.1)] for different σ. The data are for $r_0 = 0.1$, $\delta = 10^{-4}$ and $\phi = 0.208$. The straight line is a power law $t^{-6/5}$.

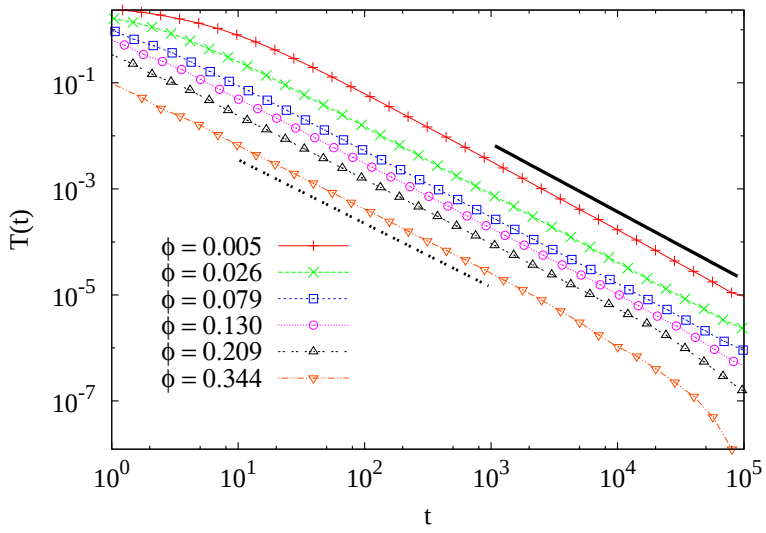

Figure 4.7: Temporal evolution of kinetic energy $T(t)$ for BA, with varying volume fraction ϕ. The bold/dotted lines are power-laws with exponents 1.283/1.202.

Volume fraction ϕ	Decay exponent θ_T^{BA}
0.005	1.283
0.026	1.269
0.079	1.247
0.130	1.216
0.209	1.206
0.344	1.202

Table 4.1: Table showing the dependence of decay exponent θ_T^{BA} on volume fraction ϕ.

particles. The newly formed aggregate may overlap with other particles leading to a chain of aggregation events. These multi-particle collisions result in the exponent θ_T^{BA} being dependent on the volume fraction ϕ. Figure 4.7 shows the temporal decay behaviour of $T(t)$ for various ϕ. We find that as ϕ increases from 0.005 to 0.344, θ_T^{BA} decreases from 1.283 ± 0.005 to 1.202 ± 0.005 and appears to converge to the $\theta_T^{mf} = 1.2$ with increasing ϕ, as shown in Table 4.1. Thus, it is remarkable that the mean field result describes well only the systems with $\phi \gtrsim 0.2$, while its derivation [15] assumes the limit $\phi \to 0$.

4.3.2 Cluster Size Distribution

The energy decay in FCGG and BA at higher densities being similar, how do other statistical properties compare? We first study clusters of particles in the inhomogeneous regime. Snapshots of FCGG and BA (see Fig. 4.8) show that clusters in FCGG are extended as opposed to compact spherical clusters (by construction) in BA. The spatial distribution of particles is partially quantified by measuring the cluster size distribution $N(m,t)$, where m is the size of cluster. For the FCGG, the simulation box is divided into boxes of side equal to the diameter of a particle. A box is said to be occupied if it contains the center of a particle. Two occupied boxes belong to the same cluster if connected by nearest neighbor occupied boxes. The cluster size distribution is then measured using the Hoshen-Kopelman algorithm [112]. $N(m,t)$ for the FCGG and BA, shown in the lower panel of Fig. 4.8, are significantly different from one another. For the FCGG, $N(m,t)$ consists of two parts: a power law ($\sim m^{-2.7}$) and a peak at large cluster sizes. The power law describes all clusters other than the largest cluster that accounts for the peak. The largest cluster contains about 75% of the particles. For BA, $N(m,t)$ is a power law for small cluster sizes ($\sim m^{-0.2}$) and exponential for cluster sizes larger than the mean cluster size. Both of these distributions are different from the mean field result for $N(m,t)$ obtained from the Smoluchowski equation describing the temporal evolution of $N(m,t)$:

$$\dot{N}(m,t) = \sum_{m_1=1}^{m-1} N(m_1,t)N(m-m_1,t)K(m_1,m-m_1) - 2\sum_{m_1=1}^{\infty} N(m_1,t)N(m,t)K(m_1,m)\ m = 1,2,\ldots, \tag{4.3}$$

where

$$K(m_1,m_2) \propto (m_1^{-1/2} + m_2^{-1/2})(m_1^{1/3} + m_2^{1/3})^2 \tag{4.4}$$

is the collision kernel [98, 113]. For this kernel, it is known that that $N(m,t) \sim \exp(-const\times m^{-1/2})$ for small m and $N(m,t) \sim \exp(-const \times m)$ for large m [98]. While the simulation results for BA matches for large m, it is different (being a power law) for small m.

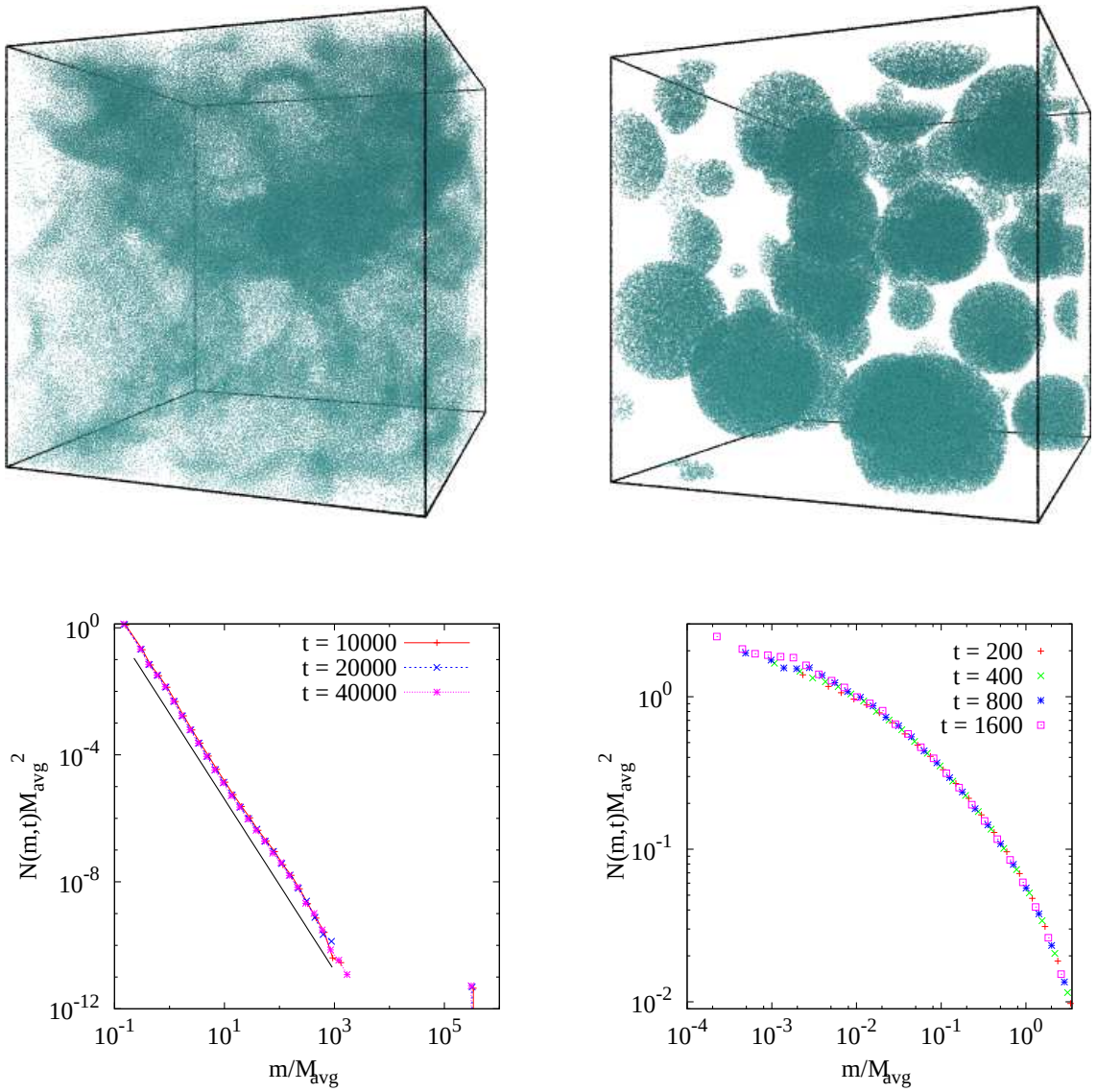

Figure 4.8: Snapshots of FCGG (upper left) and BA (upper right) in the inhomogeneous regime. The lower panel shows the scaled mass distribution for the FCGG (left) and BA (right). M_{avg} is the mean cluster size. The solid line is a power law $m^{-2.7}$. The data are for $\phi = 0.208$, $r_0 = 0.10$.

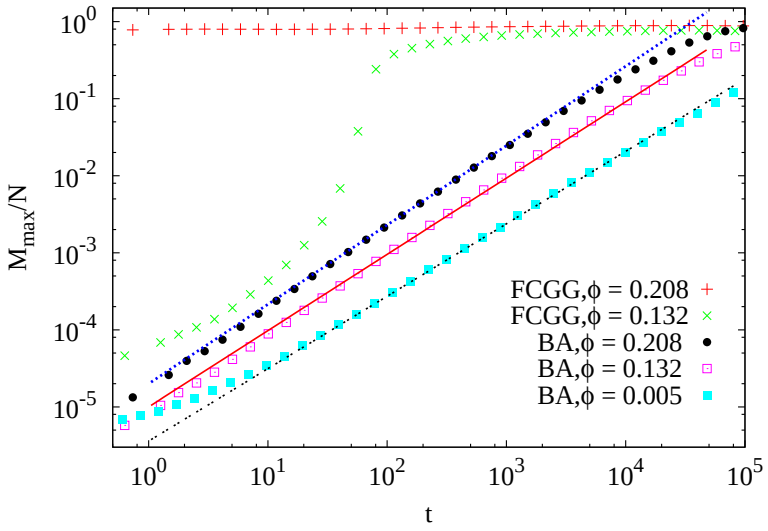

Figure 4.9: The largest mass $M_{\max}$ as a function of time t. For the FCGG, $r_0 = 0.10$, $\delta = 10^{-4}$. Straight lines are power laws $t^{0.94}$, $t^{0.99}$, $t^{1.03}$ (bottom to top).

Also, for the kernel in Eq. (4.4), it is expected that the largest cluster size $M_{\max}$ increases with time t as a power law $t^{6/5}$ [98, 113], the mean field answer. We compare this prediction with the simulations for the FCGG and BA. For the FCGG, rather than a power law growth as in one and two dimensions and in mean field, there is a rapid increase in $M_{\max}$ (see upper two curves of Fig. 4.9) at a time that coincides with the onset of the inhomogeneous cooling regime. This rapid growth is similar to the gelation transition where a gel containing a fraction of the total number of particles is formed in finite time. However the kernel for BA is non-gelling with mass dimension $1/6$, whereas the gelation transition requires mass dimension to be larger than 1 [98, 113]. For BA, $M_{\max}$ increases as a power law (see bottom three curves of Fig. 4.9), with an exponent that increases with ϕ, and possibly converges to the mean field value $6/5$. Similar behavior is seen for the growth of average cluster size of BA which grows as a power law with an exponent ranging from 1.06 for $\phi = 0.005$ to 1.19 for $\phi = 0.313$.

4.3.3 Velocity Distribution

We further compare the velocity distributions $P(v,t)$, where v is any velocity component, of the FCGG with that of BA. $P(v,t)$ has the scaling form

$$P(v,t) = \frac{1}{v_{rms}}\Phi\left(\frac{v}{v_{rms}}\right), \tag{4.5}$$

where v_{rms} is the time dependent root mean square velocity. The scaling function $\Phi(y)$ is shown in Fig. 4.10 for different times. We note that in our simulations $\Phi(y)$ does not depend on the coefficient of restitution or the initial velocity distribution, having checked for Gaussian, uniform, and exponential distributions. For the FCGG, at short times when the system is homogeneous ($t = 5, 10$ in Fig. 4.10), $\Phi(y)$ is an exponential $e^{-\alpha y}$ as predicted by kinetic theory. We find $\alpha = 2.65$, in good agreement with the kinetic theory value 2.60 [89]. For larger times ($t = 2000 - 8000$ in Fig. 4.10), $\Phi(y)$ is clearly non-Gaussian and has a tail that is overpopulated compared to the Gaussian (see comparison with Gaussian in Fig. 4.10). A quantitative measure of the deviation from the Gaussian is the kurtosis,

$$\kappa = \langle v^4\rangle/\langle v^2\rangle^2 - 5/3. \tag{4.6}$$

Its value is zero for a Gaussian distribution. Figure 4.11 shows the time evolution of kurtosis. The kurtosis after an initial increase, decreases and saturates to a non-zero value, showing quantitatively that $\Phi(y)$ is non-Gaussian.

The large y behavior of $\Phi(y)$ is shown in Fig. 4.12. The large y behavior can be understood with a heuristic argument [13, 14]. The large velocity tails are dominated by the fastest particles ($v \approx 1$) present in the system initially, who have managed to avoid any collision and are still moving with their initial velocity at time t. For such a particle to avoid collision, an interval of length $\propto t$ ahead of the particle must be empty. Now, for an initially random spatial distribution, the probability of obtaining such an empty interval decays exponentially with length, giving the survival probabil-

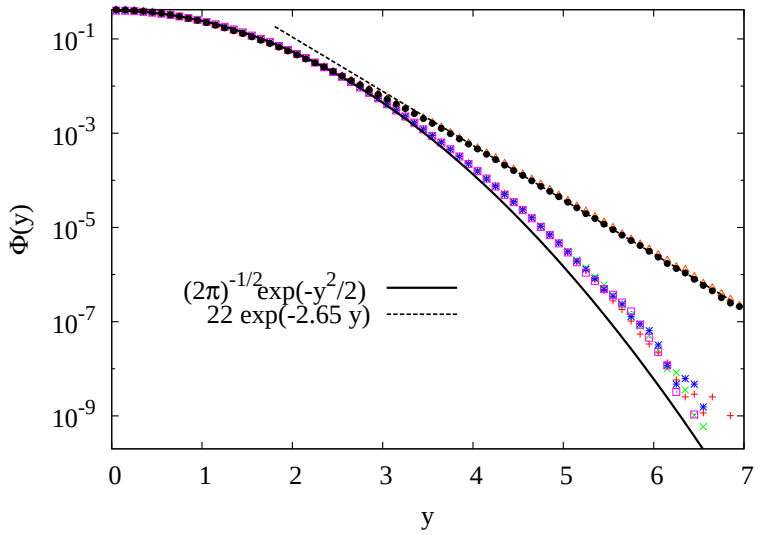

Figure 4.10: The scaled velocity distribution function $\Phi(y)$ for the FCGG at times $t = 5, 10$ (upper collapsed data) and $t = 2000, 4000, 6000, 8000$ (lower collapsed data). The solid curve is a Gaussian. The data are for $\phi = 0.208$, $r_0 = 0.10$.

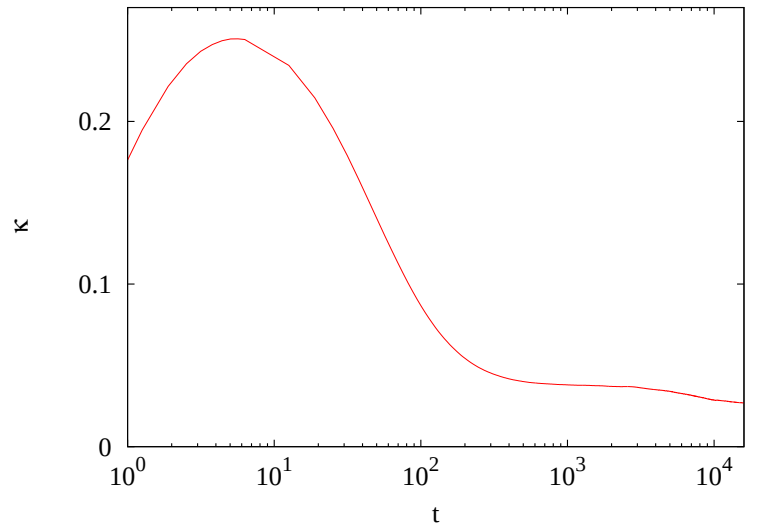

Figure 4.11: The kurtosis κ as a function of time t. The data are for $\phi = 0.208$, $r_0 = 0.10$.

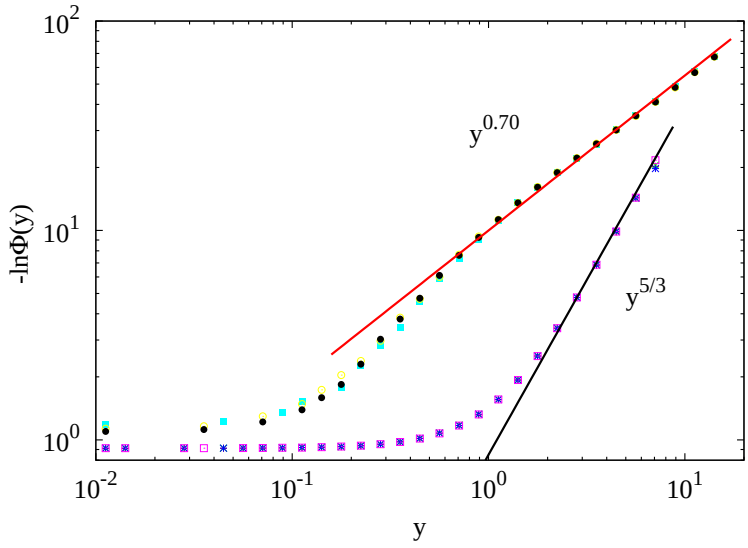

Figure 4.12: $-\ln\Phi(y)$ as a function of y for the FCGG (lower data) and BA (upper data). For FCGG, the times are $t = 2000, 4000, 6000, 8000$ and $\phi = 0.208$, $r_0 = 0.10$. For BA, the times are $t = 400, 800, 1600$ and $\phi = 0.208$.

ity $S(v = 1, t) \propto \exp(-\text{constant} \times t)$. Thus, the distribution for the fastest particles at time t, $P(1,t) = P(1,0)S(1,t) \propto \exp(-\text{constant} \times t)$. We assume a stretched exponential large-velocity tail for the scaling function $\Phi(y) \sim \exp(-\text{constant} \times |y|^\gamma)$, for $y \to \infty$, with $y = v/v_{rms} \sim vt^{\theta_T/2}$. Comparison of $P(1,t)$ from the survival probability argument with the scaling behavior $P(1,t) \sim \exp(-\text{constant} \times t^{\gamma\theta_T/2})$ gives $\gamma = 2/\theta_T$. For the FCGG (see Fig. 4.12), we find that $-\ln[\Phi(y)] \sim y^{5/3}$, consistent with the heuristic argument, with $\theta_T = 6/5$. However, for BA we find $-\ln[\Phi(y)] \sim y^{0.70}$. The deviation of BA is surprising, but may be rationalized. The argument for the exponential form of survival probability implicitly assumes that the number of clusters reach a time independent distribution resulting in a constant rate of collision. That this is true for the FCGG and not for BA can be seen from the lower panels of Fig. 4.8, where $M_{\max}$ and hence M_{avg} is nearly a constant for the FCGG and time dependent for BA (see Fig. 4.9) at large times.

Thus, in spite of having the same form of energy decay, the local environment that a particle in a FCGG sees around itself, is distinct from those in BA. In BA, two colliding clusters rearrange their masses to form a new spherical cluster at every step. Due to the lack of such dynamic cluster rearrangements, the FCGG remains locally structurally

anisotropic and disordered, as well as has a velocity distribution distinct from BA as discussed above.

4.4 Conclusion

To summarize this chapter, we studied FCGG in three dimensions using large-scale event driven molecular dynamics simulations. We found that the energy $T(t)$ of this system decreases as $t^{-\theta_T}$, with $\theta_T \approx 6/5$. This decay exponent is universal, i.e., independent of the system parameters such as volume fraction, coefficient of restitution. The energy continues to decay with the same exponent $\theta_T \approx 6/5$, when a more realistic, velocity dependent coefficient of restitution model is considered.

This rules out Burgers like equations as a description of the FCGG at large times, which predicted θ_T to be 1.5 in three dimensions. Our observed θ_T is indistinguishable from the mean field result for dilute ballistic aggregation. The relation to ballistic aggregation appears coincidental, as our direct numerical simulation of ballistic aggregation shows that the energy of the dilute ballistic gas decaying with a different exponent. In addition, the cluster size distribution as well as the velocity distribution of ballistic aggregation are strikingly different from that of the FCGG. Thus, our study concludes that the freely cooling FCGG fits to neither the ballistic aggregation or a Burgers equation description.

Chapter 5

Inhomogeneous Cooling of the Rough Granular Gas in Two Dimensions

5.1 Introduction

In Chapter 4, we studied freely cooling granular gas of hard-core smooth particles, which is also termed as smooth granular gas (SGG). In SGG, dissipation is considered only in normal direction of collision which is accounted by the coefficient of normal restitution r. However, realistic models of non-sliding collisions of hard spheres involve one more parameter, the coefficient of tangential restitution β, quantifying the dissipation in tangential direction of collisions [50, 114, 115, 116, 117]. This parameter β characterizing tangential dissipation is ignored in most studies of the freely cooling granular gas.

In this chapter, we extend our study of freely cooling granular gas by including this parameter β. When the collisions include tangential dissipation β, the translational and rotational modes are no longer independent of each other [16, 88, 118, 119, 120, 121, 122, 123, 124]. We call this model the rough granular gas (RGG). Of primary interest in this model is the evolution of the translational kinetic energy $T(t)$ and rotational energy $K(t)$ with time t,

defined in Eqs. (2.14) and (2.15).

Studies of RGG have been limited to the homogeneous cooling regime. In this regime, kinetic theory [16, 88, 118, 119, 120, 121] and simulations [16, 121] show that both translational energy $T(t)$ and rotational energy $K(t)$ decreases as t^{-2}. However, the partitioning of energy into the rotational and translational modes does not follow equilibrium equipartitioning, and depends on both r and β. In addition, the directions of the translational and angular velocities of a particle were found to be strongly correlated [122, 125].

The inhomogeneous clustered regime of RGG is poorly studied. In this chapter, we study the inhomogeneous regime of two dimensional RGG using large scale event driven molecular dynamics simulations. Let $T(t) \sim t^{-\theta_T}$ and $K(t) \sim t^{-\theta_K}$ in this regime. We show that θ_T is independent of β and is the same as that for SGG, i.e., $\theta_T \approx 1$. The exponent θ_K is also shown to be independent of the choice of r and β, $|\beta| < 1$ and to be $\theta_K = 1.60 \pm 0.04$, different from $\theta_K = 2$ in the homogeneous regime. Thus, unlike the homogeneous regime, the two exponents θ_T, θ_K differ from each other. These exponents are compared with the corresponding exponents for BA with rotational degrees of freedom. The translational energy of BA is independent of its rotational degrees of freedom and hence $\theta_T^{BA} \approx 1$ for large enough initial densities [99]. Numerically, we find that $\theta_K^{BA} \approx 1$ for BA. We conclude that the large time limit of RGG is different from that of BA, even though clustering is present. Finally, we extend the scaling arguments of Ref. [15] to BA with rotational degree of freedom. The scaling arguments predict $\theta_K^{mf} = 1$ in two dimensions. This is clearly in contradiction with the numerically obtained value of 1.6 ± 0.04. This further supports the view [19, 99, 126], as concluded in previous chapter, that the energy decay in the SGG being described accurately by $\theta_T^{mf} = 2D/(D+2)$ in D dimensions is a coincidence.

The rest of the chapter is organized as follows. In Sec. 5.2, simulation details are provided. The mean-field scaling theory of BA is recapitulated for SGG and extended to RGG in Sec. 5.3. Section 5.4 contains simulation results for RGG and BA. Finally, we conclude this chapter with a discussion in Sec. 5.5.

5.2 Simulation Details

Consider a system of N identical hard disks distributed uniformly in a two-dimensional volume of linear length L with periodic boundary conditions in both directions. The mass and diameter of the disks are taken to be unity. Initial translational and angular velocities are drawn from a Gaussian distribution with mean zero and variance 1 and 8 respectively. The variances are such that $T(0) = 2K(0)$. Thus, energy is equipartitioned between all three modes as one would expect in equilibrium. A particle moves ballistically till it collides with another particle. Particles are considered rough for which the collisions are described by the collision law, Eq. (2.5). We note that the translational kinetic energy and rotational energy are both conserved only when $r = 1$(elastic) and $\beta = -1$. In this chapter, we assume r and β to be constants, independent of the relative velocity of collision. BA with rotational degree of freedom is discussed in detail in Sec. 2.7.1.

We simulate both RGG and BA in two dimensions using event driven molecular dynamics simulations [110]. As discussed in last paragraph of Sec. 3.3.6, a cutoff velocity δ is used to avoid inelastic collapse. This cutoff velocity introduces a timescale beyond which collisions are mostly elastic, and the systems crosses over to a new regime where energy is a constant. In our simulations, we choose $\delta = 10^{-5}$ for which we check that this crossover timescale is much larger than the largest time in our simulations. Thus, the results in this chapter are independent of δ. The results are for a system of $N = 1562500$ particles and $L = 2500$ (volume fraction = 0.20).

5.3 Scaling Theory for Rotational Energy in Ballistic Aggregation

The exponent θ_K^{mf} for BA may be determined using scaling arguments. In BA, particles form spherical aggregates on collision. We first recapitulate the calculation of θ_T^{mf} =

$2D/(D+2)$ [15] as outlined in Refs. [19, 127]. Let n be the number density. It evolves in time as

$$\frac{dn}{dt} = -\frac{n}{\tau}, \tag{5.1}$$

where τ is the mean collision time. In D dimensions,

$$\frac{1}{\tau} \sim n v_{rms} R_t^{D-1}, \tag{5.2}$$

where v_{rms} is the root mean squared velocity and R_t is the radius of a typical aggregate at time t. Since total mass is conserved, $M_t n \sim 1$ or equivalently $R_t \sim n^{-1/D}$. Substituting for τ from Eq. (5.2) in Eq. (5.1),

$$\frac{dn}{dt} \sim -n^{1+1/D} v_{rms}. \tag{5.3}$$

The dependence of v_{rms} on M_t is required. An aggregate of mass M_t is formed by aggregation of M_t particles of mass 1. Conservation of linear momentum, combined with the assumption of uncorrelated momenta, gives $M_t v_{rms} \sim M_t^{1/2}$, or $v_{rms} \sim n^{1/2}$. Substituting for v_{rms} in Eq. (5.3), we obtain

$$n(t) \sim t^{-2D/(D+2)}. \tag{5.4}$$

The scaling of root mean square angular velocity ω_{rms} with time t may be obtained from conservation of angular momentum. If two particles i and j of masses m_i, m_j at $\vec{r}_i$, $\vec{r}_j$, moving with velocities $\vec{v}_i$, $\vec{v}_j$, angular velocities $\vec{\omega}_i$, $\vec{\omega}_j$, and moment of inertia I_i and I_j collide to form a particle of mass m' at $\vec{r'}$ with velocity $\vec{v'}$, and moment of inertia I', then its angular velocity $\vec{\omega'}$ is given by

$$I'\vec{\omega'} = I_i\vec{\omega}_i + I_j\vec{\omega}_j + \frac{m_i m_j}{m_i + m_j}(\vec{r}_i - \vec{r}_j) \times (\vec{v}_i - \vec{v}_j). \tag{5.5}$$

Let ω_{rms} be the root mean square angular velocity of the typical particle whose moment of inertia is $I_t \sim M_t R_t^2$. In Eq. (5.5), there are three terms on the right hand side. We

first assume that the right hand side is dominated by the first two terms. Then the angular momentum $I_t\omega_{rms}$ is a sum of M_t random variables of mean zero and variance order 1, giving

$$I_t\omega_{rms} \sim \sqrt{M_t}. \tag{5.6}$$

or equivalently $\omega_{rms} \sim M_t^{-(D+4)/(2D)}$. But the rotational energy $K(t)$ scales as $K \sim nI_t\omega_{rms}^2$. Simplifying, we obtain $K \sim t^{-2}$, independent of dimension. We now assume that the right hand side of Eq. (5.5) is dominated by the third term. Then, clearly $I_t\omega_{rms} \sim M_tR_tv_{rms}$. Using $M_tn \sim 1$, we obtain $\omega_{rms} \sim n^{(D+2)/(2D)} \sim t^{-1}$. The rotational energy $I_t\omega_{rms}^2$ now scales as $t^{-2D/(D+2)}$. This has a slower decay in time than t^{-2} obtained from assuming that Eq. (5.5) is dominated by the first two terms. The kinetic energy $T \sim nM_tv_{rms}^2$ and rotational energy K are thus given by

$$T \sim t^{-2D/(D+2)}, \tag{5.7}$$

$$K \sim t^{-2D/(D+2)}, \tag{5.8}$$

implying that $\theta_T^{mf} = \theta_K^{mf} = 2D/(D+2)$. Thus, one expects that the ratio of the two energies is a constant in the clustered inhomogeneous regime as it is in the homogeneous regime.

5.4 Simulation Results

5.4.1 Rough Granular Gas (RGG)

We now present results for RGG obtained from numerical simulations. Figures 5.1 and 5.2 show the temporal evolution of translational kinetic energy $T(t)$. Here, the coefficient of normal restitution $r = 0.1$. For this value of r, the homogeneous regime is short lived. The crossover time from the homogeneous to inhomogeneous regime depends on β, the crossover time increasing with $|\beta|$. This is expected as increasing $|\beta|$ corresponds to de-

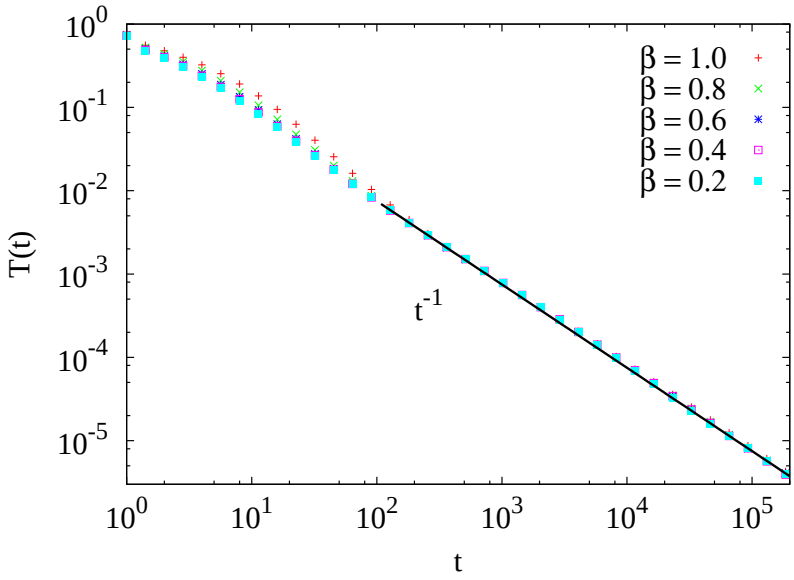

Figure 5.1: Time evolution of translational kinetic energy $T(t)$ for RGG when $\beta > 0$ for fixed $r = 0.10$.

creasing dissipation, and hence a longer homogeneous regime. For $\beta < 0$, the dependence of the crossover time on β is very weak. For all values of β, the data is consistent with $\theta_T = 1$ (see Figs. 5.1 and 5.2), same as that obtained for SGG [14]. We check that the θ_T remains the same for $r = 0.5$ and $r = 1.0$ (but $|\beta| < 1$). We conclude that θ_T for RGG is independent of the values of both r and β. These extend the results obtained earlier for SGG ($\beta = -1$), where θ_T was shown to be independent of r [13, 14, 126].

Figures 5.3 and 5.4 show the temporal evolution of rotational energy $K(t)$ for $\beta > 0$ and $\beta < 0$ respectively. The crossover to inhomogeneous regime occurs at a much later time when compared with $T(t)$. A signature of this difference in crossover times was observed in Ref. [16], where T was found to deviate from the homogeneous cooling behaviour of t^{-2} decay, while K still followed it. We also observe that the crossover times are much larger for $\beta < 0$ as compared to that $\beta > 0$. When $\beta = -1$, $K(t)$ is conserved. At large times, the data for $K(t)$ are completely independent of β (see Figs. 5.3 and 5.4). We estimate $\theta_K = 1.60 \pm 0.04$.

We also confirm that θ_K is independent of r. In Fig. 5.5, we show the dependence of $K(t)$ on r by varying r and keeping $\beta = 0.60$ fixed. $K(t)$, while decaying with a r-

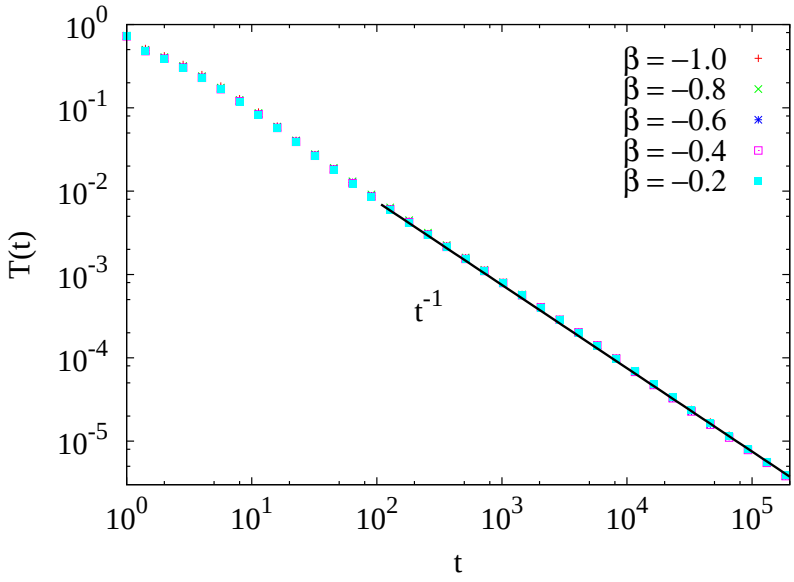

Figure 5.2: Time evolution of translational kinetic energy $T(t)$ for RGG when $\beta < 0$ for fixed $r = 0.10$.

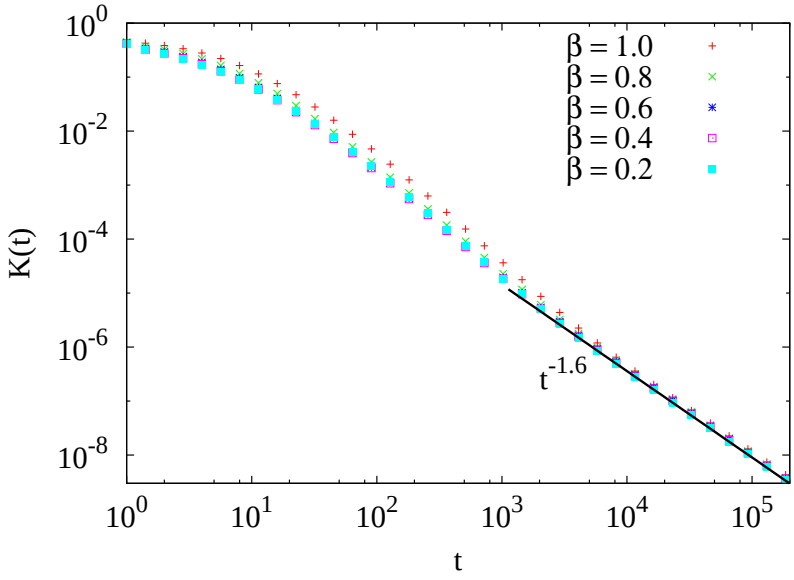

Figure 5.3: Time evolution of rotational energy $K(t)$ of RGG for $\beta > 0$ and fixed $r = 0.10$.

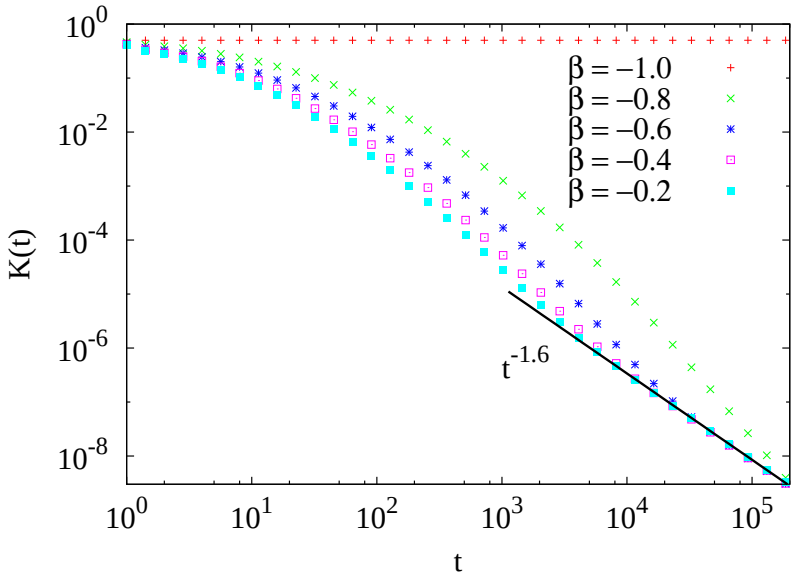

Figure 5.4: Time evolution of rotational energy $K(t)$ of RGG for $\beta < 0$ and fixed $r = 0.10$.

independent exponent, now has a r-dependent pre-factor. Thus, we conclude that at large times, $K(t) \simeq A(r)t^{-\theta_K}$, where $\theta_K \approx 1.60$ is independent of r and β.

5.4.2 Ballistic Aggregation (BA)

We now present the results from numerical simulations of BA. In these simulations, whenever two particles collide we replace them with a single spherical particle conserving mass, volume, linear and angular momenta as described in Eqs. (2.59)–(2.62). If the new particle overlaps with another particle, then these two particles aggregate. Thus, a collision between two particles may give rise to a chain of aggregation events.

For BA, it is easy to check from Eqs. (2.59) and (2.60) that including rotational degrees of freedom does not affect the translational kinetic energy $T(t)$. That being the case, we expect that θ_T^{BA} for the rough BA to be identical to that for the smooth BA. The numerical values of θ_T^{BA} for the rough BA for different initial volume fraction ϕ are tabulated in the second column of Table 5.1. θ_T^{BA} depends weakly on ϕ [19, 99, 126], and approaches 1 with increasing ϕ. $\theta_T^{BA} = 1$ for BA is consistent with the scaling arguments [see Eq. (5.7)], and is equal to θ_T for RGG.

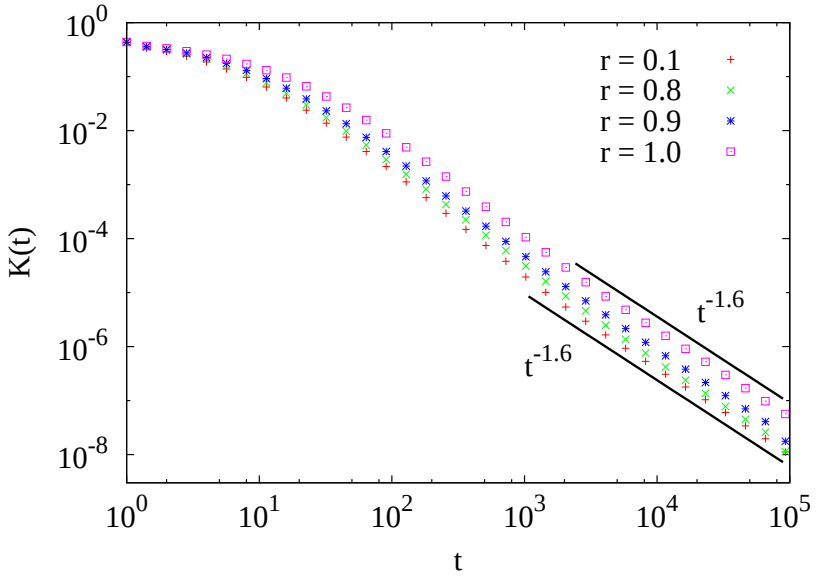

Figure 5.5: Time evolution of rotational energy $K(t)$ of RGG for different r and fixed $\beta = 0.60$.

Table 5.1: Dependence of exponents θ_T^{BA} and θ_K^{BA} on volume fraction ϕ in the BA model.

ϕ	θ_T^{BA}	θ_K^{BA}
0.008	1.12-1.13	1.10-1.12
0.079	1.05-1.06	1.07-1.08
0.196	1.01-1.02	1.03-1.04
0.393	1.01-1.02	1.00-1.01

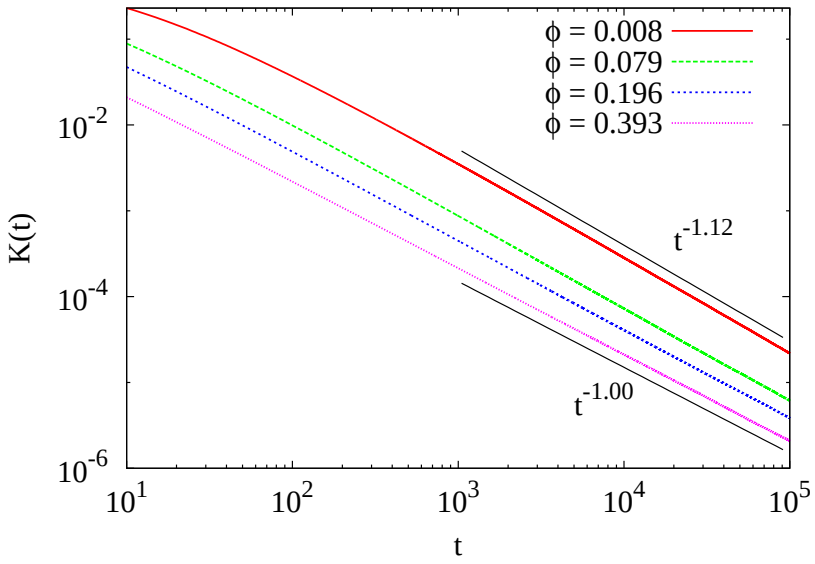

Figure 5.6: Time evolution of the rotational energy $K(t)$ of BA for different volume fractions ϕ.

The variation of the rotational kinetic energy $K(t)$ for BA with time t is shown in Fig. 5.6. Similar to θ_T^{BA}, θ_K^{BA} also decreases with increasing volume fraction ϕ (see third column of Table 5.1). With increasing ϕ, θ_K^{BA} converges to a value very close to 1, different from that obtained for RGG. Note that the scaling argument for BA predicts $\theta_K^{mf} = 1$ (see Eq. 5.8).

5.5 Conclusion

To summarize, we investigated the large time behaviour of a freely cooling rough granular gas in two dimensions using event-driven simulations. Each collision dissipates energy in both the normal and tangential directions. We showed that in the clustered inhomogeneous regime, both the translational kinetic energy $T(t)$ and the rotational energy $K(t)$ decay with time t as power-laws $A_T t^{-\theta_T}$ and $A_K t^{-\theta_K}$ where $\theta_T \approx 1.0$, and $\theta_K \approx 1.6$. These exponents are universal and independent of r and β. Within numerical errors, A_T is also independent of r and β, while A_K depends only on r. For ballistic aggregation with rotational degree of freedom, wherein particles coalesce on contact, we find that $\theta_T^{BA} \approx 1.0$ and $\theta_K^{BA} \approx 1.0$ for large enough initial volume fraction ϕ. By extending an earlier scaling

theory for BA, we obtain $\theta_K^{mf} = 1$, consistent with the numerically obtained value.

Kinetic theory for rough granular gases predicts that $K(t)/T(t)$ tends to a non-zero constant that depends on r and β [16, 118, 121]. In the inhomogeneous regime, since $\theta_T < \theta_K$ for the rough granular gas, the ratio $K(t)/T(t)$ tends to zero at large times. Violation of kinetic theory is not surprising given that it assumes that particles are homogeneously distributed, which is not the case in the inhomogeneous regime.

The clustered regime of the freely cooling granular gas has been often thought to be describable by the large time behaviour of the ballistic aggregation model. This analogy has been reinforced in particular by the fact that, within numerical error, energy decay in both systems is the same in one, two and three dimensions [13, 14, 126]. However, it has been shown that correlation functions that capture spatial distribution of particles and the velocity distributions in the granular gas are different from that of BA [9, 126]. In particular, it has been argued that a coarse grained model with aggregation and fragmentation is more suitable to study the clustered regime than one of pure aggregation as in the BA model [71]. Here, the fact that the rotational energies in the two models decay with two exponents is further evidence that the analogy should be used with care.

In the scaling arguments presented in this chapter and in Ref. [15], the correlations between velocities of colliding particles are ignored. Therefore, it has often been argued that the efficacy of the scaling arguments is a coincidence [19, 99]. In this paper, we showed that the extension of the scaling arguments to rotational energies correctly predict the numerical results for BA, albeit for larger volume fractions ϕ. We conclude that the scaling arguments are quite robust, rather the connection to granular gas is more suspect.

Chapter 6

Shock Propagation in Granular Flow Subjected to an External Impact

6.1 Introduction

In this chapter, we study the *granular explosion* model. This model is a special case of freely cooling granular gas, where all particles, except for a few localised particles, are at rest. The name granular explosion stems from the similarity of this model to a bomb/nuclear explosion [128, 129, 130], where a large amount of energy is deposited at one place giving rise to a shock wave. Locally perturbed systems are the subject matter of many recent experiments. Examples include crater formation by wind jets in the context of lunar cratering [131], viscous fingering in grains confined in a Hele-Shaw cell when displaced by gas or liquid [62, 132, 133], shock propagation in flowing glass beads following a sudden impact [6], signal propagation in dilute granular gas [134] as well as in dense static granular material (see [135] and references within), and avalanches in sand piles [136].

The granular explosion model is the inelastic version of the classic Taylor-von Neumann-

Sedov problem of shock propagation following a localized intense explosion [129]. In the latter case, the exponents characterizing the power law growth of the radius of the disturbance follows from energy conservation and simple dimensional analysis [128], while the scaling functions can be calculated exactly following a more detailed analysis [129, 130]. Theoretical, numerical and experimental studies of this problem are summarized in Refs. [137, 138]. Simulations in a hard sphere model with elastic collisions reproduce the results based on scaling arguments [139].

The granular explosion model was studied in Ref. [7] with hard inelastic particles using event driven molecular dynamics simulations, and scaling arguments. By identifying radial momentum as a conserved quantity, and using scaling arguments, the radius of disturbance $R(t)$ was predicted to increase with time t as a power law $t^{1/(D+1)}$ in D-dimensions. This result was shown to be in very good agreement with data from numerical simulations of the model.

In this chapter, we focus on an experiment [6] (henceforth referred to as BCK) on a dilute monolayer of glass beads flowing on an inclined glass plane. In the experiment, a steel ball, much larger in size than an individual glass bead, is dropped from a height onto the flowing beads. The impact generates a circular region, devoid of glass beads, whose radius increases with time. This radius was measured using high speed cameras. A theoretical model was proposed, and analyzed to derive an equation obeyed by the radius. The numerical solution of the equation was shown to match with the experimental data [6].

The inelastic granular explosion model closely resembles the experimental system in BCK, in the limit when the impact is very intense. In this chapter, we propose the power law $t^{1/3}$ ($D = 2$) as an alternate description of the radius of disturbance in the BCK experiment. By re-examining the data in BCK, we show that, there are temporal regimes in which the power law growth is a good description. At late times, the experimental data deviate from the $t^{1/3}$ behavior. This, we argue is due to the experimental system be-

coming effectively three dimensional due to accumulation of particles at the shock front, and propose a simple model incorporating this effect. Our numerical data, obtained from simulations of this model, show clearly the crossover and captures the long time behavior. Since these results are in contradiction to those presented in BCK, we further analyze the model proposed in BCK, and point out some shortcomings. In particular, we show numerically that the main assumption of BCK is not correct. Though the experimental data are not able to distinguish between the two theories because the time scales are not large enough, the simulation data clearly bring out the deficiencies of the BCK theory at large times.

A key feature of the freely cooling granular gas is the clustering due to inelastic collisions. The freely cooling gas is well understood in one dimension and progressively less understood as the dimension increases [13, 14, 15, 19, 93, 140]. Such systems are challenging experimentally because inelasticity is overwhelmed by friction and boundary effects. Friction can be eliminated in experiments on particles under levitation [83] or in microgravity [84, 85], but are expensive to perform and are limited by small number of particles and short times. In BCK, friction is balanced by gravity, and at high enough impact energies, in the center of mass frame, mimics a stationary collection of inelastic particles without friction. The boundary effects are eliminated as long as the shock does not reach the edges of the container. Thus, it is an experiment where clustering due to inelastic collisions can be studied easily.

The rest of the chapter is organized as follows. In Sec. 6.2, we define the hard core granular explosion model. The temporal patterns arising in the system are discussed in Sec. 6.3. The growth of radius of disturbance with time is obtained, using argument of radial momentum conservation. In Sec. 6.4 we describe the experimental setup of BCK, and the theoretical model reviewing the arguments that lead to the equation obeyed by the radius of the disturbance. This equation is further analyzed to derive the asymptotic long time behavior. The shortcomings of the BCK analysis are pointed out in Sec 6.5.

Our model reproduces the basic features of the experiment in BCK. The assumptions of the analysis in BCK is tested within this model and counter evidence is presented. In Sec. 6.6, we compare the experimental results in Ref. [6] with the power law growth rules obtained in Ref. [7]. The data at intermediate times are well described by these power laws. However, there is a crossover to a different behavior at large times. We examine whether this large time behavior can be explained in terms of velocity fluctuations of the particles or by making the rim three dimensional. We argue that it is plausible that the three dimensional rim is responsible for deviation from power law growth and verify this by simulation. This chapter is summarized in Sec. 6.7.

6.2 Model

The model is defined as follows. Consider a collection of identical hard sphere particles, in two dimensions. The mass and diameter of the particles are set to unity. All the particles are initially at rest and have a packing density 0.20, much smaller than the known random closed packed density 0.84 in two dimensions [141, 142]. We model an isotropic impulse by introducing four particles at the center with speed v_0 in the directions $0, \pi/2, \pi$, and $3\pi/2$. Particles move ballistically until they undergo momentum conserving, deterministic collisions with other particles. Particles are considered smooth for which the collisions are described by the collision law, Eq. (2.6). The coefficient of restitution $r = 1$ for elastic and $0 < r < 1$ for inelastic collisions. As discussed in last paragraph of Sec. 3.3.6, to avoid inelastic collapse in the inelastic system, a cutoff velocity δ is used, below which collisions are considered elastic. The cutoff δ introduces a timescale in the problem at large times, after which most of the collisions are elastic. For sufficiently small δ, the elastic crossover timescale does not show up in our simulations.

We simulate the system in two dimensions using event driven molecular dynamics [110]. The data are typically averaged over 8 different initial realizations of the particle config-

urations. All lengths are measured in units of the particle diameter, and time in units of initial mean collision time $t_0 = v_0^{-1} n^{-1/D}$, where v_0 is the initial speed, n is the number density. The value of δ is 10^{-4}, unless specified otherwise. For these values of δ, all the quantities that we measure except for the rate of collisions are independent of δ [7]. The initial speed is $v_0 = 1$ unless specified otherwise.

6.3 Analysis of the Model

In this section, we present the results obtained by the numerical simulation of the model. The numerical results are explained by analysis based on radial momentum conservation.

6.3.1 Pattern Formation

First we consider the elastic system with $r = 1$. Figure 6.1 shows the time evolution of the elastic system following an isotropic impulse. The four particles with non-zero initial velocity set off a cascade of collisions leading to the formation of a circular region of moving particles. This circular region grows outwards because of the collision of moving particles near the boundary with the outside stationary particles.

The quantity of interest is the radius of disturbance $R(t)$ which is defined as the average distance of a moving particle from the center of mass of moving particles. Its temporal growth has been obtained by using simple dimensional analysis and energy conservation [128, 129, 130]. We reproduce it using simple scaling arguments. Assuming a power-law growth for the radius of disturbance, $R(t) \sim t^{\alpha}$, the typical velocity of a moving particle is $V(t) = dR/dt \sim t^{\alpha-1}$, and the number of particles moving is $N_m(t) \sim R(t)^D \sim t^{\alpha D}$. The total energy of the system, $E(t) \sim N_m(t) V(t)^2 \sim t^{\alpha(D+2)-2}$, is constant with time,

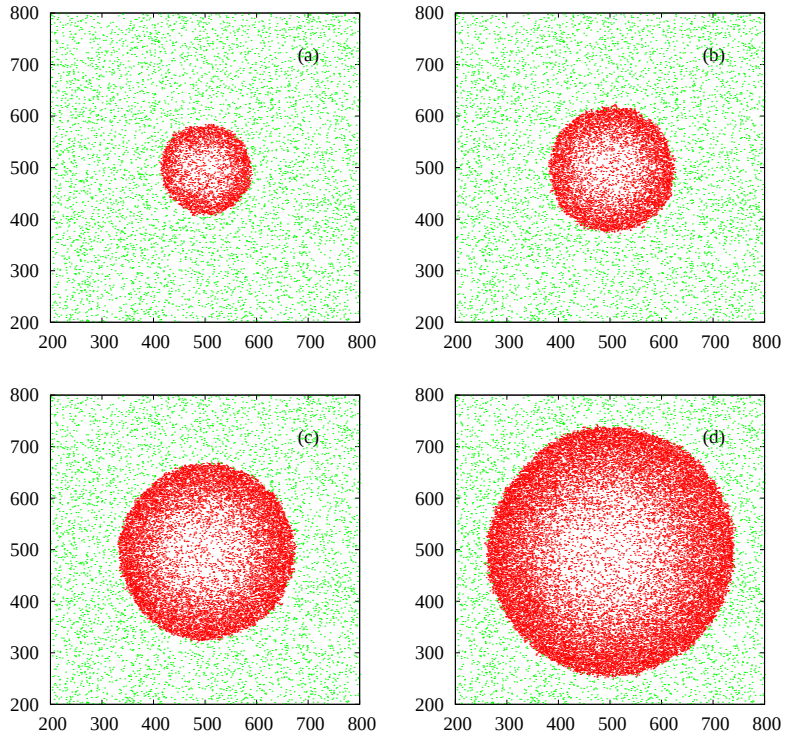

Figure 6.1: Moving (red) and stationary (green) particles at times t = (a) 1000, (b) 2000, (c) 4000 and (d) 8000, following an isotropic impulse at $(500, 500)$ at $t = 0$. The moving particles are in a circular region. The data are for elastic system, $r = 1$.

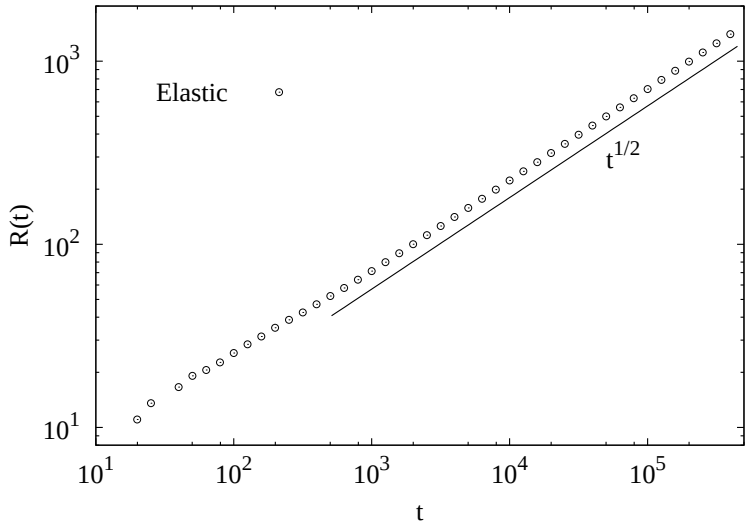

Figure 6.2: Radius of disturbance $R(t)$ vs time t for elastic system in two dimensions. The simulation data fits well with the power law $t^{1/2}$.

$E(t) \sim t^0$. Thus, the temporal growth of the radius of disturbance is given by

$$R(t) \sim t^{2/(D+2)}. \tag{6.1}$$

This power-law growth of radius [Eq. 6.1] was verified in numerical simulations [139] for one and two dimensions. We reproduced it in our simulations and is shown in Fig. 6.2 for two dimensions.

We now discuss our work where we consider the collisions to be inelastic. Throughout this chapter we discuss this inelastic system unless otherwise mentioned. In Fig. 6.3, we show the time evolution of the system following the isotropic impulse. As time increases, all the particles that were originally in a roughly circular ring, cluster together at its rim. The inside region is completely devoid of particles unlike the elastic case. We observe clustering for all the values of $r < 1$ that we have simulated, with clustering setting in at later times for larger coefficients of restitution. Temporal behavior of $R(t)$ for this system can be obtained by an argument based on radial momentum conservation, which we discuss in next subsection.

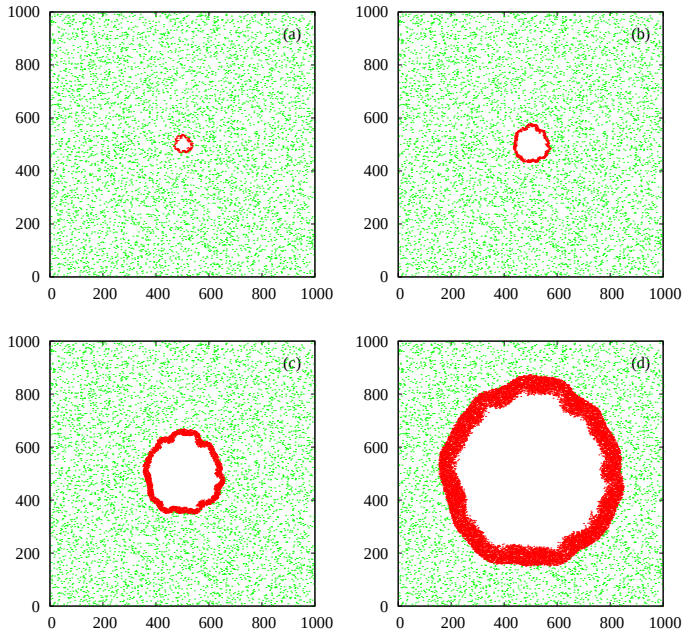

Figure 6.3: Moving (red) and stationary (green) particles at times t = (a) 10^3, (b) 10^4, (c) 10^5 and (d) 10^6, following an isotropic impulse at $(500, 500)$ at $t = 0$. The moving particles cluster together at the disturbance front. The data are for $r = 0.10$.

6.3.2 Radial Momentum Conservation

We first argue that the radial momentum in a fixed direction cannot decrease. It can decrease only if the pressure outside the growing circular ring is larger than the pressure inside. However, the outside pressure is zero since all the particles are stationary, and the inside pressure is non-negative since it is a collection of hard-core repulsive particles. Thus, the radial momentum of the system cannot decrease with time. The argument that the radial momentum cannot decrease with time puts bounds on the growth exponent of the radius of disturbance. Assuming that $R(t) \sim t^{\alpha}$ for $t \gg 1$, the number of moving particles $N_m(t) \sim t^{\alpha D}$ and the typical velocity of a particle in the ring $V(t) = dR/dt \sim t^{\alpha-1}$. Then, radial momentum that is $N_m V$ scales as $t^{\alpha(D+1)-1}$. We immediately obtain that the radius cannot grow more slowly than $R \sim t^{1/(D+1)}$, within the framework of the model.

We now argue that radial momentum is not just nondecreasing, but a constant of motion. Every collision is momentum conserving. In addition, the clustering of all the displaced particles at the rim of the ring prevents momentum being transferred in the negative radial

direction. If we further assume that once the dense rim is formed, the angular coordinates of particles do not change much, then radial momentum is a constant of motion. Therefore,

$$\Omega_D R(t)^D V(t) \Delta\theta = \text{constant}, \tag{6.2}$$

where Ω_D is the volume of a unit sphere in D-dimensions and $\Delta\theta$ is the angular spread in direction θ. The solution to Eq. (6.2) is

$$R(t) \propto t^{\alpha},\ t \gg t', \tag{6.3}$$

where $\alpha = 1/(D+1)$, and t' is the initial mean collision time.

We present numerical evidence for radial momentum being a constant of motion, as argued above. In Fig. 6.4, the temporal variation of the radial momentum is shown for different δ with fixed $r = 0.10$ and compared with the data for the elastic problem. When all collisions are elastic, radial momentum increases as $\sqrt{t}$. When collisions are inelastic, radial momentum increases very slowly with time from an initial value of 4.0 to 8.6, in nearly six decades of time (see Fig. 6.5). With the current data, it is not possible to conclude with certainty that radial momentum will become a constant at large time when $\delta \to 0$. However, one can rule out a power law growth. The radial momentum conservation is strictly valid only when collisions are completely inelastic, $r = 0$ and $\delta = 0$. However, for other value of r and δ, even after formation of the circular band, colliding particles may change their angular coordinates. Such changes in the angular coordinates of the particles will result in increase of radial momentum. We checked that the average change in angle following a collision decreases to zero with time, when δ is lowered as shown in Fig. 6.6. The power-law growth of $R(t)$ given by Eq. (6.3) which is based on radial momentum conservation fits very well with the simulation data in two dimensions as shown in Fig. 6.7.

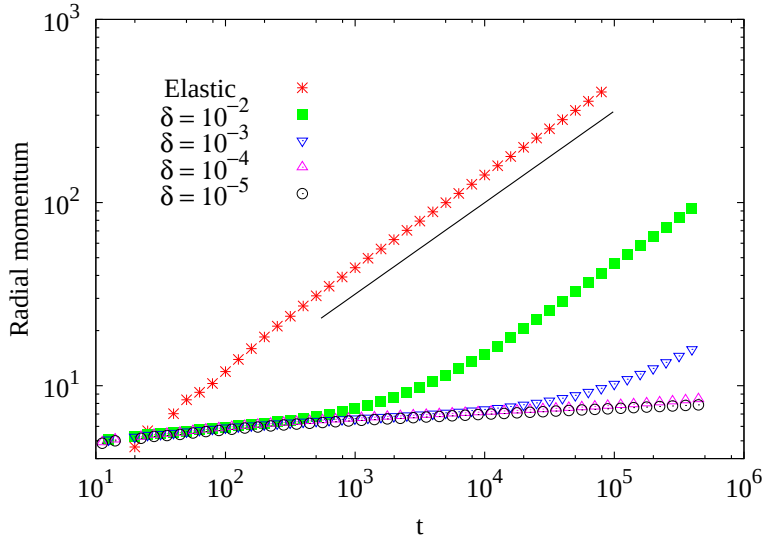

Figure 6.4: The radial momentum as a function of time t. For elastic collisions, it increases as $\sqrt{t}$ (the solid straight line is a power law $\sqrt{t}$). For inelastic collisions with $r = 0.10$, the radial momentum appears to increase very slowly with time to a constant, when $\delta \to 0$. The data for the elastic system have been scaled down by factor $1/2$.

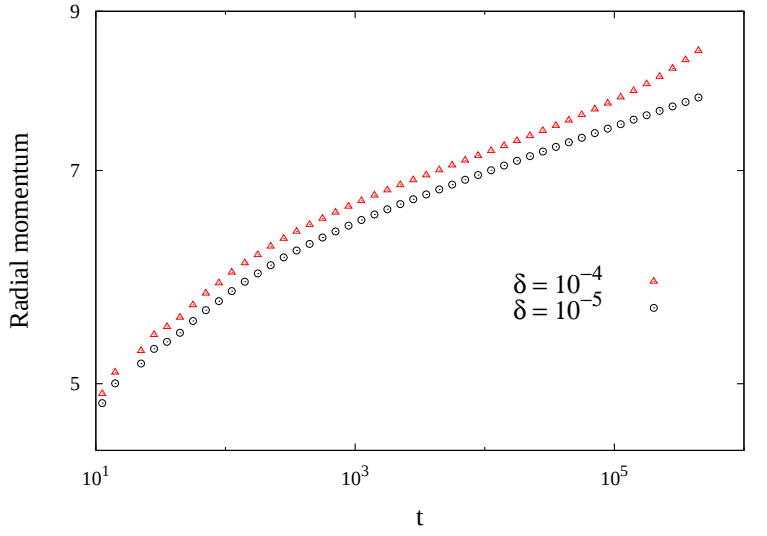

Figure 6.5: Two curves from Fig. 6.4 are plotted to show clearly the slow increase of the radial momentum.

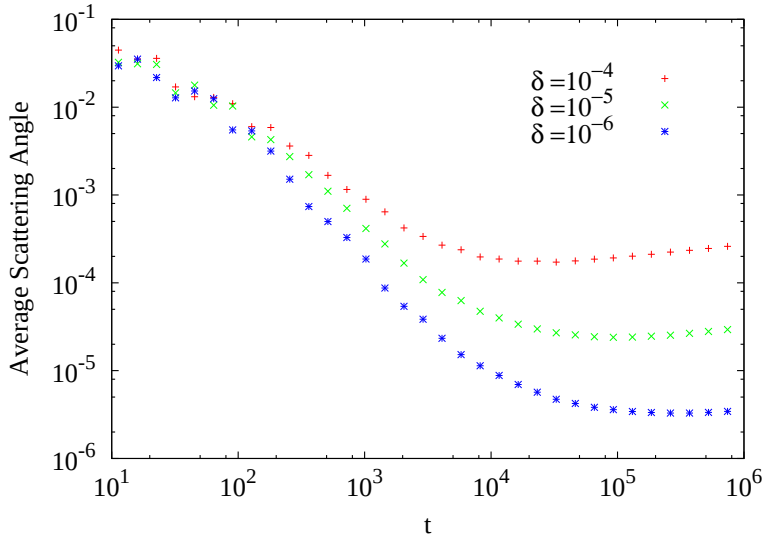

Figure 6.6: Average scattering angle on collision vs time t.

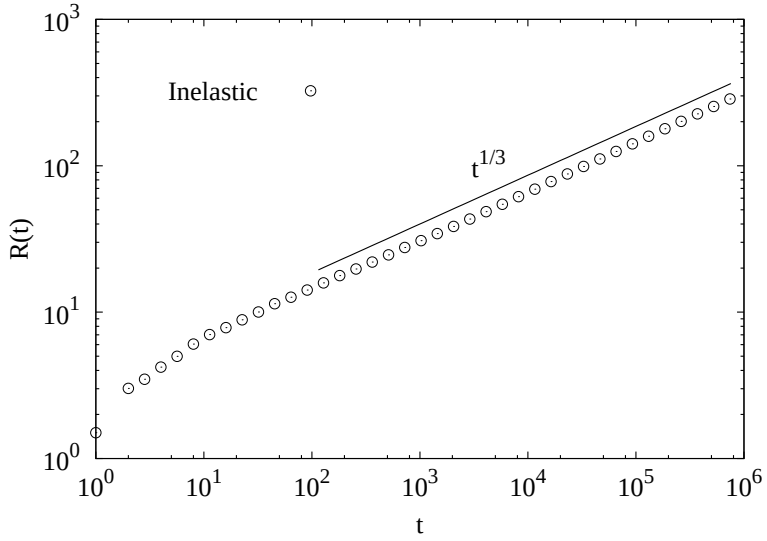

Figure 6.7: Radius of disturbance $R(t)$ vs time t for inelastic system ($r = 0.10$) in two dimensions. The simulation data fits well with the power law $t^{1/3}$.

6.4 Boudet, Cassagne and Kellay Experiment (BCK)

The inelastic granular explosion model has close resemblance to a recent experiment by Boudet, Cassagne and Kellay (BCK) [6]. In following two subsections, we first summarize the experimental setup and findings, and then the analysis done to explain the experimental data.

6.4.1 Experiment

In the experiment, a thin layer of sand (glass beads of diameter 0.3 mm) flows down on an inclined glass plane (35°, 6mm thickness). The sand is poured from a funnel shaped container, at the top end of the inclined plane in the form of a jet. The experiment was carried out on an inclined plane to cancel friction against gravity so that the flow continues. The flow is inhomogeneous and divergent, with a gradient in velocity and density, for a distance of about 10 cm near the position of jet impact. Beyond this 10 cm distance, the flow is roughly homogeneous over a distance of 30-40 cm with a lateral width of over 10cm. The experiment was carried out in this homogeneous flow region, where the velocity varies by less than 20% over a distance of 20 cm. In this region, the sand flows as a thin layer of thickness 1.2 mm approximately, with speed between 1.2 and 1.7 m/s depending on the distance from the funnel. The volume fraction of the flowing layer is controlled by varying the diameter of the funnel and it was between 5% and 20%. The produced flow is supersonic, the speed of sound in the medium was measured to be 13 ± 2 cm/s, independent of the volume fraction and the velocity of the flow for the ranges studied. Steel balls of diameter 2-16 mm were dropped vertically from a distance of about 25 cm on the flowing layer. After the first bounce of the ball on the plane, it was taken out. The effect of impact was recorded with a high speed camera (10000 frames/second), placed below the glass plate.

Figure 6.8 shows the effect of perturbing the sand flow with the steel ball impact. The

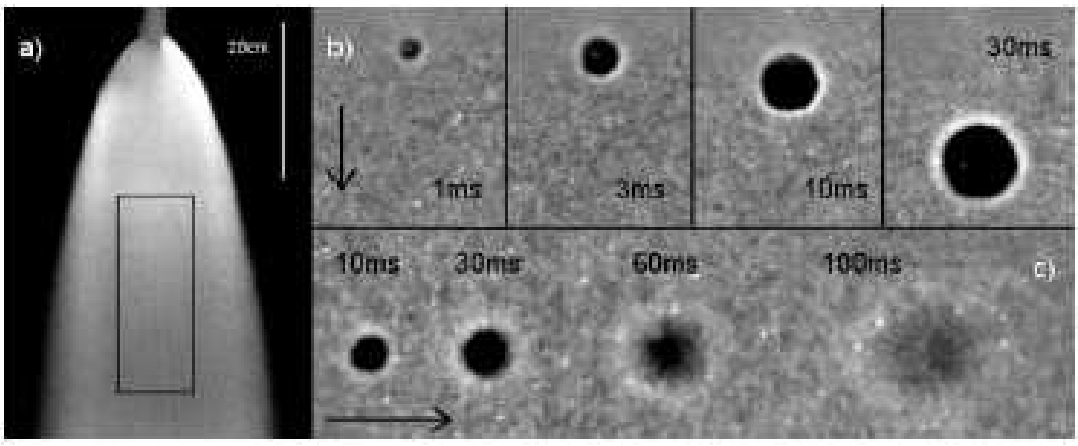

Figure 6.8: (a) An image of the flow. The experiment was carried out in the shown rectangular region where the flow is roughly homogeneous. (b) Images of expanding hole at different times after the impact of a 16 mm diameter steel sphere. Particles that were originally in a circular region have clustered into a dense rim(white rim) surrounding the hole (black circular region).(c) Impact of a 2 mm diameter sphere. The figure is taken from Ref. [6].

impact forces the sand grains to move radially outwards and form a dense rim, leaving behind an empty circular region.

6.4.2 Analysis

We review the model studied in BCK to explain the experimental data, and then generalize it to D-dimensions and derive the asymptotic behaviour for small and large times. The model is based on the experimental observation, that after the impact with the steel ball, the displaced glass beads form a growing circular ring, devoid of beads. BCK considered an idealized model where all the particles contained in a disk of radius $R(t)$ at time t accumulate at the rim (boundary of ring). The remaining particles that are outside the disk are assumed to be stationary. This mimics the experimental system when one transforms to the center of mass coordinates, and in the limit of large impact energy, when the fluctuations of the particle velocities about the mean flow may be ignored. Each particle at the rim is assumed to move radially outwards with a speed $V(t)$. As the ring moves outwards, more particles are absorbed into the ring. We reproduce the calculation in BCK,

but generalized to D-dimensions. The total kinetic energy $E(t)$ is

$$E(t) = \frac{1}{2}\rho_0 \Omega_D R(t)^D V(t)^2, \tag{6.4}$$

where ρ_0 is the initial mass density, and Ω_D is the volume of a unit sphere in D-dimensions, such that $\rho_0 \Omega_D R(t)^D$ is the total mass of displaced particles. The speed $V(t)$ is

$$V(t) = \frac{dR(t)}{dt}. \tag{6.5}$$

One more relation between $E(t)$ and $R(t)$ is required for the solution. If the particles were elastic, then total energy is conserved, $E(t) \sim t^0$, and one obtains $R(t) \propto t^{2/(D+2)}$; in particular, $R(t) \propto \sqrt{t}$ in $D = 2$ [128]. However, when particles are inelastic, there is no such conservation law, and energy decreases with time. BCK proceed by the following argument. If r is the coefficient of restitution, then the loss of energy when a particle in the rim collides with a stationary particle outside is $\frac{1}{2}(1 - r^2)V(t)^2$. Thus, when the ring moves out by a distance dR, then the change in energy dE is given by

$$dE = -\frac{1}{2}\Omega_D R(t)^D \rho_0 V(t)^2 (1 - r^2) N(t) dR, \tag{6.6}$$

where $N(t)$ is the number of collisions per particle per unit length, or equivalently, $N(t)dR$ is the number of collisions for each particle in the rim as it travels a distance dR. BCK makes the strong assumption that $N(t)$ is independent of the radius, and hence time t that is,

$$N(t) = \text{constant}. \tag{6.7}$$

Eliminating $R(t)$ and $V(t)$ in Eq. (6.6) using Eq. (6.4), one obtains

$$E(t) = E_0 \exp\left[-N(1 - r^2)R(t)\right], \tag{6.8}$$

where E_0 is the energy of impact at $t = 0$. It is now straightforward to obtain the equation satisfied by the radius $R(t)$:

$$\frac{t}{t_0} = \int_0^{R/R_0} dx\, x^{D/2} e^x, \tag{6.9}$$

where $t_0^{-1} = \sqrt{E_0[N(1-r^2)]^{D+2}/(\rho_0 \Omega_D 2^{D+1})}$ and $R_0^{-1} = N(1-r^2)/2$.

The experimental data in BCK was fitted to the numerical solution of Eq. (6.9) with $D = 2$. Although the equation describes the data well (see Fig. 4 of Ref. [6]), we argue in next section that the analysis has certain shortcomings, making the results questionable.

For later reference, it will be useful to derive the asymptotic solutions to Eq. (6.9). Let $\alpha = \ln(t/t_0)$. Then for large times, it is straightforward to derive:

$$\frac{R}{R_0} = \alpha \left[1 - \frac{D}{2}\frac{\ln\alpha}{\alpha} + \frac{D}{2}\frac{\ln\alpha}{\alpha^2} + O\left(\frac{1}{\alpha^2}\right) \right], \ \alpha \gg 1. \tag{6.10}$$

The growth is logarithmic at large times in all dimensions. For short times, by writing the exponential in Eq. (6.9) as a series, it is easy to obtain

$$\frac{R}{R_0} = \left[\frac{(D+2)t}{2t_0} \right]^{\frac{2}{D+2}} \left[1 + O\left(\left(\frac{t}{t_0} \right)^{\frac{2}{D+2}} \right) \right], t \ll t_0. \tag{6.11}$$

For small times, the power law growth of radius is identical to the elastic case [128].

6.5 Critique of BCK Analysis

First, we show by a simple calculation that the solutions Eqs. (6.8) and (6.9) do not give the correct results when $D = 1$. The solution Eqs. (6.8) and (6.9) are valid for all values of $r < 1$, including $r = 0$. In one dimension, the special case $r = 0$, when particles stick on collision, is easily solvable [7]. Let particles of mass m be initially placed equidistant from each other with inter-particle spacing a. Pick a particle at random and give it a velocity v_0 to the right. When this particle collides with its neighbor, it coalesces with

it. After k collisions, the mass of the composite particle is $(k+1)m$, its distance from the impulse is $R = ka$, and its velocity, given by momentum conservation, is $v_k = v_0/(k+1)$ towards the right. The time taken for k collisions is given by

$$t_k = \sum_{i=0}^{k-1} \frac{a}{v_i} = \frac{ak(k+1)}{2v_0}. \tag{6.12}$$

Solving for k, we obtain $k = (-1 + \sqrt{1 + 8tv_0/a})/2$. At large times $t \gg a/v_0$, the radius and energy are $R = ka \approx \sqrt{2v_0at}$ and $E(t) = mv_0^2a/(2R)$. The analysis in BCK for energy [Eq. (6.8)] and radius [Eq. (6.10)] are not consistent with the exact solution in one dimension.

Second, we show that the long time logarithmic growth of the radius of the disturbance, as in Eq. (6.10), is not possible. Suppose we assume that Eq. (6.10) is right, i.e., $R(t) \sim \ln t$. In two dimensions, the radial momentum is $R(t)^2V(t)$, where $V(t) = dR/dt \sim 1/t$. Thus the radial momentum scales as $(\ln t)^2/t$, implying that the radial momentum decreases with time, which is impossible. Therefore, within the model, the logarithmic time dependence of the radius is not possible.

Radial momentum conservation implies that $R(t)^{D/2}\sqrt{E(t)}$ is a constant of motion. Equation (6.8) is clearly not consistent with this constraint, neither is Eq. (6.10) for growth of radius consistent with Eq. (6.3).

We, therefore, conclude that the analysis of BCK is not completely satisfactory. Since the solution of BCK [Eqs. (6.8) and (6.9)] was based on the assumption that $N(t)$, the rate of collisions per particle per unit distance, is a constant, we test the validity of this assumption as well as the prediction of Eq. (6.9) in molecular dynamics simulations of a hard sphere gas.

The formation of an empty region bounded by the moving particles (as in Fig. 6.3) is the only requirement for the BCK theory to be applicable. Therefore, if the analysis in BCK is correct, then the results for radius in Eq. (6.9) should describe the disturbance in the

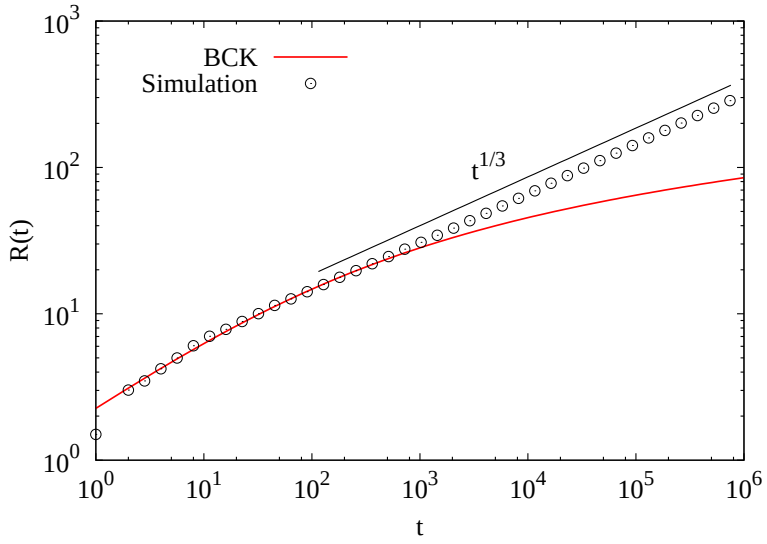

Figure 6.9: Data for radius $R(t)$ from simulations in two dimensions are compared with BCK result [Eq. (6.9)] and $t^{1/3}$. R_0 and t_0 in Eq. (6.9) are obtained by fitting the initial time simulation data to Eq. (6.9) and are $R_0 = 10.30 \pm 0.21$ and $t_0 = 35.79 \pm 2.35$. The data are for $r = 0.10$.

hard sphere model too. In numerical simulations, data can be obtained for much longer times than that in the experimental data in Ref. [6], and therefore be used to make a more rigorous test of the assumptions and the conclusions of the BCK theory.

In Fig. 6.9, we compare the BCK result Eq. (6.9) for the radius with hard sphere simulation data. The constants R_0 and t_0 in Eq. (6.9) are determined by fitting it to the numerical data at early times. It is clear that Eq. (6.9) captures only the short time behavior. On the other hand, the data at large times are consistent with the power law $t^{1/3}$. We believe that the discrepancies between the short and large time behavior are not brought out by the experimental data as the time scales are not large enough.

We now make a direct test of the BCK assumption that $N(t)$, the number of collisions per particle per unit distance is a constant in time, as assumed in BCK. The data for $N(t)$ are shown in Fig. 6.10 for three different coefficients of restitution, one of them being $r = 1$. While $N(t)$ is a constant when collisions are elastic, it is clearly not so for $r < 1$, invalidating the BCK assumption. At large times, the rate of collisions become independent of r as long as $r < 1$. This is consistent with the observations in the freely cooling granular

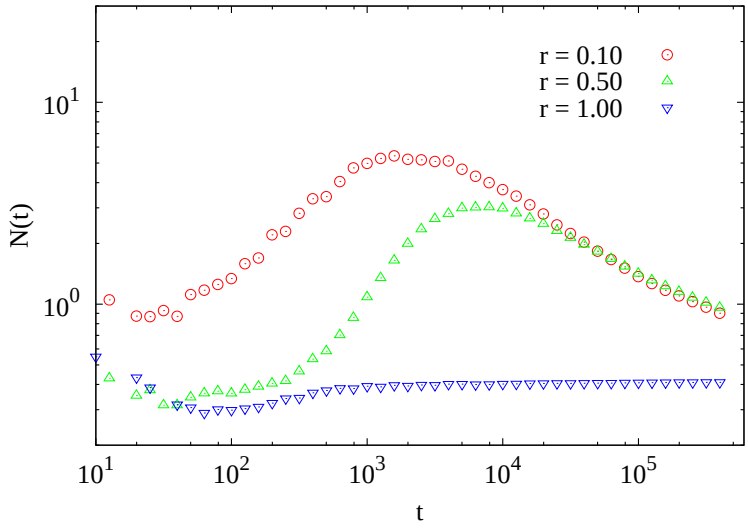

Figure 6.10: Temporal variation of $N(t)$, the number of collisions per particle per unit distance for various r. For $r < 1$, $N(t)$ is not constant as assumed by BCK.

gas [13, 14], where the long time behavior of $E(t)$ and $N(t)$ is independent of r, and hence identical to $r = 0$, the sticky limit. Thus we could think of the rim as a solid annulus made up of all the particles that have undergone at least one collision. Therefore, once the rim forms, we expect that only the collisions of the particles that are at the outer edge of the rim, with the stationary particles are relevant. Then, the collisions per particle on surface per unit time, NR, should be constant. This is confirmed in the Fig. 6.11, where NR tends to a constant independent of r, at large times. Since the relevant collisions are taking place at the outer boundary of the rim, Eqs. (6.8) and (6.9) underestimate the radius, or equivalently overestimate energy loss.

6.6 Comparison with Experimental Data

In this section, we compare the power law solution $R(t) \sim t^{1/3}$, obtained from the conservation of radial momentum, with the experimental data of Ref. [6]. We also consider modifications in our above studied hard sphere model to account for the deviation of experimental data from the power-law $t^{1/3}$ at large times.

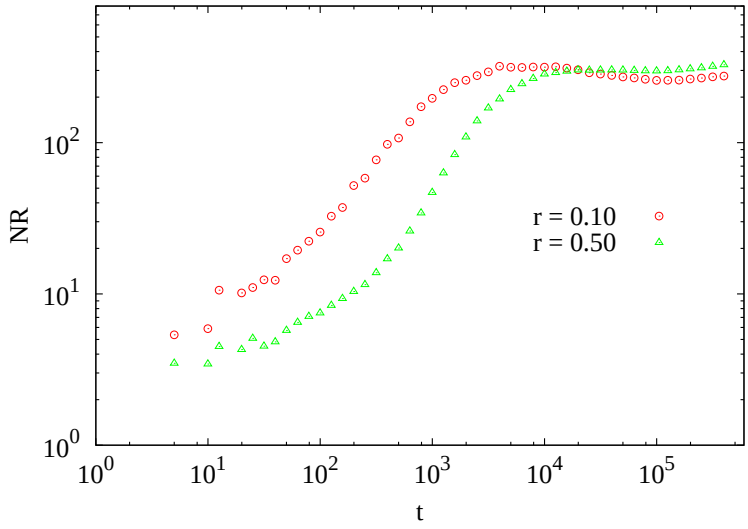

Figure 6.11: Rate of collision $N(t)$ as shown in Fig. 6.10 is multiplied by R, where R is the radius of disturbance. NR is a constant at large times for $r < 1$.

6.6.1 Experimental Data and Power-Law $t^{1/3}$

Figure 6.12 shows the experimental data (Fig. 4 of Ref. [6]) for the temporal variation of the radius of disturbance $R(t)$ following impacts with spheres of different diameter. The black solid lines are power laws $t^{1/3}$. There are temporal regimes where it matches well with the experimental data. However, there are deviations from $t^{1/3}$ at large times. There is sufficient statistics for this late time regime only for the impact with the largest sphere. For this data, we find that the data are best fitted by a power law $t^{0.18}$ (see dashed line in Fig. 6.12).

The experimental situation is more complicated than the simple hard sphere model for which the power law growth is presumably the correct result. To equate the two, we had to make approximations. First, we ignored the fluctuations of the velocities of the particles about the mean velocity. While this is reasonable for large impact velocities when typical speeds of displaced particles are much larger than typical velocity fluctuations, the fluctuations become relevant at late time. Second, we ignored the experimentally observed three dimensional nature of the rim (see discussion in last but one paragraph of Ref. [6]). Such a possibility will result in radial momentum not being conserved, thus

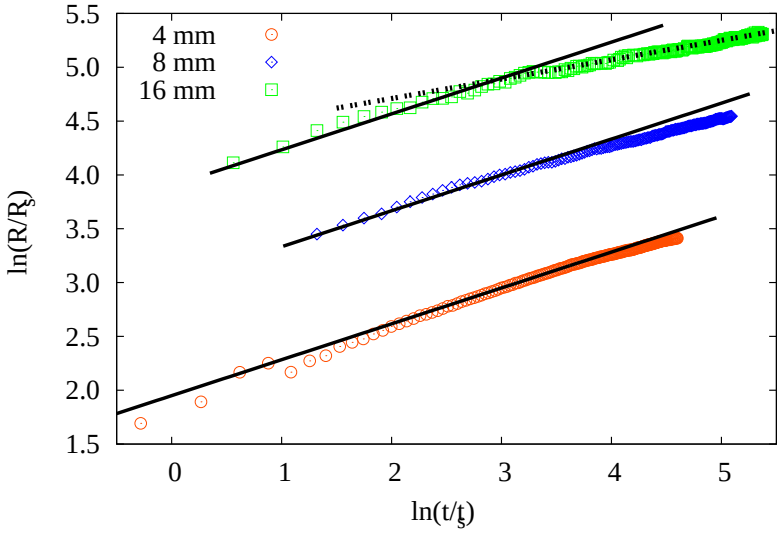

Figure 6.12: Experimental data from Ref. [6] for radius R as a function of time t following an impact by steel balls of diameter 4 mm, 8 mm and 16 mm. The solid/dashed lines have slope $1/3$ and 0.18 respectively. R_s is the diameter of a glass bead and t_s is the mean time taken by a glass bead to traverse a distance equal to its diameter. The data have been obtained from Ref. [6].

invalidating the scaling arguments in [7].

It is possible that either or both of these approximations could be responsible for the crossover seen at large times. In next two subsections, we study modified versions of the hard sphere model, which incorporates the above features. We argue that the crossover from $t^{1/3}$ law can be explained by these modified models.

6.6.2 Ambient Temperature Model

In the center of mass coordinates, all particles are not stationary but fluctuating about their mean position. When these velocity fluctuations become comparable to the velocity of the rim, then we expect the rim to destabilize, and power laws to show crossovers.

We model this situation as follows. Initially all the particles (type E) are assumed to be elastic and equilibrated at a certain fixed temperature, parameterized by $\Lambda^2 = \langle v^2 \rangle / v_0^2$, where $\langle v^2 \rangle$ is the mean velocity fluctuations and v_0, as earlier, is the speed of the perturbed

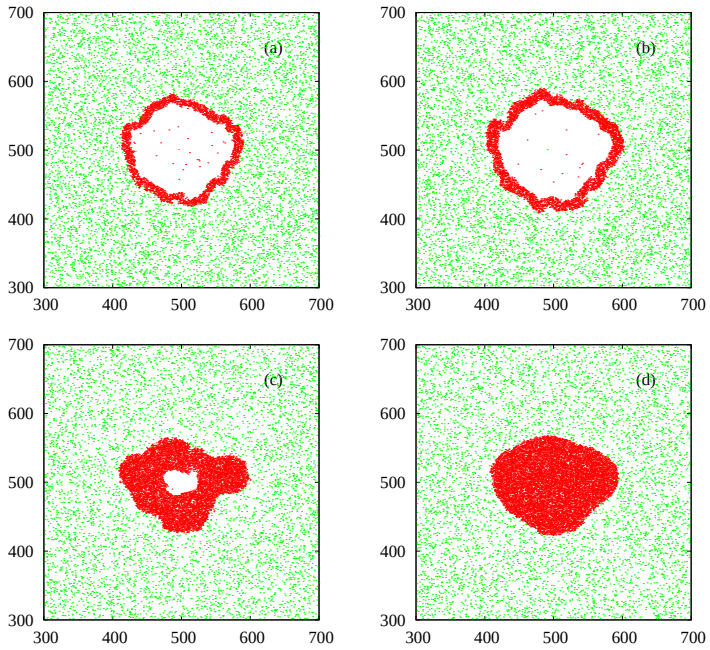

Figure 6.13: Snapshots of inelastic I particles (red) and elastic E particles (green), when $\Lambda = 1/800$, following an isotropic impulse at $(500, 500)$ at $t = 0$. The time increases from (a) to (d) and correspond to the times shown by labels a–d in Fig. 6.14. Initially, the disturbance grows as in Fig. 6.3, but at late times due to velocity fluctuations, the rim gets destabilized. The data are for $r = 0.10$.

particles. $\Lambda = 0$ corresponds to the case when all particles are initially stationary. An isotropic impulse is imparted by introducing four particles (type I) at the center with speed v_0 in the directions $0, \pi/2, \pi$, and $3\pi/2$. Collisions between E particles are elastic. Collisions involving at least one I particle are inelastic. If an E particle collides with an I particle, then it becomes type I. This model captures shock propagation in a system where all particles have some nonzero kinetic energy.

In Fig. 6.13, we show snapshots of the system at various times, when the $\Lambda = 1/800$. The sharp rim starts becoming more diffuse as the velocity of the rim decreases, until the enclosed empty region vanishes completely. These snapshots are qualitatively very similar to that seen in the experiment for low speed impacts and at large times (see Fig. 6.8).

When the rim destabilizes, $R(t)$ shows deviation from the $t^{1/3}$ power law growth (see Fig. 6.14). It is straight forward to estimate this crossover time t_c. The instability sets in when the speed of the rim is of the same magnitude as the velocity fluctuations, i.e.

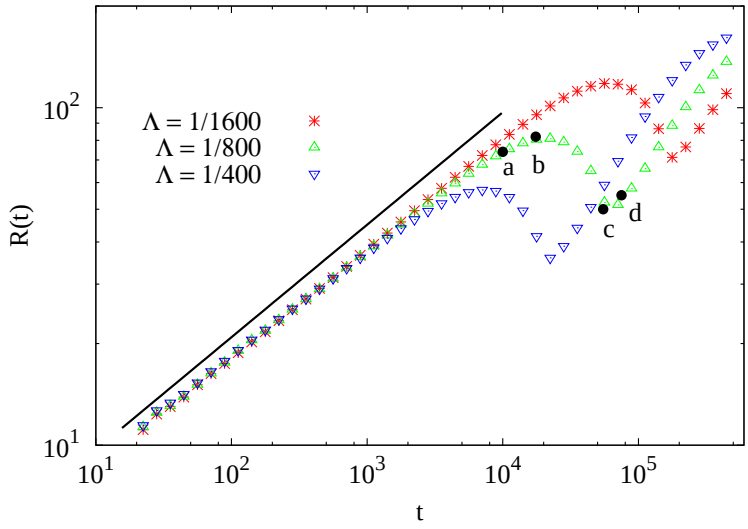

Figure 6.14: The radius of disturbance $R(t)$ as a function of time t for different values of Λ. The effect of velocity fluctuations are felt later for smaller Λ. At large times, the finite external pressure is able to compress the bubble, with $R(t)$ reaching a minimum when the density of the bubble approaches the close packing density. A solid line of slope 1/3 is drawn for reference. The data are for $r = 0.10$.

$v_{t_c} \sim \Lambda v_0$. Since $v_t \sim dR/dt \sim t^{-2/3}$, we immediately obtain $t_c \sim \Lambda^{-3/2}$. Thus, $R(t)$ should have the scaling form

$$R(t) \sim t^{1/3} f\left(t\Lambda^{3/2}\right), \tag{6.13}$$

where $f(x)$ is a scaling function with $f(x) \sim O(1)$, when $x \to 0$. The curves for different Λ collapse when scaled as in Eq. (6.13) [see Fig. 6.15].

6.6.3 Hopping Model

The introduction of a finite ambient temperature, while leading to the disintegration of the rim, does not produce the large time behavior of the data for the radius. We now ask whether the rim becoming three dimensional could be responsible for that. The rim presumably becomes three dimensional because a fast particle when hemmed in by many surrounding particles may jump out of the plane due to collision with floor and friction. The net effect is a reduction in radial momentum, which could change the growth law.

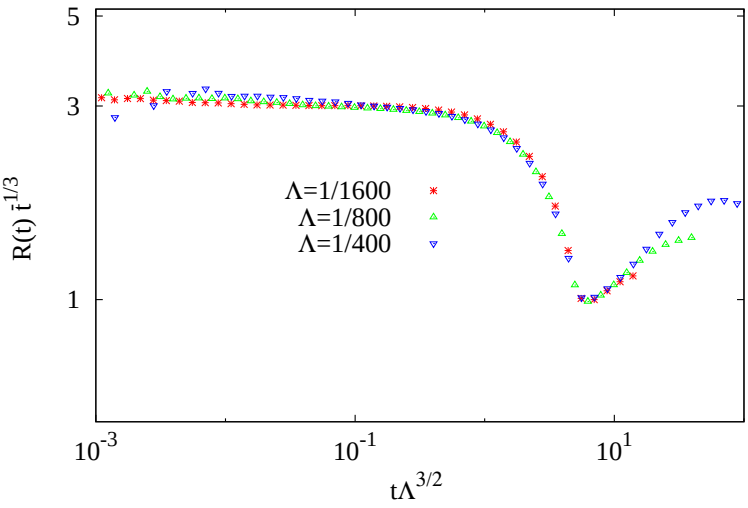

Figure 6.15: The $R(t)$ vs t data of Fig. 6.14 when scaled according to Eq. (6.13). A good collapse is obtained.

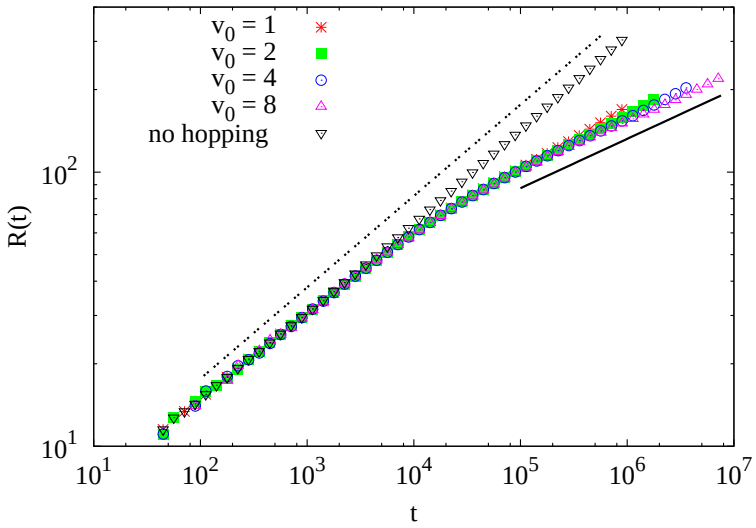

Figure 6.16: Temporal variation of radius $R(t)$ for $\kappa = 0.20$ with various initial velocity v_0. The solid line is a power law $t^{0.18}$ while the dashed line is a power law $t^{1/3}$. The data with no hopping correspond to $v_0 = 1$. All data are for $r = 0.10$.

To mimic radial momentum leakage occurring at high densities, we consider the following model. We divide the system into squares of length equal to diameter of the particles. Given the grid position of a particle, any particle which is in one of the eight neighboring squares will be called its neighbor. At any instant of time, if a particle has eight or more neighbors, then we remove the particle if its velocity $\mathbf{v}$ satisfies the hopping criterion,

$$(\mathbf{v} - \mathbf{v}_{cm}).\hat{\mathbf{v}}_{cm} > \kappa v_{cm}, \tag{6.14}$$

where $\mathbf{v}_{cm}$ is the center of mass velocity of the particle and its neighbors. In words, the longitudinal component of the velocity should be larger than v_{cm} by a factor κ.

The hopping criterion is tested for all moving particles after every 100 collisions in the system, and the results do not depend on this number provided it is not too large. The results are shown in Fig. 6.16. The results obtained are insensitive to the value of κ provided $\kappa < 0.20$. We find that at large times, the system crosses over to a different power law growth $\approx t^{0.18}$, that is very similar to the growth law seen in the experiment. While the aim of the model was to show that loss of radial momentum, at high densities, can result in crossovers at large times, we obtain a quantitative match. As of now, we have no explanation why the exponents have approximately the same numerical value, and it could be just a coincidence.

6.7 Conclusion

In summary, we studied granular explosion model, where a stationary collection of hard inelastic particles is perturbed by injecting energy to few localized particles. This initial perturbation leads to clustering of all moving particles into a shell, that propagates radially outwards in time [7]. We argued that the formation of the shell in the perturbed system conserves radial momentum. This conservation law leads to a $t^{1/(D+1)}$ power law growth for the radius of disturbance. Data from the numerical simulation of the model fits very

well to the predicted growth law of radius of disturbance.

We analyzed the recent experiment [6] of dropping spheres onto a flowing monolayer of glass beads. Our inelastic granular explosion model closely resembles this experiment. With this hard sphere system, we showed that the assumption of constant rate of collision per particle per unit distance, made in the theory [6] to describe the experimental data is correct only for elastic particles. For inelastic system, the relevant collisions are the collisions of the particles at the outer edge of the rim with the stationary particles outside. The $t^{1/3}$ ($D = 2$) growth law describes the experimental data well except at large times when the data show a crossover to a different power law growth. We attributed this crossover to the rim becoming three dimensional because of high densities and collisions with the floor. By constructing a simple model incorporating these effects, we were able to explain the crossovers at large times.

The current experimental data can not distinguish between the theory in BCK and the power law growth argued for in this chapter. If the experimental time scale is increased, then such a distinction may be possible. It will be worthwhile to make the attempt.

Acknowledgment

We thank the authors of Ref. [6] for providing us with the experimental data.

Chapter 7

Shock Propagation in a Viscoelastic Granular Gas

7.1 Introduction

In Chapter 6, we studied the granular explosion model, where a stationary collection of inelastic particles is perturbed by a localized impulse, using scaling arguments and event driven molecular dynamics simulations. By identifying radial momentum as a conserved quantity, it was argued that, the radius of the disturbance R grows with time t as $R(t) \sim t^{\alpha}$, where $\alpha = 1/(D+1)$ in D dimensions. The arguments depended crucially on the formation of a region devoid of particles, surrounded by a moving dense shell of particles.

In the numerical simulation of granular explosion studied in Chapter 6, particles were considered hard and a simplified model of constant coefficient of restitution r was used to account for the inelasticity of the collisions. Such a choice was motivated by computational efficiency. However, realistic coefficient of restitution depends strongly on the relative velocity of collision v_{rel}, $r \equiv r(v_{rel})$ [17]. Experimentally, $r(v_{rel})$ approaches 1 when the v_{rel} tends to zero, i.e., $1 - r(v_{rel}) = g(v_{rel}/\delta)$, where $g(x) \sim x^{\sigma} + O(x^{2\sigma})$, for

$x \ll 1$ and $g(x) \sim 1 - r_0$ for $x \to \infty$ [95, 96], and δ is a velocity scale. The exponent σ takes a range of values and is known to be $1/5$ for visco-elastic particles [17] (see the discussion in Sec. 2.2.3 for the visco-elastic particles). It is not clear whether the shell structure will form for such velocity dependent r. In this chapter, we study the system of visco-elastic particles in two dimensions using conventional molecular dynamics simulations. For this system, $\sigma = 1/5 < 1$, a case that cannot be studied by event driven molecular dynamics simulations performed in Chapter 6, as inelastic collapse prevents the simulation from proceeding forward [70].

The rest of the chapter is organized as follows. In Sec. 7.2, the simulation details of the model are provided. The results obtained in molecular dynamics simulations are presented in Sec. 7.3. We conclude this chapter in Sec. 7.4.

7.2 Model and Simulation Details

The system that is simulated is defined as follows. We consider a collection of mono dispersed discs distributed uniformly in two dimensions. The mass and radius of the particles are taken to be unity. All particles are initially at rest. An isotropic impulse is modeled by introducing four particles at the center with speed of unit magnitude, in the directions 0, $\pi/2$, π, $3\pi/2$. The particles move ballistically until they collide. The interaction force during the collision is given by [77] (see Sec. 2.2.3 for details)

$$F = \rho\xi^{3/2} + \frac{3}{2}A\rho\sqrt{\xi}\dot{\xi}, \tag{7.1}$$

where ξ is the overlap between the colliding particles and $\dot{\xi}$ is the time derivative of ξ. ρ and A are material parameters, characterizing the elastic and dissipative properties. Collision conserve momentum, but not energy.

We simulate the system in two dimensions using conventional molecular dynamics simu-

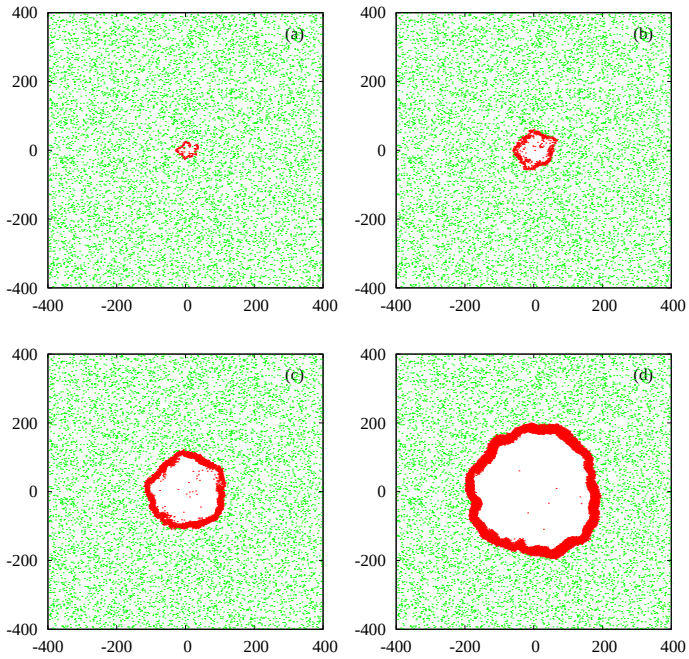

Figure 7.1: Moving (red) and stationary (green) particles at times t = (a) 10^2, (b) 10^3, (c) 10^4 and (d) 5×10^4, following an isotropic impulse at $(0, 0)$ at $t = 0$. The moving particles cluster together to form a shell.

lations, where we have used fourth order Runge-Kutta (RK4) scheme for integrating the equations of motion. The simulation data are for $\rho = 10^4$, $A = 0.028$ and volume fraction $\phi = 0.20$. The integration time step h in RK4 scheme is chosen to be $h = 0.005$, which is sufficient to resolve the full collision process. The data are typically averaged over eight different realizations of the particle configurations.

7.3 Simulation Results

Figure 7.1 shows the time evolution of the system. The four non-stationary particles at $t = 0$ move and collide with other stationary particles setting them in motion and leading to a cascade of collisions. The active particles (particles that have collided at least once) form a shell, enclosing a region devoid of particles. The shell moves out in time absorbing the particles at the boundary. Thus, similar to the hard-core system with constant r, we observe shell formation in this visco-elastic system.

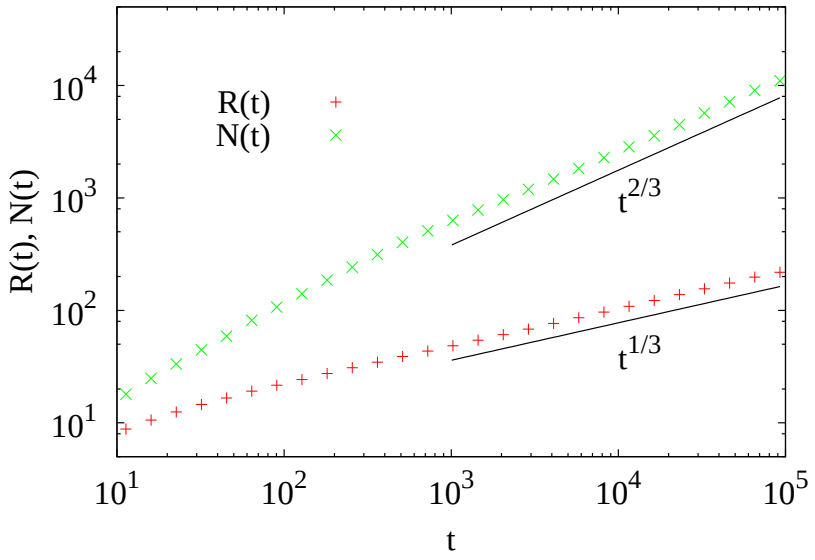

Figure 7.2: Temporal behaviour of radius of disturbance $R(t)$ and number of active particles $N(t)$.

The radial momentum conservation argument predicts that the radius of disturbance grows with t as $R(t) \sim t^{1/3}$, and the number of active particles grows as $N(t) \sim R^2 \sim t^{2/3}$ in $D = 2$. The simulation results for $R(t)$ and $N(t)$ as shown in Fig. 7.2 are in very good agreement with these predictions. The kinetic energy $E(t)$ of the shell is given by $E(t) \sim N(t)V(t)^2$, where $V(t)$ is the typical velocity of a particle in the shell and is given by $V(t) = dR/dt \sim t^{-2/3}$. Thus, the energy decreases with time as $E(t) \sim t^{-2/3}$, and as shown in Fig. 7.3 matches very well with the simulation data.

7.4 Conclusion

To summarize, we studied granular explosion model with visco-elastic particles using molecular dynamics simulations. We reproduced the formation of a dense moving shell of particles following a localized perturbation seen in hard-core granular explosion model [7] and experiments [6]. The radius of shell increases with time as $t^{1/3}$, and the energy decreases as $t^{-2/3}$ in two dimensions. We find that the results of scaling arguments for hard spheres system [7] continue to hold for visco-elastic particles, and thus is insensitive to

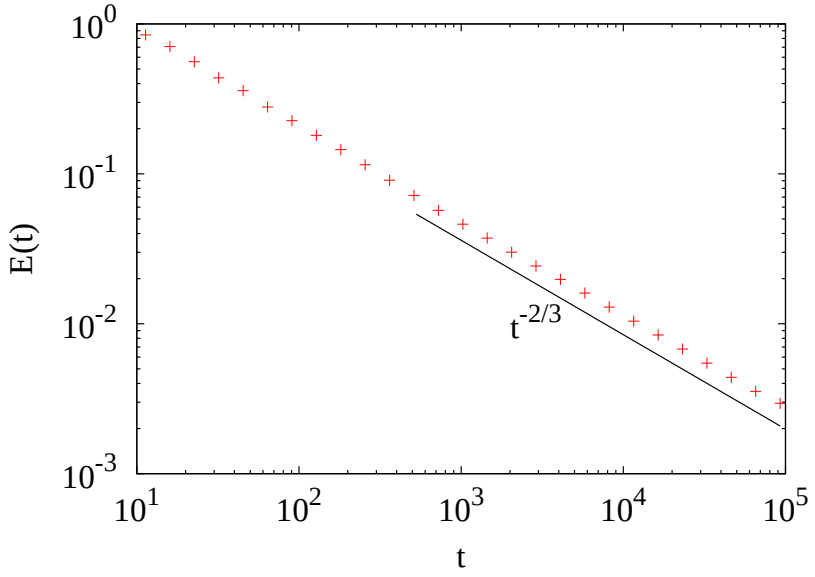

Figure 7.3: Temporal behaviour of kinetic energy $E(t)$.

the form of the coefficient of restitution.

Chapter 8

Conclusion and Discussion

We now summarize the main results of this thesis, and discuss some possible future extensions. In this thesis, we studied freely cooling granular gas using large scale molecular dynamics simulations and scaling analysis, with a particular attention on the large time behaviour. At large times, the system behaviour is dominated by strong clustering.

In **Chapter 4**, we studied the long time behaviour of the freely cooling granular gas in three dimensions using event driven molecular dynamics simulations. At large times, the translational kinetic energy $T(t)$ is found to decay with time t as a power law $t^{-\theta_T}$ with $\theta_T \approx 6/5$. This decay exponent is universal, independent of system parameters. This rules out Burgers like equation as the continuum description of the long time behaviour of granular gas, which predicted θ_T to be $3/2$ in three dimensions. Our observed θ_T is indistinguishable from the mean-field prediction for ballistic aggregation. However, our direct numerical simulation of ballistic aggregation shows that the actual decay exponent depends on density of system and differs from the mean-field prediction for dilute systems. In addition, the cluster size distribution as well as the velocity distribution of ballistic aggregation are strikingly different from that of the freely cooling granular gas. Thus, the principal conclusion that emerges from our study is that, the freely cooling granular gas fits to neither the ballistic aggregation or a Burgers equation description.

Our results clearly show the need for a new mathematical theory, beyond ballistic aggregation and Burgers equation, to write the correct continuum equations for the freely cooling granular gas, which is a very challenging task. The experimental investigation of freely cooling granular gas is limited to homogeneous cooling regime, and it is desired to design experiments to probe the inhomogeneous cooling regime.

In **Chapter 5**, we studied the large time behaviour of freely cooling granular gas of rough particles in two dimensions using event driven molecular dynamics simulations. Rough particles dissipate energy in both the normal and tangential direction of collision. We showed that at large times when the system is in clustered inhomogeneous regime, the temporal decay of translational kinetic energy $T(t)$ and rotational energy $K(t)$ is given by power laws, $T(t) \sim t^{-\theta_T}$ and $K(t) \sim t^{-\theta_K}$, with $\theta_T \approx 1$ and $\theta_K \approx 1.6$. These decay exponents are independent of coefficients of restitution. We also studied the ballistic aggregation with rotational degree of freedom. In our direct numerical simulation of this system, the decay exponents are found to be $\theta_T^{BA} \approx 1$ and $\theta_K^{BA} \approx 1$ for dense systems. Extension of an earlier scaling theory for ballistic aggregation gives $\theta_K^{mf} = 1$, consistent with the numerically obtained value. In Chapter 4, we concluded that the ballistic aggregation is not the correct description for the inhomogeneous cooling regime of freely cooling granular gas. The fact that the rotational energies in the two models decay with different exponents is a further support to our conclusion.

It has been earlier shown that in the homogeneous regime, the directions of the angular velocity and translational velocity are correlated [122]. It would be interesting to see whether this holds true in the inhomogeneous regime in three dimensions. Unfortunately, simulations in three dimensions have strong finite size effects [126] and at the same time the crossover time from the homogeneous regime to inhomogeneous regime for the rotational energy is large. This makes it difficult to obtain a large enough temporal regime where one may test for correlation. This is a promising area for future study.

Experiments have verified Haff's law for the translational kinetic energy decay in the

homogeneous cooling regime [83, 84, 85]. It will be interesting to verify the rotational energy decay behaviour of the homogeneous regime. It should not be very complicated, especially in two dimensions where there is only one rotational mode. Also desired is the investigation of the inhomogeneous cooling regime of this system.

In **Chapter 6**, we studied granular explosion model using event driven simulations and scaling analysis. The cascade of collisions created by the initial perturbation leads to clustering of all moving particles into a spherical shell. The region inside the spherical shell is devoid of particles. This formation of shell conserves radial momentum and predicts a power law growth with time t for the radius of disturbance $R(t) \sim t^{1/(D+1)}$, in D dimensions. We applied the results of granular explosion to a recent experiment [6], where a dilute monolayer of glass beads flowing down on an inclined plane was perturbed by dropping a steel ball. We showed that the growth of radius predicted in granular explosion $R(t) \sim t^{1/3}$ for $D = 2$ describes the experimental data very well except at large times. At long times, the experimental data shows a crossover to a different power law growth $\sim t^{0.18}$. We attributed this crossover to the shell becoming effectively three dimensional due to accumulation of particles at the shell front. The granular explosion model is modified to incorporate this effect. Simulation of this modified model captured the experimentally observed long time behaviour.

It will be quite interesting to see if any connection can be made between the granular explosion in which most of the particles are initially stationary and the well studied freely cooling granular gas, in which all particles initially have a nonzero kinetic energy. It may be possible to think of the freely cooling gas as a collection of many explosions initiated at different points in space, which interact when the shock fronts meet. Thus, it will be useful to make a detailed study of the case of two interacting shocks.

The data for radius show a crossover from an initial elastic behavior $t^{1/2}$ to an asymptotic $t^{1/3}$ growth law. It would be of interest to understand this crossover better. Exact solution of the shock problem in one dimension with $0 < r < 1$ would throw light on it. An

exact solution appears possible given that the freely cooling in one dimension is one of the exactly solvable model in granular physics.

Finally, in **Chapter 7**, we studied granular explosion model with visco-elastic particles using conventional molecular dynamics simulations. Visco-elastic model is a realistic model for a granular particle for which the coefficient of restitution depends strongly on relative velocity of collision. We observed that the formation of shell and scaling result for the temporal growth of radius of disturbance, earlier obtained with simplified model of constant coefficient of restitution, continue to hold for the visco-elastic system.

Bibliography

[1] H. M. Jaeger, S. R. Nagel, and R. P. Behringer, "Granular solids, liquids, and gases," *Reviews of Modern Physics*, vol. 68, pp. 1259–1273, 1996.

[2] L. P. Kadanoff, "Built upon sand: Theoretical ideas inspired by granular flows," *Reviews of Modern Physics*, vol. 71, pp. 435–444, 1999.

[3] I. S. Aranson and L. S. Tsimring, "Patterns and collective behavior in granular media: Theoretical concepts," *Reviews of Modern Physics*, vol. 78, pp. 641–692, 2006.

[4] C. S. Campbell, "Rapid granular flows," *Annual Review of Fluid Mechanics*, vol. 22, pp. 57–92, 1990.

[5] S. F. Shandarin and Y. B. Zeldovich, "The large-scale structure of the universe: Turbulence, intermittency, structures in a self-gravitating medium," *Reviews of Modern Physics*, vol. 61, pp. 185–220, 1989.

[6] J. F. Boudet, J. Cassagne, and H. Kellay, "Blast shocks in quasi-two-dimensional supersonic granular flows," *Physical Review Letters*, vol. 103, p. 224501, 2009.

[7] Z. Jabeen, R. Rajesh, and P. Ray, "Universal scaling dynamics in a perturbed granular gas," *Europhysics Letters*, vol. 89, p. 34001, 2010.

[8] L. Frachebourg, "Exact solution of the one-dimensional ballistic aggregation," *Physical Review Letters*, vol. 82, pp. 1502–1505, 1999.

[9] M. Shinde, D. Das, and R. Rajesh, "Violation of the porod law in a freely cooling granular gas in one dimension," *Physical Review Letters*, vol. 99, p. 234505, 2007.

[10] N. V. Brilliantov and T. Pöschel, *Kinetic Theory of Granular Gases*. Oxford: Oxford University Press, 2004.

[11] P. K. Haff, "Grain flow as a fluid-mechanical phenomenon," *Journal of Fluid Mechanics*, vol. 134, pp. 401–430, 1983.

[12] I. Goldhirsch and G. Zanetti, "Clustering instability in dissipative gases," *Physical Review Letters*, vol. 70, pp. 1619–1622, 1993.

[13] E. Ben-Naim, S. Y. Chen, G. D. Doolen, and S. Redner, "Shocklike dynamics of inelastic gases," *Physical Review Letters*, vol. 83, pp. 4069–4072, 1999.

[14] X. Nie, E. Ben-Naim, and S. Chen, "Dynamics of freely cooling granular gases," *Physical Review Letters*, vol. 89, p. 204301, 2002.

[15] G. F. Carnevale, Y. Pomeau, and W. R. Young, "Statistics of ballistic agglomeration," *Physical Review Letters*, vol. 64, pp. 2913–2916, 1990.

[16] S. Luding, M. Huthmann, S. McNamara, and A. Zippelius, "Homogeneous cooling of rough, dissipative particles: Theory and simulations," *Physical Review E*, vol. 58, pp. 3416–3425, 1998.

[17] R. Ramirez, T. Poschel, N. V. Brilliantov, and T. Schwager, "Coefficient of restitution of colliding viscoelastic spheres," *Physical Review E*, vol. 60, pp. 4465–4472, 1999.

[18] J. J. Brey, M. J. Ruiz-Montero, and D. Cubero, "Homogeneous cooling state of a low-density granular flow," *Physical Review E*, vol. 54, pp. 3664–3671, 1996.

[19] E. Trizac and P. L. Krapivsky, "Correlations in ballistic processes," *Physical Review Letters*, vol. 91, p. 218302, 2003.

[20] C. Coulomb, *in Memoir de Mathematique et de Physique*, vol. 7. Paris: Academie des Sciences, L'Imprimerie Royale, 1773.

[21] M. Faraday, "On the forms and states of fluids on vibrating elastic surfaces," *Philosophical Transactions of the Royal Society of London*, vol. 52, pp. 319–340, 1831.

[22] O. Reynolds, "On the dilatancy of media composed of rigid particles in contact, with experimental illustrations," *Philosophical Magazine*, vol. 20, pp. 469–481, 1885.

[23] A. Kudrolli, "Size separation in vibrated granular materials," *Reports on Progress in Physics*, vol. 67, pp. 209–247, 2004.

[24] I. Goldhirsch, "Rapid granular flows," *Annual Review of Fluid Mechanics*, vol. 35, pp. 267–293, 2003.

[25] H. M. Jaeger and S. R. Nagel, "Physics of the granular state," *Science*, vol. 255, pp. 1523–1531, 1992.

[26] A. Mehta and G. C. Barker, "The dynamics of sand," *Reports on Progress in Physics*, vol. 57, pp. 383–416, 1994.

[27] H. M. Jaeger, C. H. Liu, and S. R. Nagel, "Relaxation at the angle of repose," *Physical Review Letters*, vol. 62, pp. 40–43, 1989.

[28] T. A. J. Duke, G. C. Barker, and A. Mehta, "A monte carlo study of granular relaxation," *Europhysics Letters*, vol. 13, pp. 19–24, 1990.

[29] Y. Boguslavskii and S. Drabkin, "The kinetics of powder settlement caused by low level vibration and elastic stresses," *Physica A*, vol. 222, pp. 75–86, 1995.

[30] J. B. Knight, C. G. Fandrich, C. N. Lau, H. M. Jaeger, and S. R. Nagel, "Density relaxation in a vibrated granular material," *Physical Review E*, vol. 51, pp. 3957–3963, 1995.

[31] S. Douady, S. Fauve, and C. Laroche, "Subharmonic instabilities and defects in a granular layer under vertical vibrations," *Europhysics Letters*, vol. 8, p. 621, 1989.

[32] O. Zik and J. Stavans, "Self-diffusion in granular flows," *Europhysics Letters*, vol. 16, p. 255, 1991.

[33] F. Melo, P. Umbanhowar, and H. L. Swinney, "Transition to parametric wave patterns in a vertically oscillated granular layer," *Physical Review Letters*, vol. 72, pp. 172–175, 1994.

[34] H. K. Pak and R. P. Behringer, "Surface waves in vertically vibrated granular materials," *Physical Review Letters*, vol. 71, pp. 1832–1835, 1993.

[35] H. K. Pak, E. Van Doorn, and R. P. Behringer, "Effects of ambient gases on granular materials under vertical vibration," *Physical Review Letters*, vol. 74, pp. 4643–4646, 1995.

[36] T. Travers, M. Ammi, D. Bideau, A. Gervois, J. C. Messager, and J. P. Troadec, "Uniaxial compression of 2d packings of cylinders. effects of weak disorder," *Europhysics Letters*, vol. 4, p. 329, 1987.

[37] C. H. Liu, S. R. Nagel, D. A. Schecter, S. N. Coppersmith, S. Majumdar, O. Narayan, and T. A. Witten, "Force fluctuations in bead packs," *Science*, vol. 269, pp. 513–515, 1995.

[38] S. N. Coppersmith, C. H. Liu, S. Majumdar, O. Narayan, and T. A. Witten, "Model for force fluctuations in bead packs," *Physical Review E*, vol. 53, pp. 4673–4685, 1996.

[39] J. T. Jenkins and S. B. Savage, "A theory for the rapid flow of identical, smooth, nearly elastic, spherical particles," *Journal of Fluid Mechanics*, vol. 130, pp. 187–202, 1983.

[40] P. K. Haff, "A physical picture of kinetic granular fluids," *Journal of Rheology*, vol. 30, pp. 931–948, 1986.

[41] S. B. Savage and D. J. Jeffrey, "The stress tensor in a granular flow at high shear rates," *Journal of Fluid Mechanics*, vol. 110, pp. 255–272, 1981.

[42] P. Evesque and J. Rajchenbach, "Instability in a sand heap," *Physical Review Letters*, vol. 62, pp. 44–46, 1989.

[43] C. Laroche, S. Douady, and S. Fauve, "Convective flow of granular masses under vertical vibrations," *Journal de Physique (France)*, vol. 50, pp. 699–706, 1989.

[44] J. B. Knight, H. M. Jaeger, and S. R. Nagel, "Vibration-induced size separation in granular media: The convection connection," *Physical Review Letters*, vol. 70, pp. 3728–3731, 1993.

[45] E. E. Ehrichs, H. M. Jaeger, G. S. Karczmar, J. B. Knight, V. Y. Kuperman, and S. R. Nagel, "Granular convection observed by magnetic resonance imaging," *Science*, vol. 267, pp. 1632–1634, 1995.

[46] J. C. Williams, "The segregation of particulate materials. A review," *Powder Technology*, vol. 15, pp. 245–251, 1976.

[47] L. T. Fan, Y. M. Chen, and F. S. Lai, "Recent developments in solids mixing," *Powder Technology*, vol. 61, pp. 255–287, 1990.

[48] C. F. Harwood, "Powder segregation due to vibration," *Powder Technology*, vol. 16, pp. 51–57, 1977.

[49] W. Cooke, S. Warr, J. M. Huntley, and R. C. Ball, "Particle size segregation in a two-dimensional bed undergoing vertical vibration," *Physical Review E*, vol. 53, pp. 2812–2822, 1996.

[50] O. R. Walton, *in Particulate Two-Phase Flow*. Boston: edited by M. C. Roco (Butterworth-Heinemann), 1993.

[51] S. McNamara and W. R. Young, "Inelastic collapse and clumping in a one-dimensional granular medium," *Physics of Fluids A*, vol. 4, pp. 496–504, 1992.

[52] S. McNamara and W. R. Young, "Inelastic collapse in two dimensions," *Physical Review E*, vol. 50, pp. R28–R31, 1994.

[53] O. Pouliquen, J. Delour, and S. B. Savage, "Fingering in granular flows," *Nature*, vol. 386, pp. 816–817, 1997.

[54] Y. Forterre and O. Pouliquen, "Longitudinal vortices in granular flows," *Physical Review Letters*, vol. 86, pp. 5886–5889, 2001.

[55] J. S. Olafsen and J. S. Urbach, "Clustering, order, and collapse in a driven granular monolayer," *Physical Review Letters*, vol. 81, pp. 4369–4372, 1998.

[56] P. B. Umbanhowar, F. Melo, and H. L. Swinney, "Localized excitations in a vertically vibrated granular layer," *Nature*, vol. 382, pp. 793–796, 1996.

[57] K. Liffman, G. Metcalfe, and P. Cleary, "Granular convection and transport due to horizontal shaking," *Physical Review Letters*, vol. 79, pp. 4574–4576, 1997.

[58] G. H. Ristow, G. Straßburger, and I. Rehberg, "Phase diagram and scaling of granular materials under horizontal vibrations," *Physical Review Letters*, vol. 79, pp. 833–836, 1997.

[59] J. Rajchenbach, "Flow in powders: From discrete avalanches to continuous regime," *Physical Review Letters*, vol. 65, pp. 2221–2224, 1990.

[60] P. Tegzes, T. Vicsek, and P. Schiffer, "Avalanche dynamics in wet granular materials," *Physical Review Letters*, vol. 89, p. 094301, 2002.

[61] O. Johnsen, R. Toussaint, K. J. Måløy, and E. G. Flekkøy, "Pattern formation during air injection into granular materials confined in a circular hele-shaw cell," *Physical Review E*, vol. 74, p. 011301, 2006.

[62] B. Sandnes, H. A. Knudsen, K. J. Måløy, and E. G. Flekkøy, "Labyrinth patterns in confined granular-fluid systems," *Physical Review Letters*, vol. 99, p. 038001, 2007.

[63] I. S. Aranson, B. Meerson, P. V. Sasorov, and V. M. Vinokur, "Phase separation and coarsening in electrostatically driven granular media," *Physical Review Letters*, vol. 88, p. 204301, 2002.

[64] A. Snezhko, I. S. Aranson, and W.-K. Kwok, "Structure formation in electromagnetically driven granular media," *Physical Review Letters*, vol. 94, p. 108002, 2005.

[65] T. Pöschel and S. Luding, eds., *Granular Gases*. Berlin: Springer, 2001.

[66] T. Pöschel and N. V. Brilliantov, eds., *Granular Gas Dynamics*. Berlin: Springer, 2003.

[67] S. N. Pathak, Z. Jabeen, P. Ray, and R. Rajesh, "Shock propagation in granular flow subjected to an external impact," *Physical Review E*, vol. 85, p. 061301, 2012.

[68] S. N. Majumdar, K. Mallick, and S. Sabhapandit, "Statistical properties of the final state in one-dimensional ballistic aggregation," *Physical Review E*, vol. 79, p. 021109, 2009.

[69] S. K. Das and S. Puri, "Kinetics of inhomogeneous cooling in granular fluids," *Physical Review E*, vol. 68, p. 011302, 2003.

[70] M. Shinde, D. Das, and R. Rajesh, "Equivalence of the freely cooling granular gas to the sticky gas," *Physical Review E*, vol. 79, p. 021303, 2009.

[71] M. Shinde, D. Das, and R. Rajesh, "Coarse-grained dynamics of the freely cooling granular gas in one dimension," *Physical Review E*, vol. 84, p. 031310, 2011.

[72] L. Frachebourg, P. A. Martin, and J. Piasecki, "Ballistic aggregation: a solvable model of irreversible many particle dynamics," *Physica A*, vol. 279, pp. 69–99, 2000.

[73] R. Tribe and O. Zaboronski, "On the large time asymptotics of decaying burgers turbulence," *Communications in Mathematical Physics*, vol. 212, p. 415, 2000.

[74] S. Kida, "Asymptotic properties of Burgers turbulence," *Journal of Fluid Mechanics*, vol. 93, pp. 337–377, 1979.

[75] S. Dey, D. Das, and R. Rajesh, "Lattice models for ballistic aggregation in one dimension," *Europhysics Letters*, vol. 93, p. 44001, 2011.

[76] T. Pöschel and T. Schwager, *Computational Granular Dynamics*. Berlin: Springer, 2004.

[77] N. V. Brilliantov, F. Spahn, J.-M. Hertzsch, and T. Pöschel, "Model for collisions in granular gases," *Physial Review E*, vol. 53, pp. 5382–5392, 1996.

[78] F. G. Bridges, A. Hatzes, and D. N. C. Lin, "Structure, stability and evolution of saturn's rings," *Nature*, vol. 309, pp. 333–335, 1984.

[79] R. Greenberg and A. Brahic, *Planetary Rings*. Tucson: University of Arizona Press, 1984.

[80] H. Hertz, "Ueber die berührung fester elastischer körper," *Journal für die reine und angewandte Mathematik*, vol. 92, pp. 156–171, 1882.

[81] T. Schwager and T. Pöschel, "Coefficient of normal restitution of viscous particles and cooling rate of granular gases," *Physical Review E*, vol. 57, pp. 650–654, 1998.

[82] S. E. Esipov and T. Pöschel, "The granular phase diagram," *Journal of Statistical Physics*, vol. 86, pp. 1385–1395, 1997.

[83] C. C. Maaß, N. Isert, G. Maret, and C. M. Aegerter, "Experimental investigation of the freely cooling granular gas," *Physical Review Letters*, vol. 100, p. 248001, 2008.

[84] Y. Grasselli, G. Bossis, and G. Goutallier, "Velocity-dependent restitution coefficient and granular cooling in microgravity," *Europhysics Letters*, vol. 86, p. 60007, 2009.

[85] S. Tatsumi, Y. Murayama, H. Hayakawa, and M. Sano, "Experimental study on the kinetics of granular gases under microgravity," *Journal of Fluid Mechanics*, vol. 641, pp. 521–539, 2009.

[86] N. F. Carnahan and K. E. Starling, "Equation of state for nonattracting rigid spheres," *The Journal of Chemical Physics*, vol. 51, pp. 635–636, 1969.

[87] P. Deltour and J.-L. Barrat, "Quantitative study of a freely cooling granular medium," *Journal de Physique I*, vol. 7, p. 137, 1997.

[88] A. Goldshtein and M. Shapiro, "Mechanics of collisional motion of granular materials. Part 1. General hydrodynamic equations," *Journal of Fluid Mechanics*, vol. 282, pp. 75–114, 1995.

[89] T. P. C. van Noije and M. H. Ernst, "Velocity distributions in homogeneous granular fluids: the free and the heated case," *Granular Matter*, vol. 1, pp. 57–64, 1998.

[90] S. McNamara and W. R. Young, "Dynamics of a freely evolving, two-dimensional granular medium," *Physical Review E*, vol. 53, pp. 5089–5100, 1996.

[91] E. Efrati, E. Livne, and B. Meerson, "Hydrodynamic singularities and clustering in a freely cooling inelastic gas," *Physical Review Letters*, vol. 94, p. 088001, 2005.

[92] R. Brito and M. H. Ernst, "Extension of haff's cooling law in granular flows," *Europhysics Letters*, vol. 43, p. 497, 1998.

[93] S. Chen, Y. Deng, X. Nie, and Y. Tu, "Clustering kinetics of granular media in three dimensions," *Physics Letters A*, vol. 269, pp. 218–223, 2000.

[94] S. Miller and S. Luding, "Cluster growth in two- and three-dimensional granular gases," *Physical Review E*, vol. 69, p. 031305, 2004.

[95] C. V. Raman, "The photographic study of impact at minimal velocities," *Physical Review*, vol. 12, pp. 442–447, 1918.

[96] E. Falcon, C. Laroche, S. Fauve, and C. Coste, "Behavior of one inelastic ball bouncing repeatedly off the ground," *The European Physical Journal B*, vol. 3, pp. 45–57, 1998.

[97] L. Labous, A. D. Rosato, and R. N. Dave, "Measurements of collisional properties of spheres using high-speed video analysis," *Physical Review E*, vol. 56, pp. 5717–5725, 1997.

[98] F. Leyvraz, "Scaling theory and exactly solved models in the kinetics of irreversible aggregation," *Physics Reports*, vol. 383, pp. 95–212, 2003.

[99] E. Trizac and J.-P. Hansen, "Dynamic scaling behavior of ballistic coalescence," *Physical Review Letters*, vol. 74, pp. 4114–4117, 1995.

[100] P. L. Krapivsky and E. Ben-Naim, "Aggregation with multiple conservation laws," *Physical Review E*, vol. 53, pp. 291–298, 1996.

[101] J. M. Burgers, *The Non-Linear Diffusion Equation: Asymptotic Solutions and Statistical Problems*. Boston: Reidel, 1974.

[102] K. Shida and T. Kawai, "Cluster formation by inelastically colliding particles in one-dimensional space," *Physica A*, vol. 162, pp. 145–160, 1989.

[103] N. Schörghofer and T. Zhou, "Inelastic collapse of rotating spheres," *Physical Review E*, vol. 54, pp. 5511–5515, 1996.

[104] D. Goldman, M. D. Shattuck, C. Bizon, W. D. McCormick, J. B. Swift, and H. L. Swinney, "Absence of inelastic collapse in a realistic three ball model," *Physical Review E*, vol. 57, pp. 4831–4833, 1998.

[105] S. Luding and S. McNamara, "How to handle the inelastic collapse of a dissipative hard-sphere gas with the TC model," *Granular Matter*, vol. 1, pp. 113–128, 1998.

[106] S. E. Esipov and T. J. Newman, "Interface growth and Burgers turbulence: The problem of random initial conditions," *Physical Review E*, vol. 48, pp. 1046–1050, 1993.

[107] S. E. Esipov, "Energy decay in Burgers turbulence and interface growth: The problem of random initial conditions. II," *Physical Review E*, vol. 49, pp. 2070–2081, 1994.

[108] S. Luding, "Structure and cluster formation in granular media," *Pramana*, vol. 64, pp. 893–902, 2005.

[109] D. C. Rapaport, "The event scheduling problem in molecular dynamic simulation," *Journal of Computational Physics*, vol. 34, pp. 184–201, 1980.

[110] D. C. Rapaport, *The Art of Molecular Dynamics Simulations*. Cambridge: Cambridge University Press, 2004.

[111] T. Pöschel, N. V. Brilliantov, and T. Schwager, "Long-time behavior of granular gases with impact-velocity dependent coefficient of restitution," *Physica A*, vol. 325, pp. 274 – 283, 2003.

[112] J. Hoshen and R. Kopelman, "Percolation and cluster distribution. I. Cluster multiple labeling technique and critical concentration algorithm," *Physical Review B*, vol. 14, pp. 3438–3445, 1976.

[113] C. Connaughton, R. Rajesh, and O. Zaboronski, "Kinetics of cluster-cluster aggregation," in *Handbook of Nanophysics: Clusters and Fullerenes* (K. D. Sattler, ed.), Taylor and Francis, 2010.

[114] A. Zippelius, "Granular gases," *Physica A*, vol. 369, pp. 143–158, 2006.

[115] S. F. Foerster, M. Y. Louge, H. Chang, and K. Allia, "Measurements of the collision properties of small spheres," *Physics of Fluids*, vol. 6, pp. 1108–1115, 1994.

[116] O. Herbst, M. Huthmann, and A. Zippelius, "Dynamics of inelastically colliding spheres with coulomb friction: Relaxation of translational and rotational energy," *Granular Matter*, vol. 2, pp. 211–219, 2000.

[117] I. Goldhirsch, S. H. Noskowicz, and O. Bar-Lev, "Nearly smooth granular gases," *Physical Review Letters*, vol. 95, p. 068002, 2005.

[118] M. Huthmann and A. Zippelius, "Dynamics of inelastically colliding rough spheres:Relaxation of translational and rotational energy," *Physical Review E*, vol. 56, pp. R6275–R6278, 1997.

[119] J. T. Jenkins and M. W. Richman, "Kinetic theory for plane flows of a dense gas of identical, rough, inelastic, circular disks," *Physics of Fluids*, vol. 28, pp. 3485–3494, 1985.

[120] C. K. K. Lun, "Kinetic theory for granular flow of dense, slightly inelastic, slightly rough spheres," *Journal of Fluid Mechanics*, vol. 233, pp. 539–559, 1991.

[121] S. McNamara and S. Luding, "Energy nonequipartition in systems of inelastic, rough spheres," *Physical Review E*, vol. 58, pp. 2247–2250, 1998.

[122] N. V. Brilliantov, T. Pöschel, W. T. Kranz, and A. Zippelius, "Translations and rotations are correlated in granular gases," *Physical Review Letters*, vol. 98, p. 128001, 2007.

[123] B. Gayen and M. Alam, "Orientational correlation and velocity distributions in uniform shear flow of a dilute granular gas," *Physical Review Letters*, vol. 100, p. 068002, 2008.

[124] E. Ben-Naim and A. Zippelius, "Singular energy distributions in driven and undriven granular media," *Journal of Statistical Physics*, vol. 129, pp. 677–697, 2007.

[125] R. Rongali and M. Alam, "Higher-order effects on orientational correlation and relaxation dynamics in homogeneous cooling of a rough granular gas," *Physical Review E*, vol. 89, p. 062201, 2014.

[126] S. N. Pathak, Z. Jabeen, D. Das, and R. Rajesh, "Energy decay in three-dimensional freely cooling granular gas," *Physical Review Letters*, vol. 112, p. 038001, 2014.

[127] E. Ben-Naim, P. L. Krapivsky, F. Leyvraz, and S. Redner, "Kinetics of ballistically-controlled reactions," *Journal of Physical Chemistry*, vol. 98, pp. 7284–7288, 1994.

[128] G. Taylor, "The formation of a blast wave by a very intense explosion. I. Theoretical discussion," *Proceedings of the Royal Society of London A*, vol. 201, pp. 159–174, 1950.

[129] L. Sedov, *Similarity and Dimensional Methods in Mechanics*. Florida: CRC Press, 10 ed., 1993.

[130] J. von Neumann in *Collected Works*, p. 219, Oxford: Pergamon Press, 1963.

[131] P. T. Metzger, C. D. Immer, C. M. Donahue, B. M. Vu, R. C, L. III, and M. Deyo-Svendsen, "Jet-induced cratering of a granular surface with application to lunar spaceports," *Journal of Aerospace Engineering*, vol. 21, p. 24, 2009.

[132] X. Cheng, L. Xu, A. Patterson, H. M. Jaeger, and S. R. Nagel, "Towards the zero-surface-tension limit in granular fingering instability," *Nature Physics*, vol. 4, pp. 234–237, 2008.

[133] S. F. Pinto, M. S. Couto, A. P. F. Atman, S. G. Alves, A. T. Bernardes, H. F. V. de Resende, and E. C. Souza, "Granular fingers on jammed systems: New fluid-like patterns arising in grain-grain invasion experiments," *Physical Review Letters*, vol. 99, p. 068001, 2007.

[134] W. Losert, D. G. W. Cooper, and J. P. Gollub, "Propagating front in an excited granular layer," *Physical Review E*, vol. 59, pp. 5855–5861, 1999.

[135] S. Luding, "Granular media-information propagation," *Nature*, vol. 435, pp. 159–160, 2005.

[136] A. Daerr and S. Douady, "Two types of avalanche behaviour in granular media," *Nature*, vol. 399, p. 241, 1999.

[137] Y. B. Zel'dovich and Y. P. Raizer, *Physics of Shock Waves and High Temperature Hydrodynamic Phenomena*. New York: Dover Publications, Inc., 2002.

[138] J. P. Ostriker and C. F. McKee, "Astrophysical blastwaves," *Reviews of Modern Physics*, vol. 60, pp. 1–68, 1988.

[139] T. Antal, P. L. Krapivsky, and S. Redner, "Exciting hard spheres," *Physical Review E*, vol. 78, p. 030301, 2008.

[140] E. Trizac and A. Barrat, "Free cooling and inelastic collapse of granular gases in high dimensions," *The European Physical Journal E*, vol. 3, pp. 291–294, 2000.

[141] D. E. G. Williams, "Packing fraction of a disk assembly randomly close packed on a plane," *Physical Review E*, vol. 57, pp. 7344–7345, 1998.

[142] D. Bideau and J. P. Troadec *J. Phys. C*, vol. 17, p. L371, 1984.